Technical Report ITL-93-1
July 1993

US Army Corps
of Engineers
Waterways Experiment
Station

Computer-Aided Structural Engineering (CASE) Project

Theoretical Manual for Analysis of Arch Dams

by Yusof Ghanaat
QUEST Structures

Approved For Public Release; Distribution Is Unlimited

Prepared for Headquarters, U.S. Army Corps of Engineers

Computer-Aided Structural Engineering (CASE) Project

Technical Report ITL-93-1
July 1993

Theoretical Manual for Analysis of Arch Dams

by Yusof Ghanaat

QUEST Structures
1900 Powell St.
Suite 210
Emeryville, CA 94608

Final report

Approved for public release; distribution is unlimited

Prepared for U.S. Army Corps of Engineers
Washington, DC 20314-1000

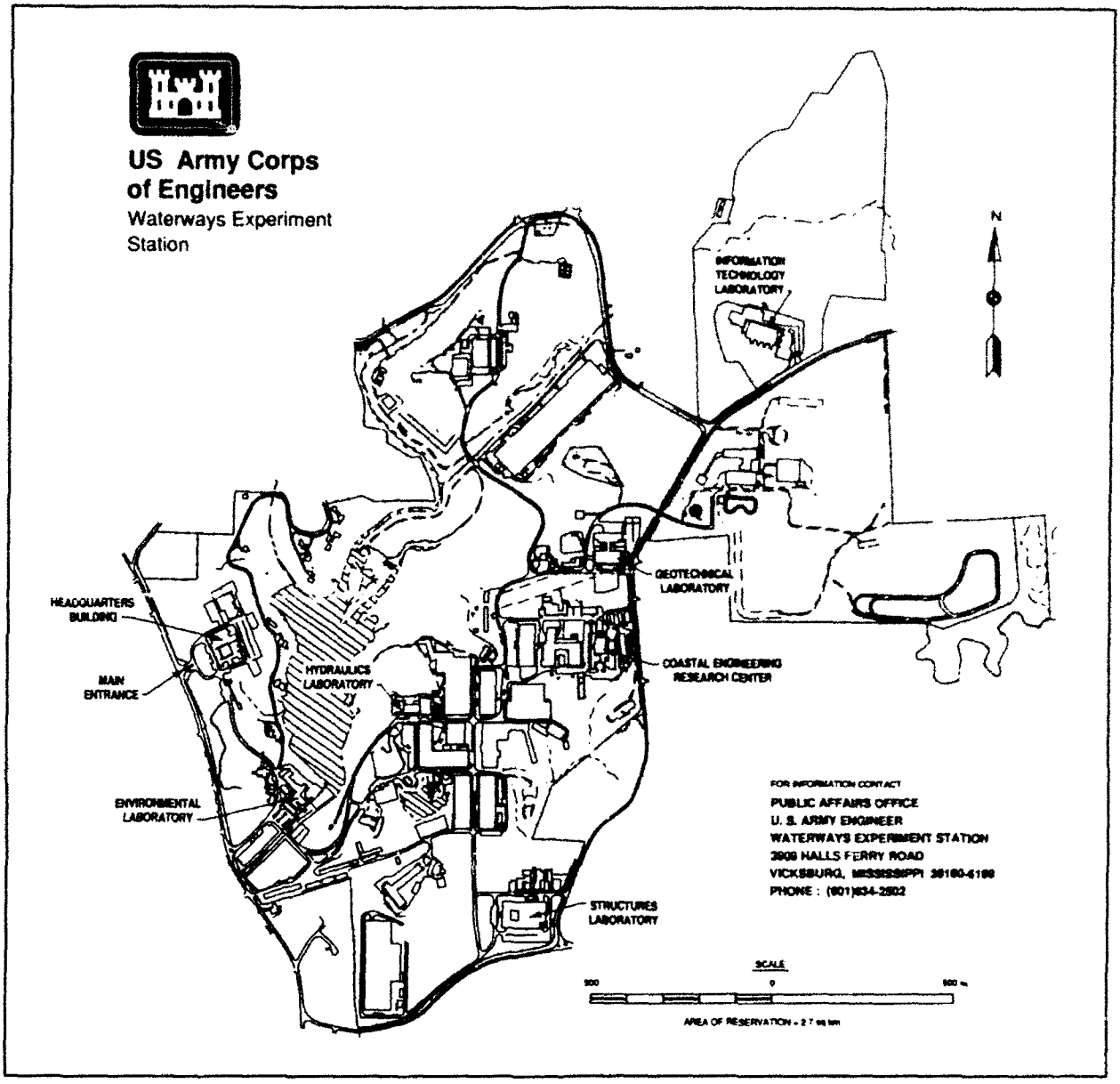

Waterways Experiment Station Cataloging-in-Publication Data

Ghanaat, Yusof.
Theoretical manual for analysis of arch dams / by Yusof Ghanaat ; prepared for U.S. Army Corps of Engineers.
108 p. : ill. ; 28 cm. — (Technical report ; ITL-93-1)
Includes bibliographical references.
1. Arch dams — Earthquake effects — Mathematical models. 2. Structural analysis (Engineering) 3. Finite element method. 4. Structural dynamics. I. United States. Army. Corps of Engineers. II. U.S. Army Engineer Waterways Experiment Station. III. Computer-aided Structural Engineering Program. IV. Title. V. Series: Technical report (U.S. Army Engineer Waterways Experiment Station) ; ITL-93-1.
TA7 W34 no.ITL-93-1

TABLE OF CONTENTS

4. SYSTEM IDEALIZATION

5. ISOPARAMETRIC ELEMENT FORMULATION

6. STATIC ANALYSIS PROCEDURE

7. EARTHQUAKE ANALYSIS PROCEDURE

TABLE OF FIGURES

Figure

PREFACE

This report provides a theoretical background and describes the procedures for the linear structural analysis of concrete arch dams. The analytical procedures described are employed in the **G**raphics-based **D**am **A**nalysis **P**rogram (GDAP). An overview of the trial load method of arch dam design and analysis is also presented. Funding for the development of this manual was provided by Headquarters, US Army Corps of Engineers (HQUSACE), under the Computer-Aided Structural Engineering (CASE) Project, and the Civil Works Guidance Update Program, in an effort to provide the Corps with engineering manuals.

This manual was written under the direction of and is a product of the CASE Arch Dam Task Group. The manual was written by Dr. Yusof Ghanaat (QUEST Structures/consultant under contract DAC39-88-C-005-P003). Task group members during the development of this manual were:

Mr. Byron J. Foster	CESAD-EN (Chairman)
Mr. G. Ray Navidi	CEORH-ED
Mr. William K. Wigner	CESAJ-EN
Mr. Terry W. West	FERC (formerly CESAJ-EN)
Mr. Jerry L. Foster	CECW-ED (formerly FERC)
Mr. Donald R. Dressler	CECW-ED
Mr. H. Wayne Jones	CEWES-IM-DS (Task Group Coordinator)
Mr. David A. Dollar	USBR
Mr. Larry K. Nuss	USBR
Dr. Yusof Ghanaat	Consultant - QUEST Structures
Prof. Ray W. Clough	Consultant
Mr. Merlin D. Copen	Consultant - USBR (retired)
Mr. Howard L. Boggs	Consultant - USBR (retired)

The work was accomplished under the general supervision of Dr. N. Radhakrishnan, Director, Information Technology Laboratory (ITL), U.S. Army Engineer Waterways Experiment Station (WES), and under the direct supervision of Mr. H. Wayne Jones, Chief, Scientific Engineering and Applications Center (SEAC), Computer-Aided Engineering Division (CAED), ITL, WES. Prof. Clough and Mr. Boggs provided invaluable comments and recommendations in the review of this manual. The technical monitor for HQUSACE was Mr. Don Dressler.

At the time of publication of this report, Director of WES was Dr. Robert W. Whalin. Commander was COL Leonard G. Hassell, EN.

1. INTRODUCTION

1.1 Purpose

This manual is a companion to Engineer Manual (EM) 1110-2-2201, "Engineering and Design: Arch Dam Design" (Headquarters, Department of the Army 1993), and is intended to provide a theoretical background for the linear structural analysis of concrete arch dams. It is also designed to describe analytical procedures employed in the computer program, Graphics-Based Dam Analysis Program (GDAP)(Ghanaat 1993), and to provide an overview of the trial load method of arch dam design and analysis.

1.2 Scope

The manual contains an overview and discussion of the general aspects of the finite element procedures, including system idealization, isoparametric element formulation, and solution techniques for the static and dynamic analyses of arch dams used in the computer program GDAP. It also presents general discussions on the concepts, assumptions, and limitations of the trial load method.

1.3 Methods of Analyses and Assumptions

This manual primarily deals with the linear-elastic methods of analyses under which a linear behavior is assumed for the concrete dam, impounded water, and foundation rock. Nonlinear effects such as concrete cracking, water cavitation, construction joints opening during earthquake shaking, or geometric nonlinearity are not considered.

2. TRIAL LOAD METHOD OF ANALYSIS

2.1 Introduction

The basic steps in designing an arch dam include preparation of a preliminary layout, computation of stresses due to static loads, evaluation of the stress results, and modifications of the layout by adjusting the dam shape. This overall process of design of arch dams is fully discussed by the U.S. Bureau of Reclamation (USBR) (1977) and in EM 1110-2-2201, "Arch Dam Design." The primary objective in the design of arch dams is to establish a layout by determining the arches which will fit the site topography most favorably and distribute the load with the minimum use of materials within allowable stress limitations. To produce a satisfactory design, the four design steps are repeated until stress distributions developed throughout the dam structure are acceptable. The estimation of stresses in arch dams, however, is a difficult and complex problem. It should be based on an analysis procedure which provides reasonably accurate results and yet is simple enough for the design purposes. One such analysis procedure is the trial load method which was developed prior to 1940 and later was expanded and programmed for the digital computers by the USBR.

A complete description of the theory of the trial load method and its computerized version known as Arch Dam Stress Analysis System (ADSAS) is given by the USBR (1977). This chapter provides an overview of the method for introductory purposes. The presentation in this chapter closely follows the USBR presentation to facilitate further study of the method.

2.2 Overview of Trial Load Method

The trial load method assumes that an arch dam is made of two systems of structural members -- horizontal *arch units* and vertical beams or *cantilever units* (Figure 2-1). Each system occupies the entire body of the dam and the loading is assumed to be divided between the two systems in such a way that the resulting arch and cantilever deflections for any point in the dam are equal. In general, the agreement between the arch and cantilever deflections must be made in radial and tangential directions as well as in rotational directions. This agreement is accomplished by subjecting representative arch and cantilever units to a succession of self-balancing trial loads and solving the simultaneous equations involved. The solution is normally obtained by computers using a trial load program such as

ADSAS. The resulting load distribution required to achieve deflection agreement is then used to compute stresses in the dam.

The stresses in arch dams are computed more accurately using the finite element method. This method, which will be discussed in later chapters, divides the dam structure into small but *finite elements* interconnected at a discrete number of points. The displacements of these nodal points are the basic unknowns. They are obtained from the solution of equilibrium equations for the entire system, assembled by combining the stiffness matrices and the load vectors of the individual elements. The stresses are then obtained from the computed displacements using the stress-displacement relationship for each finite element. Although the finite element method provides more accurate stress results, subdivision of the dam and its foundation to small finite elements is a laborious task. As a result, the finite element procedure is usually not a preferred method for the iterative design process of arch dams. However, a specialized finite element program such as GDAP (Ghanaat 1993), which includes automatic mesh generation capabilities, offers simplified input data and can easily be used to perform design calculations.

One advantage of the trial load method is that the necessary data for analyzing the dam structure using ADSAS are directly taken from the layout drawings. Thus, modifications of the dam layout during the iterative design process can easily be incorporated in the trial load analysis by changing only a few parameters. Another important advantage includes the overall design philosophy of arch dams which has evolved on the basis of the trial load method of analysis, an insight shared by many arch dam designers. For these reasons, the trial load method continues to be the preferred method of analysis by many designers and is discussed in the remainder of this chapter.

2.2.1 Horizontal Arch Units

In the trial load method, the entire body of the dam is divided into a series of slices called *arch units*. Each arch unit is bounded by two horizontal planes one unit apart. In most cases, only several representative arch units are selected for the analysis (Figure 2-1).

2.2.2 Vertical Cantilever Units

The dam is also divided into a continuous series of vertical slices called *cantilever units*. Each cantilever unit is bounded between two vertical planes radial to the upstream face and spaced one unit apart at the dam axis. It should be noted that the cantilever units for arch dams other than constant-center type are bounded by warped surfaces. This is because vertical radial planes are not possible for the variable-radius arch dams, where the direction of the radius on a given vertical varies with elevation. Similar to the arch units, only a few representative cantilever units are required for the trial load analysis.

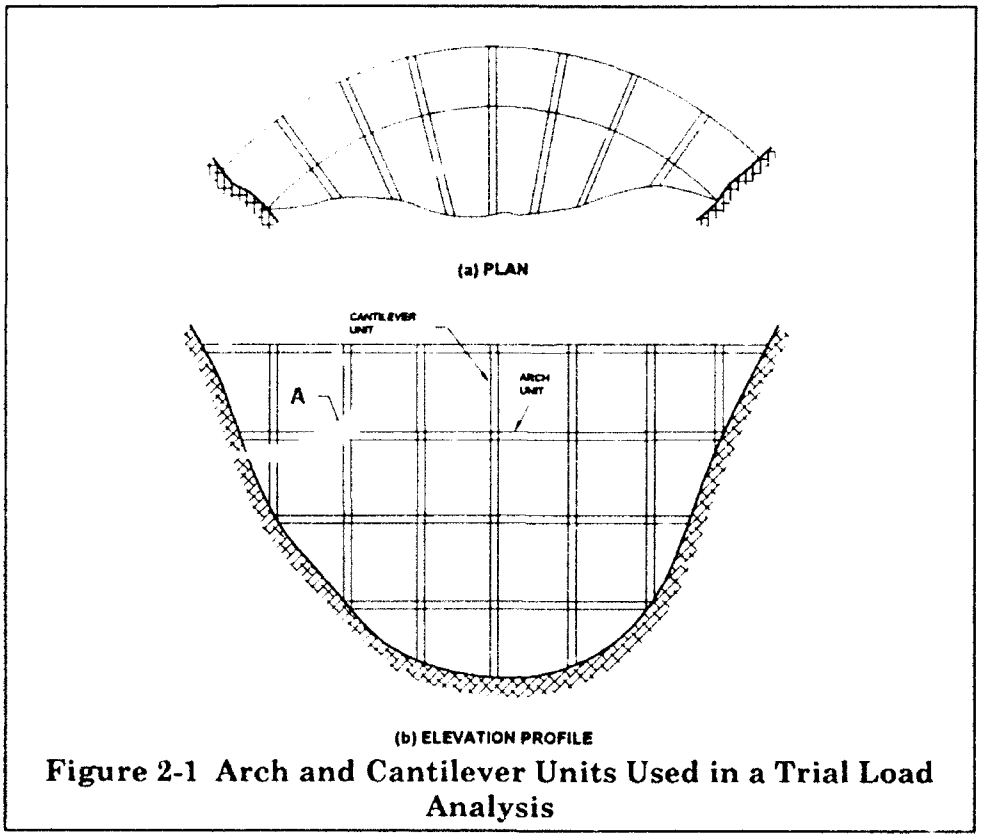

Figure 2-1 Arch and Cantilever Units Used in a Trial Load Analysis

2.2.3 Interaction of Arch and Cantilever Units

The representative arch and cantilever units are assumed to be connected at their intersection volumes. Figure 2-2 represents one of the arch and one of the cantilever units in Figure 2-1 which intersect in a common volume A. The load applied on the face of this volume will be resisted partly by the arch, with the remainder going to the cantilever. Similar load distributions also take place at other points on the faces

of both the arch and the cantilever, with the result being a deflection of the arch and cantilever units to a new position. The intersecting volume A moves from its initial position to A_2 in such manner that the new position A_2 in the deformed cantilever coincides with its position in the deformed arch. This movement generally consists of three translational and three rotational components. But as illustrated in Figure 2-2, two translations in the radial and tangential directions and two rotations in horizontal (θ_V) and vertical (θ_H) planes are the most important components. Vertical movements and rotations in vertical tangential planes are considered to be negligible.

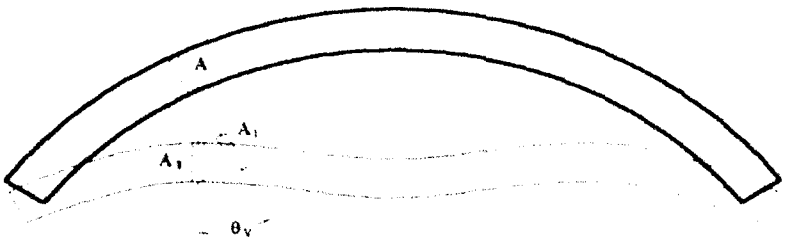

(a) Deflected Arch

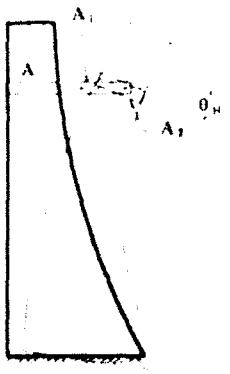

(b) Deflected Cantilever

Figure 2-2 Linear and Rotational Deflections of Arch and Cantilever Units

Simple radial loads on the cantilever will not produce the required tangential and rotational displacements. These movements are produced by internal forces in the dam, but in the trial load method they are treated as external loads applied on individual arch and cantilever units and are determined by trial.

2.3 Types of Trial Load Analyses

Trial load analyses may be performed with varying degrees of accuracy and refinement consistent with different phases of the design. Progressing from the simplest to the most comprehensive, they include crown-cantilever adjustment, radial deflection adjustment, and complete adjustment analyses.

2.3.1 Crown-cantilever Analysis

The most important factors in division of external loads between arch and cantilever units are the radial loads and radial deflections. In the simplest form, this division is accomplished by a crown-cantilever analysis which involves adjustment of radial deflections at the crown cantilever with the corresponding deflections at the crown of the arches. This analysis assumes a uniform distribution of radial loads on the arches and neglects the effects of tangential shear and twist. The analysis produces only a crude estimate of the actual stresses, but it is usually adequate for preliminary studies, particularly in a constant radius dam.

2.3.2 Radial Deflection Analysis

In this analysis, the radial deflections at the arch quarter points are brought into agreement with several corresponding cantilevers by an adjustment of the radial loads between these units. The radial loads in this case no longer need to be distributed uniformly from the crowns to abutments of arches. This permits to apply a more realistic load distribution, which will result in an improved estimate of the stresses compared with those obtained from a crown-cantilever analysis. The results, however, are still incomplete because the effects of tangential displacement and twist are not considered. A radial deflection analysis may be used for the feasibility studies.

2.3.3 Complete Adjustment Analysis

None of the preceding analyses provides a complete representation of the displacements and internal forces in an arch dam. The actual situation can be

analyzed by a complete trial load analysis, in which agreement of three translational and three rotational displacements is achieved by appropriate division of the radial, tangential, and twist loads between arch and cantilever units. This analysis provides reasonable results for a specifications design. The accuracy of results is limited only by the basic assumptions of the method, and the level of error permitted in the calculations.

2.4 Outline of Analysis Procedure

The arch dam to be analyzed is divided into a representative series of arch and cantilever units similar to those shown in Figure 2-1. The actual dimensions of these units are obtained from the layout drawing of the dam. The analysis then proceeds with a division of loads between representative arch and cantilever units in such a way that the deflections or movements of these units are equal. To accomplish this, the trial load method assumes elastic material properties for the dam and employs the theory of elasticity to fulfill the requirements for equilibrium, continuity, and boundary conditions that must be met to obtain correct stress results.

The deflections or movements in an arch dam generally include three translational and three rotational components. These are radial, tangential, and vertical translations, and rotations in horizontal, vertical radial, and vertical tangential planes. However, deflections in the vertical direction and rotations in vertical tangential planes are small and usually are ignored in the trial load analysis. The remaining four deflections are computed for the arches and cantilevers using the usual arch and beam formulas by subjecting these structural units to radial, tangential, and twist loads. It should be recognized that the arch analysis must include bending effects as well as rib-shortening and transverse shear. Similarly, the beam formula used for the analysis of cantilevers must include shear deformations in addition to the bending.

Following the procedures described in the following paragraph, a set of self-balancing trial loads required to produce equal deflections in the arches and cantilevers is determined. From these loads, the stresses in the arch are then computed by assuming a linear stress distribution through the thickness.

2.4.1 Adjustment for Radial Deflection

The first trial load division of external loads, such as the water load, begins with a transfer of load which will produce equal arch and cantilever deflections in the radial direction. The type of loads needed for this agreement are illustrated on the intersecting volume A shown in Figure 2-3. Loads are applied to the cantilever by introducing a pair of shear forces on the cantilever sections, such as V_c shown on the top and bottom faces of the volume A. The differences in these forces are balanced by the shear forces, V_a, which are assumed to be present on the arch sections from the application of external loads. These shear force pairs satisfy the equilibrium condition in the radial direction, but they also exert moments on volume A. The moments produced by the shear couples are balanced by differences between the cantilever bending moments, M_c, and the arch bending moments, M_a, applied on the faces of volume A to ensure equilibrium against rotation. These forces known as self-balancing, provide a mechanism for transfer of loads from arch units to cantilever units, without altering the total loads applied to the dam. The magnitudes of the radial self-balancing loads are determined by trial.

Once a set of self-balancing radial loads has been selected, bending moments in the arch and cantilever units and the corresponding deflections are computed. If the agreement between the radial deflections of the arch and cantilever units is not satisfactory, the self-balancing loads are modified and the process repeated.

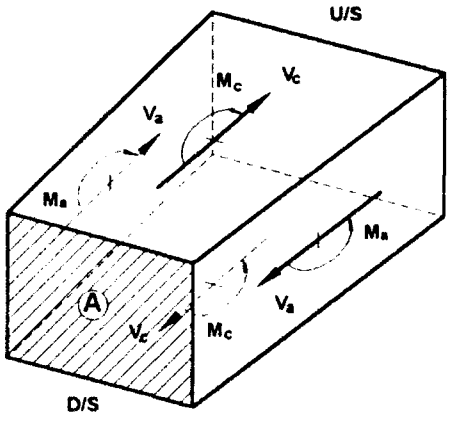

Figure 2-3 Self-balancing Loads for Radial Adjustment

2.4.2 Adjustment for Tangential Deflection

The tangential displacements shown in Figure 2-2a are adjusted by a procedure similar to that described for the radial displacements. The required set of self-balancing loads for tangential adjustment are depicted in Figure 2-4. In this case, the equilibrium is maintained by balancing the difference between the tangential shear forces, V_{TA}, at the top and bottom faces with the arch thrusts, H, applied to the sides of volume A. Similarly, a difference between the vertical shear forces on the side faces is compensated with a difference in the thrusts, W_c, applied to the top and bottom faces. Since shear forces for the tangential adjustments are assumed to be equal, no equilibrium against rotation about a radial line need be considered. However, the effects of small differences in shear forces, if necessary, can be accounted for with the twist adjustment.

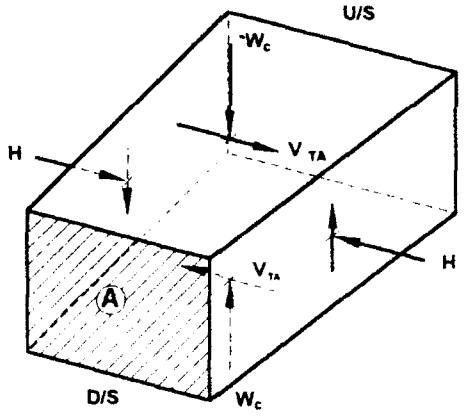

Figure 2-4 Self-balancing Loads for Tangential Adjustment

2.4.3 Adjustment for Twist

In addition to radial and tangential deflections, the arch and cantilever units must be twisted to conform to the angular deflection of one another as demonstrated in Figure 2-2. This is accomplished by applying twist loads to the arches and cantilevers to rotate them simultaneously into angular agreement. As shown in

Figure 2-5, the self-balancing loads consist of twisting moments M_{TW} and M'_{TW}, applied to the top and bottom and to the sides of volume A, respectively. To satisfy equilibrium conditions, the difference in M_{TW} is balanced by the difference between bending moment M_a applied to the sides. Similarly, the difference between M'_{TW} is balanced by a corresponding difference introduced between the bending moment M_c at the top and bottom. It should be noted that the twisting moments applied per unit of height and per unit of length must be equal for the shear stresses induced in the vertical and horizontal planes of the volume to also be equal.

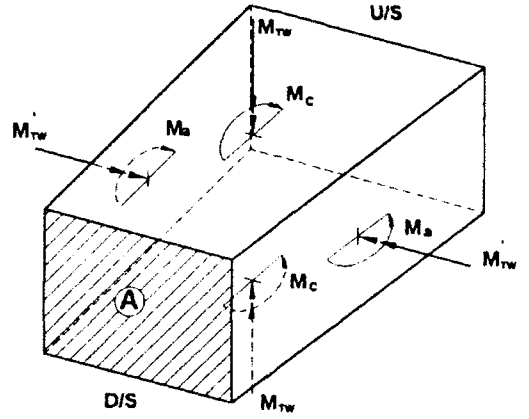

Figure 2-5 Self-balancing Loads for Twist Adjustment

2.4.4 Readjustment of Radial, Tangential, and Twist Deflections

Each adjustment described above is carried out for a set of self-balancing loads associated only with that particular adjustment, while ignoring the effects of added loads employed in the other adjustments. The past experience indicates that such procedure usually succeeds when the adjustments for separate self-balancing loads are made in the order described previously. Nevertheless, the loads applied in each succeeding adjustment will always introduce some errors which will reduce the accuracy of the adjustments already made. Such deficiencies can be corrected by making readjustments that follow the same order and procedure described for the adjustments, except in the readjustments the effects of all loads on the deflections are considered.

2.4.5 Adjustment for Poisson's Ratio

Arch thrusts applied to the volume A shorten its length in the arch direction and extend its height according to Poisson's ratio. The circumferential shortening of the arch, not being constant from face to face, influences both linear and angular deflections of the arch. Similarly, the change of shape produced by bending moments in the arch and cantilever affects the arch and cantilever deflections, but the rotations are more important in this case. Such deflections produced by the influence of Poisson's ratio may be included in the computation, if desired. This can be accomplished by computing the deflections caused by the lateral strains and including them in the readjustment calculations.

2.4.6 Effects of Foundation Deformations

Elastic deformations of the foundation supporting the arches and cantilevers of an arch dam have significant effects on the deflections and stresses developed in the dam. When included in a trial load analysis, they increase deflections of the arch and cantilever units. However, the stresses are generally reduced near the abutment and foundation regions, but may increase in the interior portion of the dam. In the trial load analysis, the effects of foundation are approximated by a series of independent springs supporting the dam. The elastic constants of these springs are determined from the Vogt's flexibility coefficients of a semiinfinite isotropic foundation as fully described by the USBR (1977).

2.5 Types of Loads

The static loads used in the trial load analysis are classified into external, internal, and unit loads.

2.5.1 External Loads

In a trial load analysis, all deflections are measured from a reference line representing the concrete-weighted position. Deflections due to concrete weight are not considered, but the resulting stresses are combined with the stresses due to other loads to obtain the total stresses in the dam. The remaining external loads to be considered include headwater, tailwater, silt, ice, and loads due to the temperature changes. All external loads, except horizontal water load, are initially applied to either arches or cantilever. In the subsequent application of trial loads,

however, external loads are appropriately redistributed between arches and cantilevers .

Vertical components of headwater, tailwater, silt, and the superstructure loads, as well as any horizontal ice and horizontal tailwater, are usually assigned to cantilevers as initial condition. Vertical deflections are usually ignored in the analysis, but contributions of these initial loads to radial deflections of cantilevers are accounted for. The effects of temperature changes are normally confined to the arches only. Temperature changes are specified at elevations of the arches and may vary linearly from face to face.

2.5.2 Internal Loads

The internal loads are the self-balancing loads used to bring the arch and cantilever units into deflection agreement without changing the total external loads applied on the dam. As described, they are always applied in pairs, one acting on the arch and the other acting on the cantilevers. Furthermore, they must be equal in magnitude and opposite in direction to satisfy the equilibrium condition.

2.5.3 Unit Loads

The unit loads are standard load patterns used in the trial load analysis to facilitate the application of external and internal loads as well as the computation of deflections. Deflections computed for these unit loads provide a convenient basis for the estimation of total deflections for various trial loads.

2.5.3.1 Unit Cantilever Loads

The unit load patterns for cantilevers are shown in Figure 2-6. Unit radial loads are triangular loads applied on the face of the cantilever in the radial direction. They vary from a unit pressure value at one arch elevation to zero pressure at the two adjacent arch elevations as shown in Figure 2-6a. It should be obvious that any radial force with linear variation between successive arch elevations can easily be represented by a combination of these unit loads. Tangential unit loads are also triangular in shape, except that they represent shear forces applied along the centerlines of the cantilevers for computing tangential deflections (Figure 2-6b). Unit twist loads are twisting moments applied to cantilevers to compute the angular movements. As shown in Figure 2-6c, unit twist loads are also triangular loads.

2.5.3.2 Unit Arch Loads

Unit load patterns, similar to those described for cantilevers, are also applied to the arches to simplify the arch analysis. The unit radial load patterns are shown in Figure 2-7a. They include a uniform load acting on the entire arch length and triangular loads with a maximum pressure at one abutment and zero pressure at the arch quarter-points. In addition, to allow for the effects of foundation movements, a concentrated shear force is also considered at the abutment.

Unit tangential loads required for the computation of tangential deflections are applied as the uniform and triangular thrusts along the arch centerlines as shown in Figure 2-7b. A concentrated unit thrust is also employed to account for the abutment movements.

Unit twist loads are also employed in the form of uniform, triangular, and concentrated loads. They are unit twisting moments applied along the arch centerlines as demonstrated in Figure 2-7c.

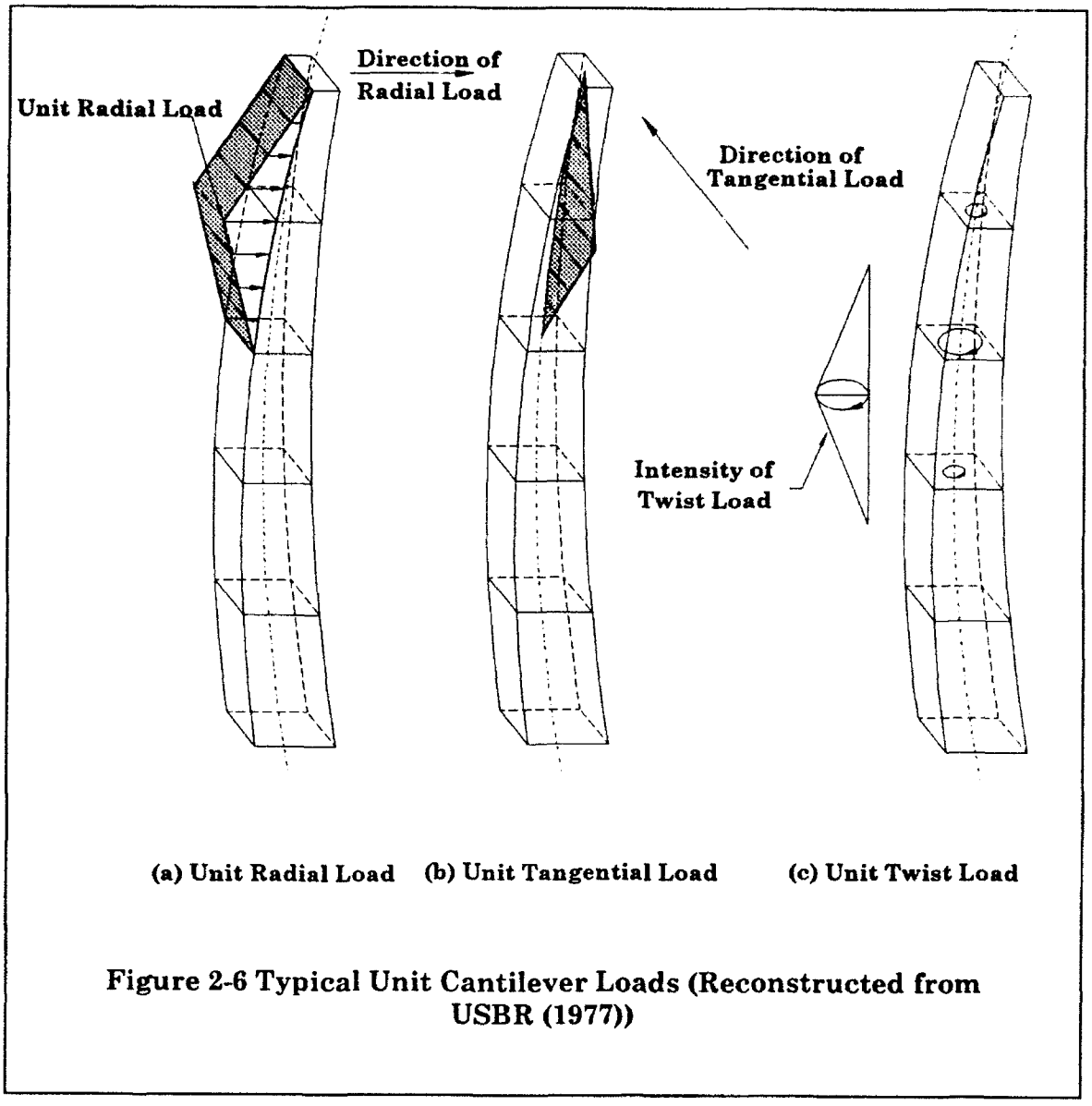

Figure 2-6 Typical Unit Cantilever Loads (Reconstructed from USBR (1977))

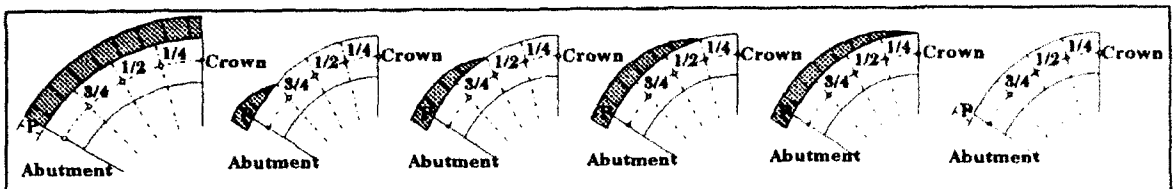

(a) Radial Load Patterns

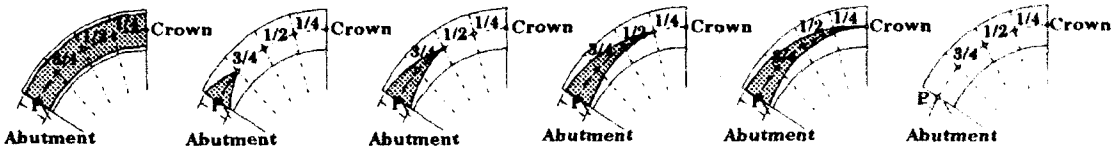

(b) Tangential Load Patterns

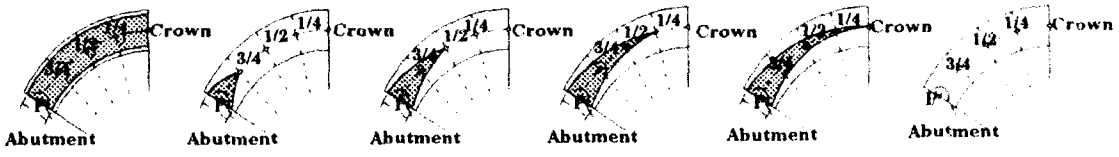

(c) Twist Load Patterns

Figure 2-7 Unit Arch Load Patterns (Reconstructed from USBR (1977))

3. FINITE ELEMENT METHOD OF ANALYSIS

3.1 Introduction

The concept of the finite element method (FEM) is very broad. The method is used in a number of different formulations and is also applied to the analysis of non-structural problems such as heat transfer, seepage, and general flow problems. The most common FEM formulation, which is widely used for the solution of practical structural systems, is the displacement-based FEM. Most general-purpose analysis programs use this formulation for its simplicity, generality, and good numerical properties (Pilkey, Saczalski, and Schaffer 1974). This manual describes only this formulation. Other formulations such as the *equilibrium, hybrid, and mixed models* that use stresses or a combination of nodal displacements and stresses as the field variables are not discussed here. Therefore, in this manual, the term "finite element method" (FEM) implies "displacement-based finite element method" for the analysis of structural systems.

The FEM is a numerical method of analysis by which a structure such as an arch dam is idealized as an assemblage of subdivisions (finite elements), interconnected at a discrete number of nodal points having a finite number of unknowns (Figure 3-1). The displacements of these nodal points located at the boundaries of each finite element represent the basic unknown variables. The behavior of each finite element is approximated by a set of assumed functions which represent displacements within the element region in terms of the element nodal displacements. These displacement functions are often in a form that ensures continuity among adjacent elements and, therefore, throughout the complete structure. With displacements being known at all points within the element, the strains at any point will also be available in terms of the nodal displacements. These strains, together with any initial strains and the stress-strain relationship of the material, will define the state of stresses throughout the element and its boundaries. Using the strain-displacements and stress-displacements relationships, the stiffness of each element can be obtained by satisfying the force-equilibrium condition between a system of equivalent nodal forces with the boundary stresses and any distributed load acting on the element.

Finally, the equilibrium equations for the entire system are obtained by combining the individual elements in a manner which satisfies the conditions of equilibrium and compatibility at the junctions of these elements. The equilibrium equations,

which are essentially a system of algebraic equations, are solved using numerical methods.

3.2 General Formulation of FEM

The finite element procedure outlined in the previous paragraph is presented here in mathematical form. The general finite element discretization procedure and derivation of equilibrium equations are summarized in this section (Zienkiewicz 1971, Bathe and Wilson 1976). A three-dimensional (3-D) finite element, such as that used in Figure 3-1, is considered, and the element displacements, strains, stresses, and stiffness properties are derived.

3.2.1 Displacement Functions

The basic assumption of the displacement-based finite element analysis is that the displacements within the entire system **u** can be expressed in terms of element interpolation functions **N** and the vector of nodal displacements **U**:

$$\{\mathbf{u}\} = [\mathbf{N}]\{\mathbf{U}\} \tag{3.1}$$

The most important feature of the method is that the interpolation functions are applied separately to each element m thus:

$$\{\mathbf{u}\}^m = [\mathbf{N}]^m\{\mathbf{U}\}^m = \left[N_i, N_j, N_k, \cdots\right]\begin{Bmatrix} U_i \\ U_j \\ U_k \\ \vdots \end{Bmatrix} \tag{3.2}$$

where m indicates that each quantity is referred to element "m" only

The interpolation functions $\mathbf{N_i}$, $\mathbf{N_j}$, $\mathbf{N_k}$ are described in Sections 5.1, 5.2, and 5.3, but in general, they satisfy the following relationships:

$$\mathbf{N}_i^m(x_i, y_i, z_i) = \mathbf{I}$$
$$\mathbf{N}_i^m(x_j, y_j, z_j) = \mathbf{N}_i^m(x_k, y_k, z_k) = 0$$

3.2.2 Strains

With displacements known at all points, the strains at any point can be obtained by appropriate differentiation of the assumed displacements. The strains in matrix notation are given by:

$$\{\varepsilon\} = [\mathbf{B}]\{\mathbf{U}\} \tag{3.3}$$

For a 3-D problem, the six strain components are defined as follows (Timoshenko and Goodier 1970):

$$\{\varepsilon\} = \begin{Bmatrix} \varepsilon_x \\ \varepsilon_y \\ \varepsilon_z \\ \gamma_{xy} \\ \gamma_{yz} \\ \gamma_{zy} \end{Bmatrix} = \begin{Bmatrix} \frac{\partial u}{\partial x} \\ \frac{\partial v}{\partial y} \\ \frac{\partial w}{\partial z} \\ \frac{\partial u}{\partial y} + \frac{\partial v}{\partial x} \\ \frac{\partial v}{\partial z} + \frac{\partial w}{\partial y} \\ \frac{\partial w}{\partial x} + \frac{\partial u}{\partial z} \end{Bmatrix} \tag{3.4}$$

The element strain interpolation function matrix [B] is easily obtained by combining Equations 3.2 and 3.4.

3.2.3 Stresses

The stresses in a finite element are related to the element strains using the material constitutive law and are given by:

$$\{\sigma\} = [\mathbf{D}]\{\varepsilon\} + \{\sigma_0\} \tag{3.5}$$

where [D] = the elasticity matrix

$\{\sigma_0\}$ = the element initial stresses

The material law stated in [D] for each element can be arbitrary. However, isotropic material properties are used in most cases, and orthotropic material properties are applied to special situations (Malvern 1969).

3.2.4 Loads

The external loads acting on a general 3-D body are surface tractions $\mathbf{f}^S$, body forces $\mathbf{f}^B$, and concentrated forces $\mathbf{F}^I$. These forces, in general, consist of three components corresponding to the three coordinate axes:

$$\left\{\mathbf{f}^B\right\} = \begin{bmatrix} f_X^B \\ f_Y^B \\ f_Z^B \end{bmatrix} \; ; \; \left\{\mathbf{f}^S\right\} = \begin{bmatrix} f_X^S \\ f_Y^S \\ f_Z^S \end{bmatrix} \; ; \; \left\{\mathbf{F}^I\right\} = \begin{bmatrix} F_X^I \\ F_Y^I \\ F_Z^I \end{bmatrix} \tag{3.6}$$

3.2.5 Element Stiffness

The simplest approach to obtain the stiffness matrix for a finite element is to use the *principle of virtual displacements* (Zienkiewicz 1971, Bathe and Wilson 1976). This principle states that the equilibrium of the body requires that for any kinematically compatible small virtual displacements imposed onto the body, the total internal virtual work be equal to the total external virtual work, thus:

$$\int_V \varepsilon^T \sigma dV = \int_V \mathbf{U}^T \mathbf{f}^B dV + \int_S \mathbf{U}^S \mathbf{f}^S dS + \sum_I U^T F^I \tag{3.7}$$

The left-hand side of Equation 3.7 corresponds to internal work. It is equal to the actual stresses σ going through the virtual strains ε that correspond to the imposed virtual displacements **U**. Substituting Equations 3.3 and 3.5 in the left-hand side of Equation 3.7, the finite element stiffness matrix expressed in terms of element nodal degrees of freedom (DOF) $\{\mathbf{U}\}^m$ is obtained:

$$[\mathbf{k}]^m = \int_{V^m} \left[[\mathbf{B}]^T [\mathbf{D}][\mathbf{B}]\right]^m dV^m \tag{3.8}$$

The right-hand side of Equation 3.7 is equal to work done by the actual element forces $\mathbf{f}^B$, $\mathbf{f}^S$, and $\mathbf{F}^i$ going through the virtual displacements {U} and will lead to equivalent nodal forces.

3.2.6 Equilibrium Equations

The virtual work of Equation 3.7 is easily applied to an entire structure, approximated as an assemblage of discrete finite elements. This is accomplished by rewriting Equation 3.7 as a sum of integrations over the volume and areas of all finite elements and assuming that the displacements within each element are expressed in terms of the nodal displacements of the entire structure, i.e.;

$$\sum_m \int_V \left[\varepsilon^T \sigma dV\right]^m = \sum_m \int_V \left[\mathbf{U}^T \mathbf{f}^B dV\right]^m + \sum_m \int_S \left[\mathbf{U}^S \mathbf{f}^S dS\right]^m + \sum_i U'^T F' \qquad (3.9)$$

where $m = 1, 2, \ldots, N$

N = number of finite elements

One important feature to note is that the integrations are performed separately for each element, and, thus, local element coordinates may be used for convenience. This will be discussed further in Section 5.1, 5.2, and 5.3. Substituting element displacements, strains, and stresses in Equation 3.9, we obtain:

(3.10)

$$\begin{aligned}\mathbf{U}^T \left\{\sum_m \int_{V^m} \left[[\mathbf{B}]^T [\mathbf{D}][\mathbf{B}] dV\right]^m\right\} \mathbf{U} = {} & \mathbf{U}^T \left\{\sum_m \int_{V^m} \left[[\mathbf{N}]^T \{\mathbf{f}^B\} dV\right]^m\right\} \\ & + \mathbf{U}^T \left\{\sum_m \int_{S^m} \left[\left[\mathbf{N}^S\right]^T \{\mathbf{f}^S\} dS\right]^m\right\} \\ & - \mathbf{U}^T \left\{\sum_m \int_{S^m} \left[[\mathbf{B}]^T \sigma' dV\right]^m\right\} \\ & + \mathbf{U}^T \mathbf{F}\end{aligned}$$

where **F** is now a vector of nodal forces applied at the nodal points of the assembled structure

By imposing unit virtual displacements $\mathbf{U}^T = \mathbf{I}$, the familiar static equilibrium equations of the element assemblage is obtained:

$$\mathbf{k}\,\mathbf{u} = \mathbf{p} \tag{3.11}$$

where

$$\mathbf{p} = \mathbf{p}_B + \mathbf{p}_S - \mathbf{p}_I + \mathbf{p}_C \tag{3.12}$$

The matrix **k** is the stiffness of the complete structure and is equal to the left-hand side of Equation 3.10. The load vector **p** includes the effects of element body forces, surface forces, initial stresses, and concentrated loads.

Furthermore, the element inertia and damping forces can be included as part of the body forces to represent dynamic behavior of the system. Approximating the element accelerations and velocities by the same interpolation functions as in Equation 3.2, gives:

$$\mathbf{p}_B = \sum_m \int_{V^m} \left[[\mathbf{N}]^T \left[\{\mathbf{f}^B\} - \rho \mathbf{N}\ddot{\mathbf{u}} - \lambda \mathbf{N}\dot{\mathbf{u}} \right] dV \right]^m \tag{3.13}$$

where $\dot{\mathbf{u}}$ and $\ddot{\mathbf{u}}$ = vectors of nodal velocities and accelerations

ρ = mass density

λ = damping parameter of the element m

Thus, equilibrium equations of the entire structure for a dynamic case are given by:

$$\mathbf{m}\ddot{\mathbf{u}} + \mathbf{c}\dot{\mathbf{u}} + \mathbf{k}\mathbf{u} = \mathbf{p} \tag{3.14}$$

where **m** and **c** are mass and damping matrices of the structure, respectively

In practice, however, damping parameters are not defined for individual elements. Rather, the matrix **c** is approximated using the mass and stiffness matrices of the complete structure.

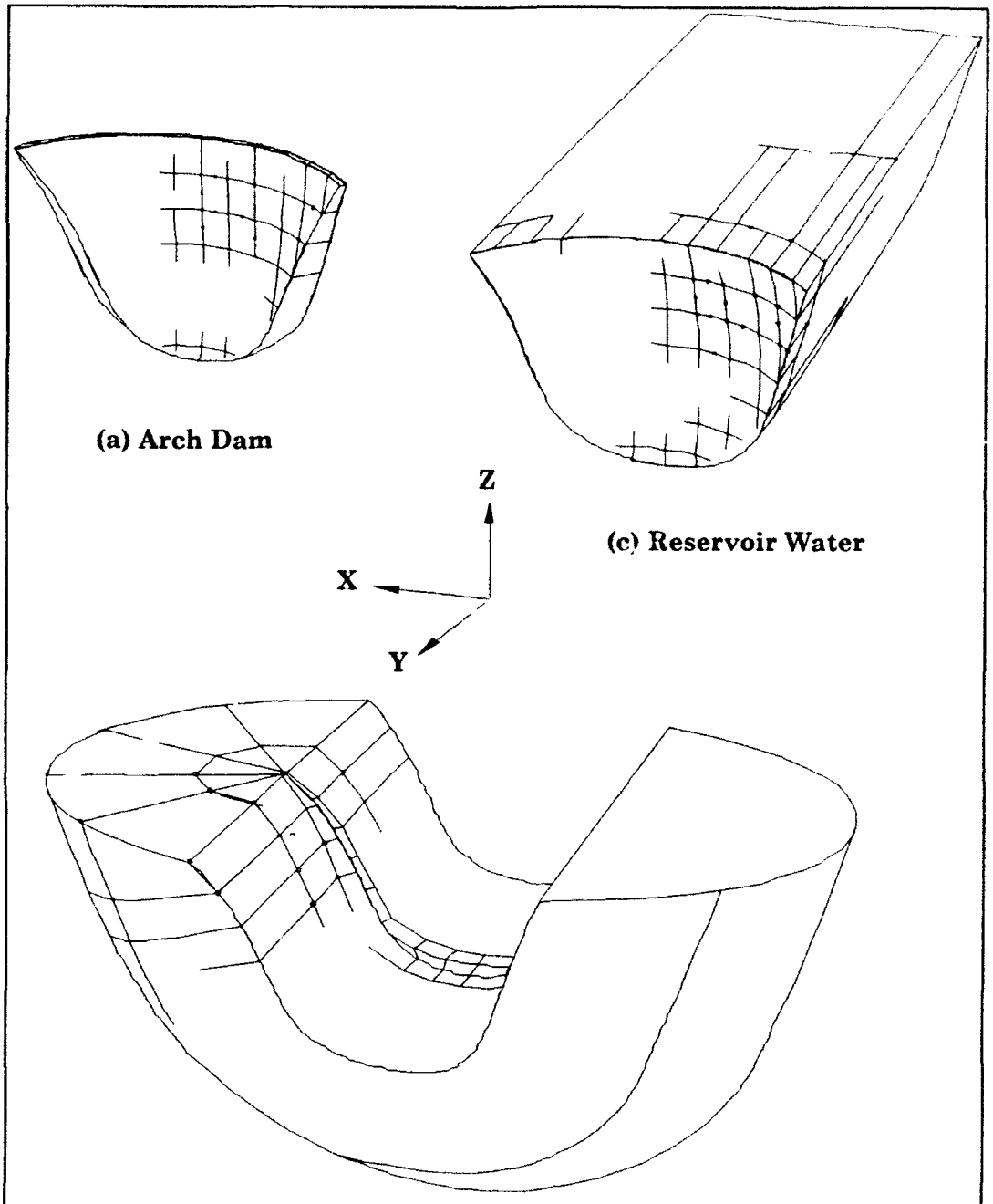

Figure. 3.1 Dam, Foundation Rock, and Reservoir Water Divided into Finite Elements

4. SYSTEM IDEALIZATION

4.1 Introduction

The standard finite element formulation previously presented is applicable to analysis of arch dams, but certain simplified assumptions are needed before the method can be implemented. Arch dams are distinguished from other problems in structural dynamics by their complex geometry as dictated by the canyon shape and by significant interaction with the impounded water and the foundation rock (Chopra 1988). The analysis of arch dams is especially complicated for seismic effects because they must be treated as 3-D systems consisting of the concrete arch, the reservoir water, and the foundation rock (Figure 4-1). The finite element discretization of each component under the assumption of linear elastic behavior is described in the following section.

4.2 Arch Dam

Arch dams are constructed as a system of monolithic blocks separated by vertical joints. The joints are later grouted under high pressure to form a complete monolithic structure in compression (USBR 1977). These joints, however, can take little or no tension and may open under severe winter temperature loading conditions or when subjected to intense earthquake ground motions. Such nonlinear joint opening or slippage is not considered in the linear-elastic analysis, because arch dams are assumed to be monolithic structures.

Using the standard finite element discretization procedure, the monolithic arch structure is idealized as an assemblage of finite elements of appropriate shapes and types. In principle, any reasonably accurate 3-D element and mesh arrangement may be used. In practice, however, isoparametric solid and shell elements of the types included in the GDAP program (Ghanaat 1993) are best suited for the analysis of arch dams. The curved surfaces of an arch dam are directly represented by curved isoparametric elements, and element matrices are conveniently evaluated with respect to the local coordinates of each element. The isoparametric element formulations of several finite elements are discussed in Chapter 5.

The finite element mesh of an arch dam may be defined by specifying spatial coordinates of arbitrary nodal points, but it is more appropriate to arrange the element mesh mathematically. It is obvious that all the element exterior nodes that

are also defined mathematically must lie on the upstream and downstream surfaces of the dam. The element nodes on the surfaces of the dam, if arranged on a grid of vertical and horizontal lines, would appropriately relate to the arches and cantilevers of the trial load procedure described in Chapter 2. This discretization procedure is the technique that has been adopted in GDAP for the automatic mesh generation of arch dams of arbitrary geometries (Ghanaat 1993). Figure 4-1 is an example of an arch dam model generated by GDAP. Thick-shell elements were used in the interior regions of the dam, and the regions near the abutments were modeled by 3-D shell elements (see Section 5.2) which also provided an easy connection between the thick-shell elements of the dam and the solid elements of the foundation rock. Guidelines regarding the size of the dam mesh are presented in the EM 1110-2-2201, "Arch Dam Design."

4.3 Foundation Rock

Ideally, a foundation model should include the significant geological features of the rock and should also extend to a distance at which the interaction with the dam becomes negligible. It is generally impossible to account for all the discontinuities in the rock in a realistic manner because geological data of the underlying rock are not available or require as much judgment as measurement to obtain and also because the foundation must be analyzed under the assumptions of anisotropy and nonlinear behavior for the rock. A foundation model which extends to infinity or extends to finite distance, but includes wave-transmitting boundaries, is also not possible because appropriate analytical procedures for such models are not available. Another important factor is that it is virtually impossible to define free-field motions at the dam-foundation contact points, because neither realistic analytical procedures nor sufficient recorded data are available.

For these reasons, an extremely simple idealization of the deformable foundation rock is commonly used in practical applications (Clough 1980). Specifically, an appropriate portion of the deformable foundation rock is idealized as part of the arch dam finite element model which only includes the flexibility of the foundation rock. Thus, the inertial and damping effects of the foundation rock are ignored in the dynamic analysis. Linearly elastic material properties are assumed, but the effects of geology are partially accounted for by using the modulus of deformation rather than the modulus of elasticity of the rock.

As shown in Figure 4-1, the foundation rock supporting the arch dam is represented as an assemblage of 3-D solid elements and is constructed on semicircles drawn on planes cut into the canyon walls and oriented normal to the rock-concrete interface. The geometry of the foundation rock model may be assumed arbitrarily, but should match the finite element meshes of the dam at the dam-foundation contact, and should extend to sufficiently large distances in all directions from the contact surface at the base of the dam. For practical purposes, the foundation models of GDAP are especially useful because they are generated automatically and include different degrees of mesh refinement. Guidelines for selecting an appropriate size for the foundation rock model are given in the EM 1110-2-2201, "Arch Dam Design."

4.4 Impounded Water

Interaction between the impounded water and an arch dam has a significant effect on earthquake response of the dam and should be considered in the analysis. This interaction is influenced by the reservoir geometry and the energy absorption of the reservoir bottom. A reservoir behind an arch dam may extend a great distance in the upstream direction. The geometry of a reservoir is usually of a complicated shape, depending on the topography of the site. The energy absorption at the reservoir bottom is affected by the bottom geological conditions for which no measured data are available.

Currently, three procedures are available for idealization of the impounded water. They vary from a simple reservoir model based on the Westergaard added-mass, to a more advanced idealization which considers a more realistic dam-reservoir interaction mechanism.

4.4.1 Generalized Westergaard Model

The simplest and least refined reservoir idealization is an extension of the Westergaard formulation (Westergaard 1933). This approach, also known as the *Generalized Westergaard Method* (Clough 1977), employs the same added-mass concept introduced by Westergaard for the incompressible reservoirs. However, unlike the standard method, the *Generalized Westergaard Method* takes account of the dam curvature and its flexibility by assuming that hydrodynamic pressure at any point on the upstream face of the dam is proportional to the *total* acceleration acting *normal* to the dam at that point. This approach is available in the program GDAP as an option and is computationally efficient, because finite element

discretization of the fluid domain is not required. But the method only provides a rough estimate of the hydrodynamic forces acting on the face of an arch dam, and its use should be limited to the feasibility or preliminary studies.

4.4.2 Incompressible Reservoir Model

If water compressibility is ignored, interaction effects of the impounded water can be represented by an equivalent added-mass matrix. To compute the added-mass matrix, reservoir water is idealized as an assemblage of incompressible liquid elements using a finite element formulation (Zienkiewicz 1971, Kuo 1982). In general, any complicated reservoir geometry can be represented by the finite element discretization, but a prismatic model extending to a finite distance in the upstream direction is sufficient for practical purposes (Figure 4-1). The effects of surface waves are usually ignored, and, thus, pressures at the free surface are assumed to be zero. At other reservoir boundaries, the acceleration boundary conditions are satisfied by establishing proportionality between the pressure gradient and the normal component of acceleration.

The INCRES program, a module of GDAP (Ghanaat 1993), computes the incompressible added-mass matrix using the finite element procedure. However, it ignores accelerations at the reservoir floor and at the upstream section by assuming them to be rigid. Previous studies show that assuming zero accelerations at the upstream boundary will have very little or no effect on the incompressible added mass. Also, if the upstream reach of the reservoir model is at least three times the water depth (Clough et al. 1984 (Apr)(Nov)), then the reservoir motions beyond this distance are essentially zero. The implication of zero accelerations at the reservoir floor is that earthquake ground motions are not applied to the reservoir bottom, and, thus, their effects on the hydrodynamic pressures exerted on the dam are ignored. It is not known how much this would influence the dam response, but this reservoir model would be more effective if the earthquake ground motions were applied to the reservoir floor adjacent to the dam (Clough and Chang 1987).

4.4.3 Compressible Reservoir Model

Recent studies of Morrow Point Dam show that water compressibility can be important for the interaction between the dam and reservoir, as determined by field measurements (Duron and Hall 1988) and by analytical procedures (Fok and

Chopra 1985). When water compressibility is considered, interaction between the dam and impounded water requires a solution in the frequency domain. One effective approach (Fok and Chopra 1985) is to idealize the fluid domain as a finite region adjacent to the dam connected to a prismatic body of water extending to infinity; this provides for proper transmission of pressure waves in the upstream direction. The finite region is represented as an assemblage of liquid finite elements (similar to the incompressible case), while the infinite region is treated as an assemblage of subchannels of infinite length for which a continuum solution is available. Furthermore, this analytical procedure allows for the energy loss into the reservoir floor by assuming absorptive boundaries. The dissipation of energy into the reservoir boundaries is characterized by the wave reflection coefficient, α, which is the ratio of the amplitude of the reflected to the amplitude of the incident pressure wave.

The interaction effects of compressible water depend on the dam and reservoir geometries and are influenced by the α factor and the characteristics of the earthquake ground motions. Such elaborate analysis may not be necessary for all dams, especially when the fundamental resonant frequency of the reservoir is greater than the fundamental frequency of the dam with an empty reservoir by at least a factor of 2. For relatively high dams, when strong coupling exists between the dam and the impounded water, compressibility of water may be considered but several analyses based on different values of the α factor may be required.

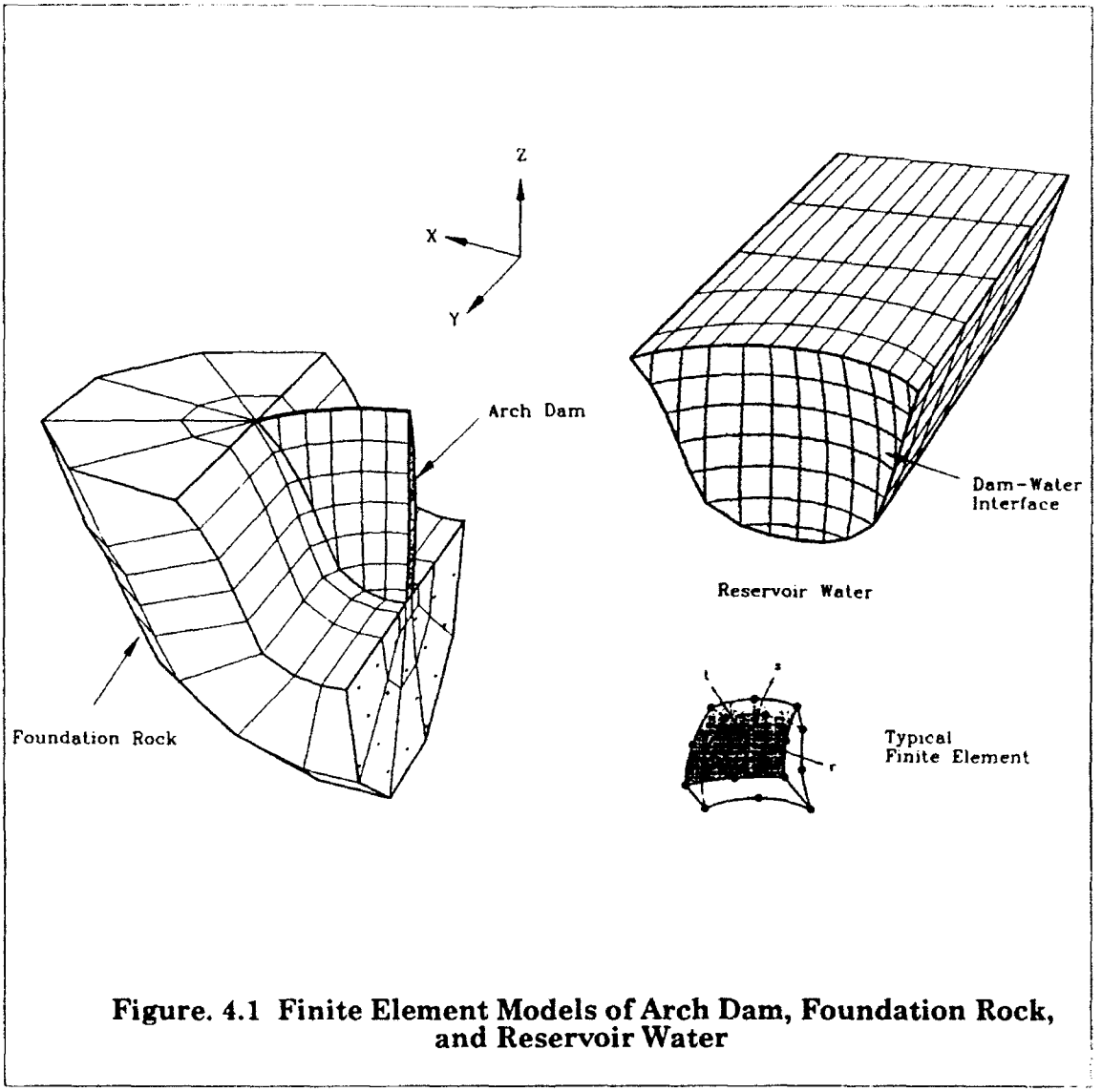

Figure. 4.1 Finite Element Models of Arch Dam, Foundation Rock, and Reservoir Water

5. ISOPARAMETRIC ELEMENT FORMULATION

5.1 Introduction

In this section another very important aspect of the finite element analysis, i.e. formulation of element matrices, is presented, and several elements especially developed for the analysis of arch dams are described.

Finite elements most appropriate for the analysis of arch dams are of the *isoparametric* family for which both the element coordinates and element displacements are defined using the same (*iso-*) parameters or interpolation functions (Zienkiewicz 1971, Bathe and Wilson 1976). They are constructed by mapping a nondimensionalized rectangular element with a specified number of nodes into the actual curved-surface element in the manner shown in Figures 5-1 through 5-4. The element transformation is carried out using interpolation functions that are conveniently defined in the natural coordinate system.

5.2 Eight-Node Solid Elements

The standard eight-node solid element is a linear-displacement isoparametric element developed by Zienkiewicz (Zienkiewicz 1971). A refined version of this element included in GDAP (Ghanaat 1993) uses incompatible deformation modes (Ghaboussi, Wilson, and Taylor 1971) for improved bending behavior. Both isotropic and orthotropic material properties can be specified. This element is used to model the foundation rock or thick section of gravity arch dams.

Element Geometry. Figure 5-1 shows the eight-node solid element. The element geometry is described in terms of the nodal coordinates using the following isoparametric relationship:

$$\mathbf{X} = \sum_{i=1}^{8} N_i X_i \; ; \quad \mathbf{Y} = \sum_{i=1}^{8} N_i Y_i \; ; \quad \mathbf{Z} = \sum_{i=1}^{8} N_i Z_i \qquad (5.1)$$

where X, Y, Z = global coordinates at any point within the element
X_i, Y_i, Z_i = coordinates of node i

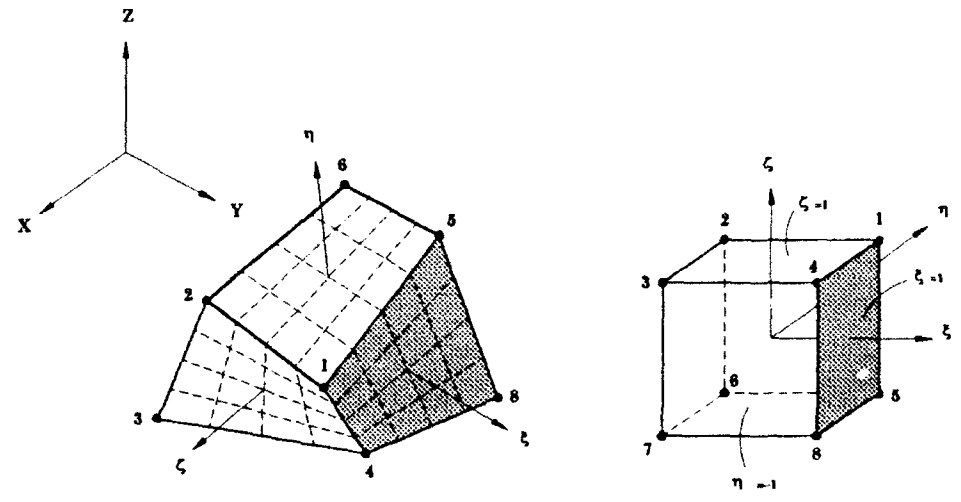

(a) Local and Global Coordinate System (b) Natural Coordinate System

Figure 5-1 Eight-Node Solid Element

The interpolation functions are specified in the natural coordinate system:

$$N_i = \tfrac{1}{8}(1+\xi_i\xi)(1+\eta_i\eta)(1+\zeta_i\zeta) \qquad i = 1,2,\cdots,8 \tag{5.2}$$

where ξ_i , η_i, ζ_i are +1 or -1 and represent the coordinates of node i

Element Displacements. Displacement approximation of the modified eight-node element includes three additional terms in each direction and the total expansion is of the form:

$$\begin{aligned}
\mathbf{u} &= \sum_{i=1}^{8} N_i u_i + N_9 q_1 + N_{10} q_2 + N_{11} q_3 \\
\mathbf{v} &= \sum_{i=1}^{8} N_i v_i + N_9 q_4 + N_{10} q_5 + N_{11} q_6 \\
\mathbf{w} &= \sum_{i=1}^{8} N_i w_i + N_9 q_7 + N_{10} q_8 + N_{11} q_9
\end{aligned} \tag{5.3}$$

where

$$N_9 = (1-\xi^2); \quad N_{10} = (1-\eta^2); \quad N_{11} = (1-\zeta^2)$$

The displacement amplitudes q_i are additional DOF's that may be visualized as displacements of midedge nodes that are eliminated by static condensation in the subsequent analysis operations.

Element Stiffness Matrix. The element stiffness corresponding to the natural coordinate system shown in Figure 5.1b is:

$$[\mathbf{k}] = \int_{-1}^{1}\int_{-1}^{1}\int_{-1}^{1} [\mathbf{B}]^T [\mathbf{D}][\mathbf{B}] \mathbf{detJ}\, d\xi d\eta d\zeta \tag{5.4}$$

where matrices [B] and [D] are defined in Equations 3.3 and 3.5, and detJ is the determinant of the Jacobian operator. The Jacobian operator which relates the natural coordinate derivatives to the local coordinate derivatives is given by

$$\mathbf{J} = \begin{bmatrix} \partial x/\partial\xi & \partial x/\partial\eta & \partial x/\partial\zeta \\ \partial y/\partial\xi & \partial y/\partial\eta & \partial y/\partial\zeta \\ \partial z/\partial\xi & \partial z/\partial\eta & \partial z/\partial\zeta \end{bmatrix} \tag{5.5}$$

Element Mass Matrix. Mass matrix for an eight-node solid element can be obtained from the inertia forces given in Equation 3.13. The mass matrix expressed in the natural coordinate system is:

$$[\mathbf{m}] = \rho \int_{-1}^{1}\int_{-1}^{1}\int_{-1}^{1} [\mathbf{N}]^T [\mathbf{N}] \mathbf{detJ}\, d\xi d\eta d\zeta \tag{5.6}$$

This is called the *consistent mass* matrix because the interpolation functions used here are the same as were used in the evaluation of the stiffness matrix. The consistent mass formulation requires more computer effort than does a simple lumped mass matrix but provides greater accuracy and is more appropriate for the analysis of arch dams.

Element Surface Loads. Surface loads included in the eight-node element are hydrostatic water and silt pressures; uniform pressure distributions can also be

specified. The nodal forces due to distributed surface pressures are obtained from Equation 3.10 and, in the natural coordinate system, are given by:

$$\{\mathbf{R}_S\} = \int_{-1}^{1}\int_{-1}^{1} [\mathbf{N}^S]^T \{\mathbf{f}^S\} \mathbf{detJ}\, d\xi d\eta \tag{5.7}$$

where $[\mathbf{N}^S]$ are interpolation functions corresponding to the surface on which pressures $\{\mathbf{f}^S\}$ are acting

Element Loads Due to Initial Strains. The initial strains due to the temperature changes in the element are given by:

$$\varepsilon_0 = [\beta_x \theta, \beta_y \theta, \beta_z \theta, 0, 0, 0]^T \tag{5.8}$$

where β_x, β_y, β_z = coefficients of thermal expansion in the x, y, and z directions

θ = temperature change from the stress-free state

For an isotropic material, coefficients of thermal expansion are the same in all directions. The temperature changes at any point within the element are obtained from the nodal temperature values using the displacement interpolation functions given in Equation 5.2:

$$\theta = \sum_{i=1}^{8} N_i \theta_i \tag{5.9}$$

The vector of initial nodal forces is obtained by substituting $\mathbf{e}_0$ in Equation 3.10 and expressing the integration in the natural coordinate system:

$$\{\mathbf{R}_i\} = \int_{-1}^{1}\int_{-1}^{1}\int_{-1}^{1} [\mathbf{B}]^T [\mathbf{D}] \{\beta\} \theta \mathbf{detJ}\, d\xi d\eta d\zeta \tag{5.10}$$

Numerical Integration of Element Matrices. The element matrices presented in integral forms must be evaluated numerically. The numerical integrations are most effectively obtained using Gauss quadrature scheme (Zienkiewicz 1971). For example numerical integration of the element stiffness is given by:

$$\mathbf{k} = \sum_i \sum_j \sum_k w_i w_j w_k \mathbf{B}^T(\xi_i, \eta_j, \zeta_k)\mathbf{D}\mathbf{B}(\xi_i, \eta_j, \zeta_k) \qquad (5.11)$$

where w_i, w_j, w_k = weight factors for the integration points corresponding to ξ_i, η_j, ζ_k

The number of Gauss integration points used to evaluate a specific element matrix depends on the order of the function to be integrated. For eight-node solid elements, two integration points in each direction are usually used.

5.3 Three-Dimensional Shell Elements

The eight-node element described is the simplest 3-D element in the isoparametric family. It can be extended to more refined elements by assuming higher order interpolation functions and expressing them in terms of an appropriately increased number of nodal points. The 3-D shell element shown in Figure 5-2 is such an element. It is a 16-node, curved solid element which uses quadratic displacement and geometry interpolation functions on two faces and linear interpolation functions through the thickness (Ghaboussi, Wilson, and Taylor 1971). The element also includes incompatible deformation modes to improve the bending behavior and thus its accuracy. This element has been very effective in the analysis of arch dams, and usually one element in the thickness direction is adequate.

Element Geometry. Figure 5-2 shows the 16-node shell element in the natural, local, and global coordinate systems. The element geometry is expressed in terms of the nodal coordinates through a set of interpolation functions:

$$\mathbf{X} = \sum_{i=1}^{16} N_i X_i \; ; \quad \mathbf{Y} = \sum_{i=1}^{16} N_i Y_i \; ; \quad \mathbf{Z} = \sum_{i=1}^{16} N_i Z_i \qquad (5.12)$$

where

$$
\begin{aligned}
N_1 &= \tfrac{1}{8}(1+\xi)(1+\eta)(1+\zeta)(\xi+\eta-1)\\
N_2 &= \tfrac{1}{8}(1-\xi)(1+\eta)(1+\zeta)(-\xi+\eta-1)\\
N_3 &= \tfrac{1}{8}(1-\xi)(1-\eta)(1+\zeta)(-\xi-\eta-1)\\
N_4 &= \tfrac{1}{8}(1+\xi)(1-\eta)(1+\zeta)(\xi-\eta-1)\\
N_5 &= \tfrac{1}{8}(1+\xi)(1+\eta)(1-\zeta)(\xi+\eta-1)\\
N_6 &= \tfrac{1}{8}(1-\xi)(1+\eta)(1-\zeta)(-\xi+\eta-1)\\
N_7 &= \tfrac{1}{8}(1-\xi)(1-\eta)(1-\zeta)(-\xi+\eta-1)\\
N_8 &= \tfrac{1}{8}(1+\xi)(1-\eta)(1-\zeta)(\xi+\eta-1)\\
N_9 &= \tfrac{1}{4}(1-\xi^2)(1+\eta)(1+\zeta)\\
N_{10} &= \tfrac{1}{4}(1-\xi)(1-\eta^2)(1+\zeta)\\
N_{11} &= \tfrac{1}{4}(1-\xi^2)(1-\eta)(1+\zeta)\\
N_{12} &= \tfrac{1}{4}(1+\xi)(1-\eta^2)(1+\zeta)\\
N_{13} &= \tfrac{1}{4}(1-\xi^2)(1+\eta)(1-\zeta)\\
N_{14} &= \tfrac{1}{4}(1-\xi)(1-\eta^2)(1-\zeta)\\
N_{15} &= \tfrac{1}{4}(1-\xi^2)(1-\eta)(1-\zeta)\\
N_{16} &= \tfrac{1}{4}(1+\xi)(1-\eta^2)(1-\zeta)
\end{aligned}
$$

Element Displacements. The displacements within the element are approximated by:

$$
\begin{aligned}
\mathbf{u} &= \sum_{i=1}^{16} N_i u_i + N_{17}q_1 + N_{18}q_2 + N_{19}q_3 + N_{20}q_4 + N_{21}q_5\\
\mathbf{v} &= \sum_{i=1}^{16} N_i v_i + N_{17}q_6 + N_{18}q_7 + N_{19}q_8 + N_{20}q_9 + N_{21}q_{10}\\
\mathbf{w} &= \sum_{i=1}^{16} N_i w_i + N_{17}q_{11} + N_{18}q_{12} + N_{19}q_{13} + N_{20}q_{14} + N_{21}q_{15}
\end{aligned}
\qquad (5.13)
$$

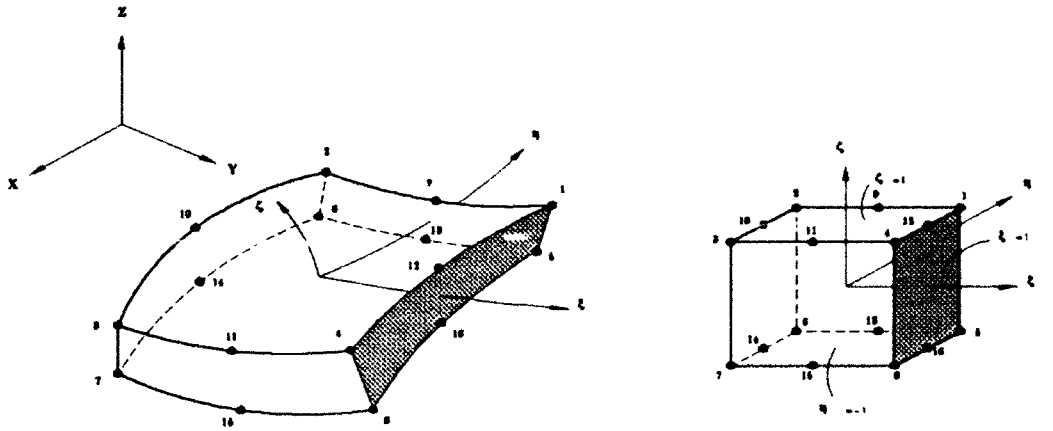

(a) Local and Global Coordinate Systems

(b) Natural Coordinate System

Figure 5-2 Three-Dimensional Shell Element

where

$$N_{17} = \xi(1-\xi^2); \quad N_{18} = \eta(1-\eta^2); \quad N_{19} = \zeta(1-\zeta^2)$$
$$N_{20} = \xi\eta(1-\xi^2); \quad N_{21} = \eta\xi(1-\eta^2)$$

An important feature of the element is that any midside node can be eliminated by introducing a kinematic constraint along that side. This is done by assuming that the side remains straight during the element deformation, and, thus, the midside displacements can be expressed in terms of the corresponding corner displacements. This feature permits a 16-node shell element to be attached to an 8-node solid element used in the foundation while maintaining displacement compatibility.

Element Matrices. The stiffness matrix, consistent mass matrix, and the nodal load vectors for 16-node shell elements are obtained using the procedures outlined. All matrix integrals are evaluated numerically using the Gauss quadrature procedure. The integrals are evaluated exactly using a 3 × 3 Gauss integration in the surface direction combined with 2 points through the thickness, i.e. a total of 18 points for the element. The temperature changes within the element are related to nodal

temperature values, using the same quadratic interpolations on two faces and linear interpolations through the thickness.

5.4 Thick-Shell Elements

Another specialized element for the analysis of shell structures such as an arch dam is the thick-shell element included in GDAP. This element is based on an isoparametric formulation using quadratic displacement and geometry variations in the surface directions and linear variation through the thickness. However, the surface nodes are reduced to only eight nodes lying on the midsurface, half-way between the corresponding surface nodes (Pawsey 1970). Each node on the midsurface has five DOF's, three translations in the global directions, and two rotations about two axes perpendicular to the midsurface normal (Figure 5-4). The sixth DOF, associated with the change of thickness of the element, is replaced by a zero stress condition ($\sigma_{nn} = 0$) in the normal direction. The element also uses a reduced integration scheme which excludes the excessive shear strain energy in the stiffness matrix and, thus, improves the bending behavior. The resulting element provides an efficient tool for representing the shell behavior of an arch dam. It permits for a significant transverse shear distortion and is applicable to both moderately thick and thin arch dams.

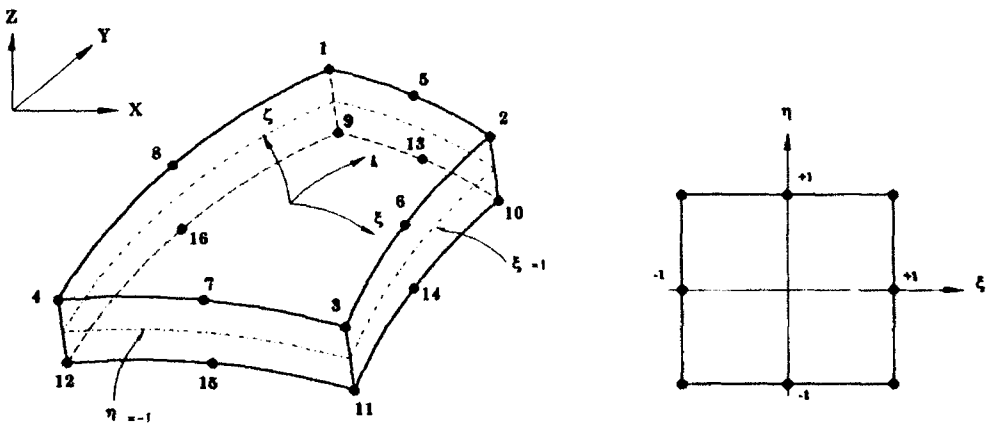

(a) Local and Global Coordinate Systems

(b) Natural Coordinate System

Figure 5-3 Curved Thick-Shell Element

Element Geometry. The geometry of the element surfaces are defined by 16 nodal points, 8 on each curved surface (Figure 5-3). The coordinates of any point within the element are described in terms of the midsurface coordinates and a vector connecting the two upper and lower points, as shown in Figure 5-4:

$$\begin{Bmatrix} X \\ Y \\ Z \end{Bmatrix} = \sum_i N_i \begin{Bmatrix} X_i \\ Y_i \\ Z_i \end{Bmatrix}_{mid.} + \sum_i N_i \frac{\zeta}{2} V_{3i} \qquad (5.14)$$

where

$$V_{3i} = \begin{Bmatrix} X_i \\ Y_i \\ Z_i \end{Bmatrix}_{up} - \begin{Bmatrix} X_i \\ Y_i \\ Z_i \end{Bmatrix}_{down}$$

The interpolation functions N_i are the standard quadratic functions of a two-dimensional (2-D) element and are defined with respect to the natural coordinate system shown in Figure 5-3b:

(5.16)

$$\begin{aligned}
N_1 &= \tfrac{1}{4}(1-\xi)(1+\eta) - N_5/2 - N_8/2 \\
N_2 &= \tfrac{1}{4}(1+\xi)(1+\eta) - N_5/2 - N_6/2 \\
N_3 &= \tfrac{1}{4}(1+\xi)(1-\eta) - N_6/2 - N_7/2 \\
N_4 &= \tfrac{1}{4}(1-\xi)(1-\eta) - N_7/2 - N_8/2 \\
N_5 &= \tfrac{1}{2}(1-\xi^2)(1+\eta) \\
N_6 &= \tfrac{1}{2}(1-\eta^2)(1+\xi) \\
N_7 &= \tfrac{1}{2}(1-\xi^2)(1-\eta) \\
N_8 &= \tfrac{1}{2}(1-\eta^2)(1-\xi)
\end{aligned}$$

Element Displacements. Figure 5-4 illustrates displacements and various local and global axes of the thick-shell element. The displacements at any point within the element are defined by three translations of the midsurface nodes and by two rotations of the nodal vectors V_{3i} about two orthogonal directions V_{1i} and V_{2i}. If γ_i and δ_i represent the two rotations at node i, and v_{2i} and v_{1i} denote the two-unit

vectors in the V_{2i} and V_{1i} directions, the displacement at any point is defined in the form:

$$\begin{Bmatrix} u \\ v \\ w \end{Bmatrix} = \sum_i N_i \begin{Bmatrix} u_i \\ v_i \\ w_i \end{Bmatrix} + \sum_i N_i \frac{t_i}{2} [v_{1i} - v_{2i}] \begin{Bmatrix} \gamma_i \\ \delta_i \end{Bmatrix} \qquad (5.16)$$

where u, v, and w = displacements in the global directions

u_i, v_i, and w_i = displacement components of the midsurface node i

t_i = element thickness at this node

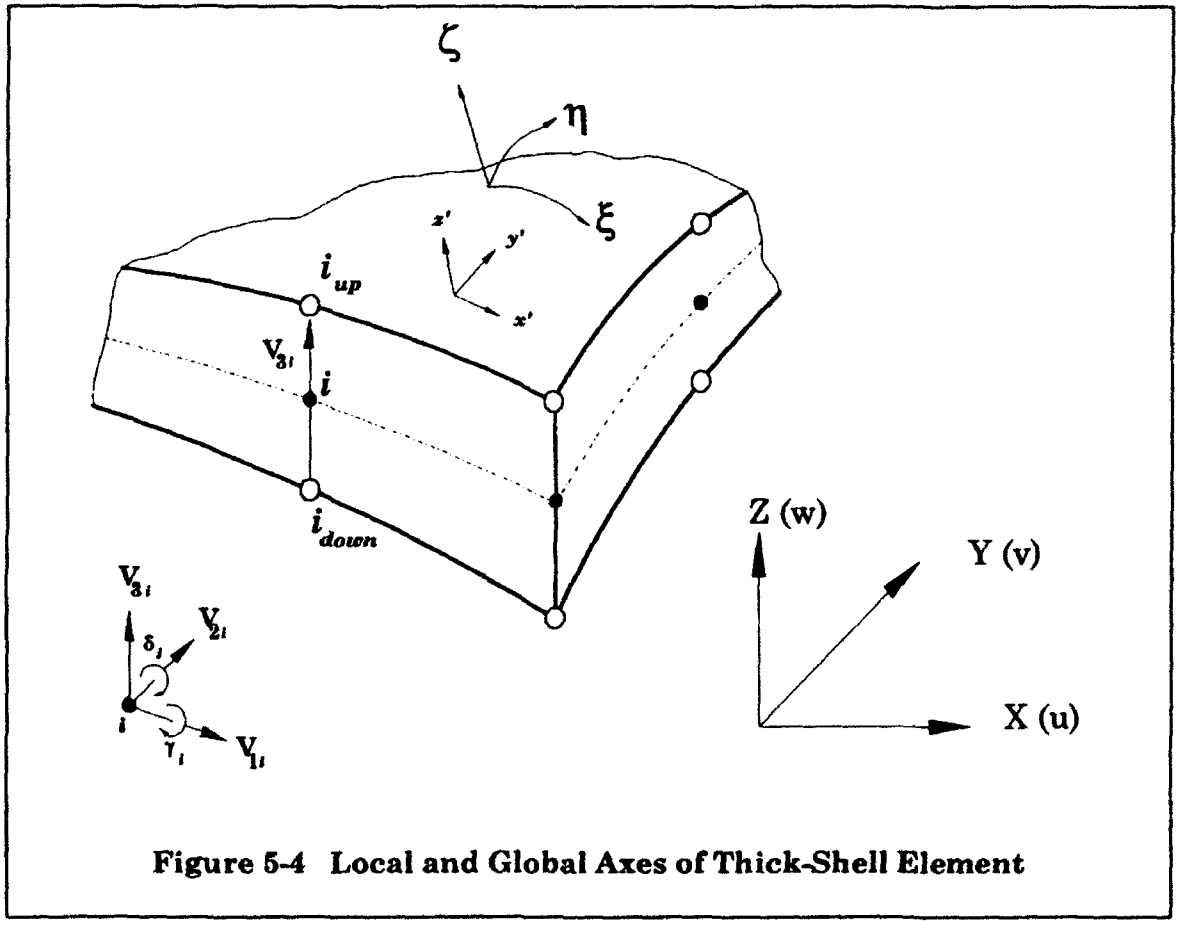

Figure 5-4 Local and Global Axes of Thick-Shell Element

Element Matrices. The element property matrices are derived following the standard procedures described previously, except that for the thick-shell elements, strain and stress components at any point on the surface are defined with respect to mutually perpendicular local axes at that point, and, thus, an additional transformation is necessary. The local axes are constructed such that z' is normal and the orthogonal x', and y' axes are tangent to the element surface (Figure 5-4). The first transformation which relates the global displacements to curvilinear coordinates is carried out as in the case of 3-D elements using the relationship given in Equation 5.15. The global derivatives of displacements are then transformed to the local derivatives of the local displacements using the standard coordinate transformation. From this transformation, the element strain-displacement matrix [B] is obtained; other relevant element matrices are easily established following the standard procedures discussed earlier.

Numerical Integration of Element Matrices. All element matrices are evaluated using a reduced integration scheme to improve accuracy of the solution (Pawsey 1970). Pure bending deformations of finite size elements are always accompanied by extraneous shear stresses that actually do not exist under the shell theory. The contribution of this shear strain energy to the stiffness matrix results in a stiffer element. In the limit, the extraneous strain energy vanishes because it becomes smaller as the element size decreases. However, such restriction on the element size can be easily removed by reducing the integration order (Pawsey 1970).

The thick-shell element included in GDAP uses two integration points in the thickness direction (ζ) but uses different reduced integration grids in the surface directions (ξ, η) for evaluation of the strain energy due to various strain components. For example, ε_{xx} and ε_{yy} are integrated using 2×3 and 3×2 grids, respectively, rather than the usual 3×3 Gauss quadrature points. Similar reduced integration orders are also used to calculate the transverse shear energy from γ_{zx} and γ_{zy}.

6. STATIC ANALYSIS PROCEDURE

6.1 Introduction

This chapter presents linear-elastic response analysis of arch dams under the static loads. A typical finite element static analysis involves the following basic steps:

1. Idealization of the dam and an appropriate portion of the foundation rock as an assemblage of finite elements

2. Evaluation of the stiffness properties of the elements, and the element load vectors

3. Formulation of the equations of static equilibrium for the entire structure by direct addition of the stiffness matrices and the load vectors of the individual elements, as well any externally applied concentrated nodal loads

4. Solution of the system of equilibrium equations by numerical methods to obtain displacements at nodal points of the assembled structure

5. Determination of the element stresses from the computed nodal displacements and the element stress-displacement relationship

Finite element idealization of the concrete arch dam and the foundation rock are based on the procedures described in Chapter 4. The concrete arch as shown in Figure 4-1 is usually modeled by a combination of the thick-shell and 3-D shell elements. The main body of the dam is represented by the thick-shell elements, and the regions near the abutments where the shell behavior diminishes are modeled using the 3-D elements. The foundation rock as described earlier is represented by the eight-node solid elements and should at least extend one dam height in the upstream, downstream, and downward directions. Guidelines for the appropriate selection of the element types, size of the dam finite element mesh, and the size of the foundation rock region are provided in EM 1110-2-2201, "Arch Dam Design."

The stiffness properties and the load vectors for each element type are calculated following the formulations given in Chapter 5; linearly elastic material properties are assumed. Finite elements used in the body of the dam are usually assumed to be isotropic, but orthotropic properties may be specified for the eight-node solid elements to represent the foundation rock.

The system equations of equilibrium for the complete structure approximated as an assemblage of finite elements are formed using the principle of virtual displacements. The solution of this algebraic system of equations, the static loads relevant to the analysis of arch dams, and the results of a typical static analysis are discussed in this chapter.

6.2 System Equations of Equilibrium

The linear system of equations that arises in a typical linear-elastic static analysis of arch dams are given for the entire assembled dam-foundation system by

$$\mathbf{k}\,\mathbf{u} = \mathbf{p} \qquad (6.1)$$

where $\mathbf{k}$ = stiffness matrix
$\mathbf{u}$ = displacement vector
$\mathbf{p}$ = load vector

The assembled stiffness matrix **k,** which is obtained from the *symmetric* stiffness matrices of the individual elements, is also a symmetric matrix. Thus, only the main diagonal and the terms on one side of the main diagonal must be stored. Another important feature of the matrix **k** is that the stiffness coefficient corresponding to a particular DOF is influenced only by the DOF's associated with the elements connecting to that DOF; the stiffness coefficients associated with nonconnecting DOF's are zero. Therefore, the global stiffness matrix usually contains many more zero terms in each row than nonzero terms. In a typical stiffness matrix, the nonzero terms are clustered in a band centered along the main diagonal called *bandwidth.* In a finite element analysis it is important that all the zero terms outside the bandwidth not be included in the equation solution. The computer program GDAP (Ghanaat 1993) , like many other finite element programs stores only those terms in the banded region that are on and above the main diagonal, and usually a term known as the *half-bandwidth* is used instead of the bandwidth. This scheme reduces both the storage requirements and the number of operations needed in the solution process. It is obvious that greater efficiency can be achieved by minimizing the bandwidth of the stiffness matrix. This often can be accomplished by appropriate node numbering so that the maximum difference in

global DOF's in any one of the finite elements is minimized. However, this is not always easy to generate, and various automatic bandwidth minimization schemes are currently available that can be used. The load vector **p**, in general, consists of the concentrated forces or moments applied at the nodal points and the consistent loads due to the distributed element loads. The element loads include the gravity, water, and temperature loads that are discussed later.

6.3 Solution by Gauss Elimination

In practice, the linear system of equations for an arch dam structure may include several thousand equations that must be solved simultaneously. The number of equations increases with the number of finite elements used to approximate the actual dam-foundation and the appurtenant structures. For example, the number of equations for finite element analysis of a multiple arch dam can easily approach or exceed 10,000 equations. Thus, it is obvious that the cost of analysis and its practical feasibility depend to a great degree on the effectiveness of the available solution algorithms. The most effective algorithms for the solution of the linear system of equations with symmetric banded matrix, which is obtained in a finite element structural analysis, are applications of Gauss elimination (Dahlquist and Bjorck 1974). The basic concept of the Gauss elimination method is to eliminate the unknowns in a systematic way and to produce an upper triangular matrix from which the unknown displacements **u** are solved by a back substitution. A detailed description of the standard Gauss elimination scheme and other various applications of the method are given by Bathe and Wilson (1976).

6.4 Static Loads

The most common loads considered in the static analysis of arch dams are weight of the dam, hydrostatic pressures of the impounded water, silt pressures, and the temperature changes in the concrete. The contribution of less common loads, such as the tail water, ice, uplift or pore pressures, and the loads due to the appurtenant structures should also be included when they are significant. Arch dams should be designed for all appropriate combinations of such loads. Combination of transient loads whose simultaneous occurrence at any given time is highly improbable is not appropriate and should not be considered. The loading combinations applicable to

arch dams include usual, unusual, and the extreme loading combinations and are described in EM 1110-2-2201 on arch dam design.

6.4.1 Gravity Loads

Gravity loads due to dead weight of the dam are calculated from a uniform weight density throughout each element. They are distributed body forces that are easily obtained using the standard procedures outlined in Chapter 3. Calculation of the nodal loads for each individual element is straight forward, but the way gravity loads are applied to the dam structure depends on the construction and joint grouting sequence.

Concrete arch dams are constructed as a system of cantilever blocks separated by vertical joints (Figure 6-1). The joints are open during the construction to permit cooling and shrinkage to take place independently in each cantilever, but later they are grouted under high pressure to form a monolithic structure. The gravity loads imposed on the individual cantilevers separated by joints are assumed to be transmitted vertically to the foundation without any arch action. The actual construction process, especially for the large dams with overhanging sections, is more complicated and may proceed in several layers as shown in Figure 6-1. In each layer, cantilevers are constructed independently, but the joints are grouted before the next layer is built. In principle, stress analysis for gravity loads should approximately follow the construction sequence, but the calculation process is quite tedious. In practice, the construction process is simulated by a series of independent cantilevers with the vertical joints being open along the entire height of the cantilevers as shown in Figure 6-1d. The static analysis for the gravity loads is then performed in two steps. First, gravity loads are applied to alternate cantilevers by setting the modulus of elasticity to zero for the remaining cantilevers. In the second analysis, modulus of elasticity is switched on for the alternate cantilevers and set to zero for the first set.

Alternatively, the gravity loads may be applied to the continuous and completely finished dam in a preliminary design calculation. In fact, this assumption may actually be more realistic for dams in narrow canyons where arch action exists

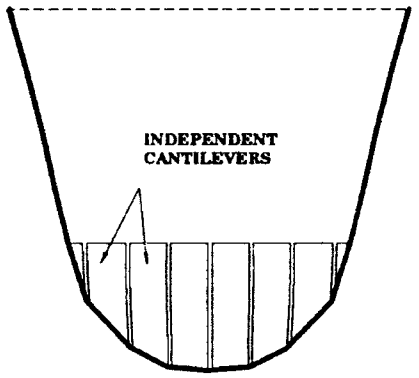

(a) Construction Sequence 1

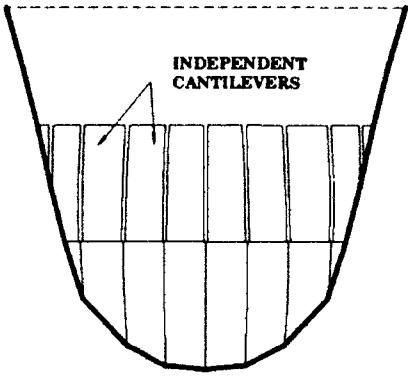

(b) Construction Sequence 2

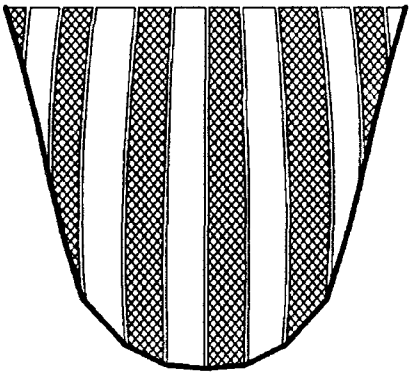

(d) Idealized Gravity Load Model

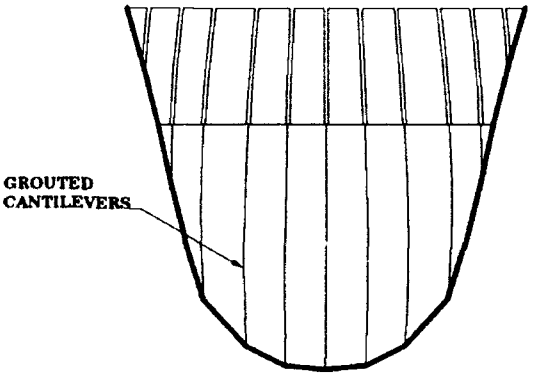

(c) Construction Sequence 3

Figure 6-1 Construction Sequence and Idealized Gravity Load Model

even without grouting. In either case, it is obvious that gravity loads should not be applied within the foundation rock.

6.4.2 Hydrostatic Loads

When the reservoir is filled after the contraction joints are grouted, the compressive stresses across the joints are further increased, so the dam resists the hydrostatic loads as a truly monolithic structure. The static analysis for the hydrostatic loads uses the complete dam-foundation model, and the water loads are applied as external surface loads acting on the dam and foundation rock. The weight of impounded water causes deformations of the foundation rock at the valley floor and

flanks which affect deformations and stresses in the dam. These foundation effects may not be negligible and should be included in the analysis (EM 1110-2-2201, Herzog 1989).

6.4.3 Temperature Loads

Temperature loads play an important part in the design and safety evaluation of arch dams, especially when operating under severe temperature variations. Operating temperature loads are applied to the monolithic dam structure after the contraction joints are grouted. The element nodal loads due to temperature changes are obtained using the procedures discussed in Chapter 4. In general, temperature distributions within a dam vary in a nonlinear manner but they are usually approximated by a combination of uniform and linear variations in practical applications. The computer program GDAP permits temperature changes to vary with elevation, across arch sections, and through the dam thickness. However, when nodal temperature values are generated by the program, constant temperatures are assumed across each arch section. Only operating temperature loads are discussed in this report. Thermal studies to determine appropriate placing and closure temperatures during the construction are discussed in EM 1110-2-2201.

When a temperature change occurs in an arch dam, the resulting volumetric change, if restrained by the dam boundaries, induces thermal stresses in the dam. The magnitudes of the temperature loads depend on the difference between the closure temperature and concrete temperatures expected during operation (USBR 1965). The closure temperature is the mean concrete temperature at the time the contraction joints are grouted to form a monolithic structure. This temperature is very important because it directly affects the thermal stresses induced in the dam. The adverse effects of the extreme operating temperature variations can be minimized by selection of an appropriate closure temperature.

Concrete temperatures to be expected during operation of a dam are determined from studies that consider the ambient air temperatures, reservoir water temperatures, and solar radiation. These studies are made using the measured thermal properties of the materials, recorded air and water temperatures at the dam site, and accurate analytical calculations.

6.4.4 Silt Loads

Silt loads are treated in the same manner as the impounded water loads. They are applied as hydrostatically varying surface loads using an appropriate weight density.

6.4.5 Concentrated Loads

Any concentrated force or moment can be applied at a given nodal point. This may include dead weight of the appurtenant structures such as gates and bridges or any static load approximated as a point load. These loads are applied after grouting of contraction joints, and, thus, are resisted by both the arch and cantilever units of the monolithic dam structure.

6.4.6 Ice Loads

Ice pressures exerted on a dam are represented by a distributed surface load or by equivalent concentrated loads applied at appropriate nodal points. The magnitude of ice pressures depends on many parameters that are not easily available. Some estimates of ice pressures are given in EM 1110-2-2201.

6.4.7 Uplift Pressures

Uplift or pore pressures develop when water enters the interstitial spaces within the body of an arch dam as well as in the foundation joints, cracks, and seams. The effect of uplift pressures is to reduce the normal compressive stresses on horizontal sections within the concrete and to increase the corresponding tensile stresses should they exist. Uplift pressures have negligible effects on the stress distribution in thin arch dams, but their influence on thick gravity-arch dams may be significant and should be included in the analysis.

The effects of uplift pressures generally are not incorporated as part of the regular finite element analysis of arch dams. This is partly due to the minor stress changes they cause in thin arch dams, and also to the lack of accurate data associated with the magnitudes and distributions of uplift pressures. The uplift pressure distributions at the dam-foundation interface and within the foundation rock depend

on the depth and size of drains, grout curtain, rock porosity, jointing, faulting, and any geological features that may affect the flow of water through the system.

The effects of uplift pressures, if significant, can be accounted for by using Terzaghi's *effective stress* concept which states that a pore pressure P_u in a rock causes the same reduction in peak normal stress that would be caused by a reduction of the confining pressure by an amount equal to P_u. The effective stress at a particular location can be obtained as the algebraic sum of the total stress and the uplift pressure at that location. The uplift pressures can be determined by measurements or may be estimated by analytical methods from flow nets. The positive uplift pressures are then added algebraically to the horizontal and vertical components of the total stresses computed in a finite element analysis ignoring the uplift. When a crack exists in the dam, uplift pressures exerted on the surfaces of the crack are applied as external hydrostatic pressures.

6.5 Results of Static Analysis

The results of a typical static analysis include nodal displacements and element stresses computed at various locations for all expected loading combinations. The appropriate loading combinations for an arch dam are discussed in EM 1110-2-2201.

At each nodal point, three displacement components corresponding to a global system of axes are computed. They may be presented in the form of 3-D plots showing the deflected shape of the entire dam or as 2-D plots along the arch and cantilever sections as shown in Figure 6-2. The magnitudes and deflected shapes of the resulting displacements provide important data that can be used to visually evaluate the acceptability of a new design or the overall behavior of an existing dam.

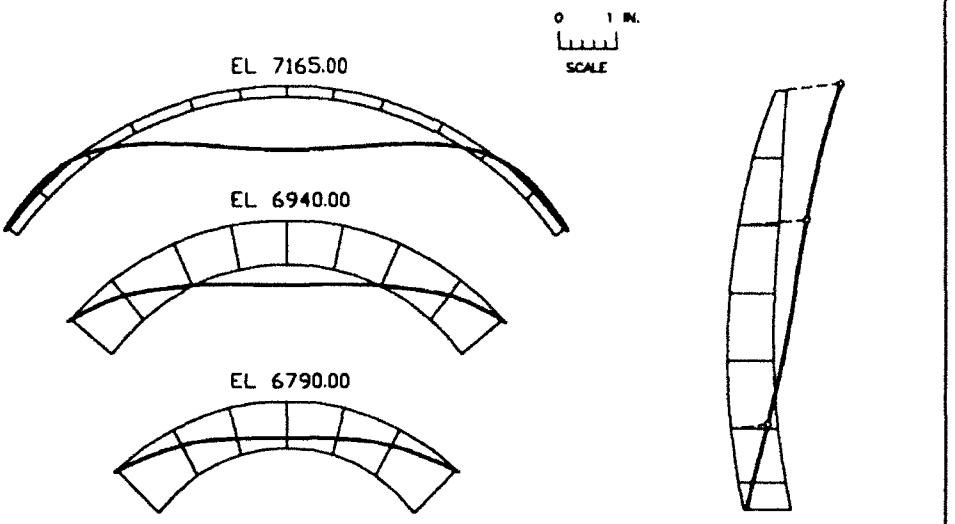

Figure 6-2 Nodal Displacement due to Water Load

The most meaningful stress results for evaluation of an arch dam are the surface stresses in the arch and cantilever directions. In general, six stress components -- three normal and three shear stresses -- are computed at each stress point of a 3-D element; thick-shell elements have only five stress components, because the stress component normal to the element surface is assumed to be zero. If such stresses are calculated with respect to a global coordinate system, they should be transformed to arch and cantilever stresses by suitable transformation. The computer program GDAP which has been especially developed for the analysis of arch dams, automatically provides arch, cantilever, and shear stresses on the surfaces of each element, and then uses this information to calculate the magnitude and direction of the principal stresses on the upstream and downstream faces of the dam. The arch and cantilever stresses are usually presented in the form of stress contours, whereas the principal stresses are shown as vector plots containing both the magnitude and the stress direction. Figure 6-3 shows an example of surface stresses computed for the impounded water loads.

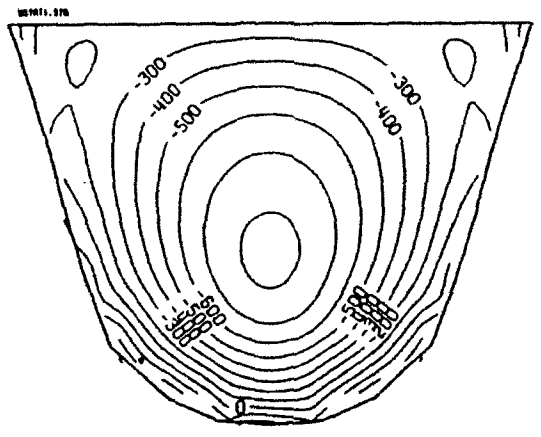

U/S Arch Stresses

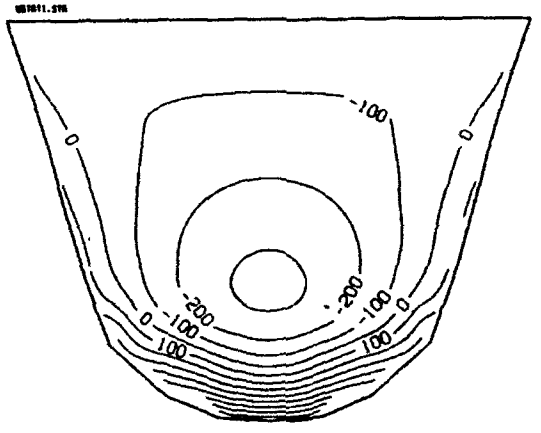

U/S Cantilever Stresses

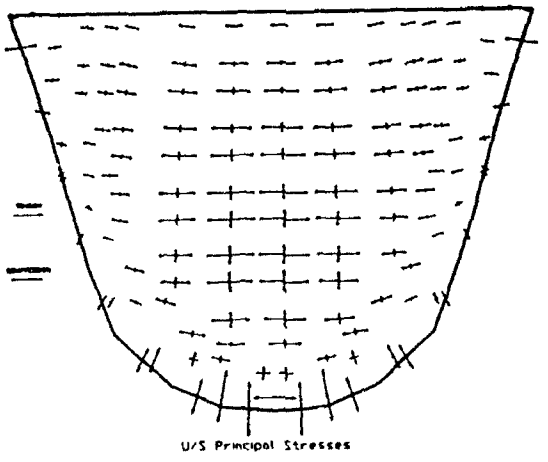

U/S Principal Stresses

Figure 6-3 Arch and Cantilever Stress Contours and Vector Plots of Principal Stresses

7. EARTHQUAKE ANALYSIS PROCEDURE

7.1 Introduction

The earthquake response analysis of concrete arch dams generally is performed by the standard dynamic FEM. However, prediction of the dam response during earthquakes is more complex than a typical problem in structural dynamics. The response of an arch dam to earthquakes is significantly influenced by its dynamic interactions with the deformable foundation rock and the impounded water. It may also be considerably affected by the variation of earthquake ground motion over the width and height of the canyon. Analytical procedures are now available to account for the interaction with the reservoir water using three different levels of sophistication (Chapter 4). But interaction with the foundation rock is still represented by the oversimplified massless foundation model, due partly, to the uncertainties and difficulties associated with definition of the seismic input. During intense earthquake motions, the dam response is further complicated by the opening and slippage of the vertical contraction joints; tensile cracks may occur; and the impounded water may momentarily separate from the upstream face of the dam at the locations of negative pressures, resulting in cavitation. These types of responses are nonlinear in nature and are very difficult to model and calculate reliably. The linear-elastic earthquake response analysis of arch dams is summarized in this section. A typical earthquake response analysis involves several steps as follows:

1. Finite element idealization of the dam-foundation system

2. Idealization of the impounded water by the Westergaard added-mass assumption or as an assemblage of finite element fluid elements

3. Evaluation of the stiffness, damping, and mass properties of the finite elements

4. Evaluation of the effective earthquake forces due to the mass of the dam structure, as well as the hydrodynamic forces due to the earthquake-induced motions of the reservoir, to formulate the equations of motion

5. Evaluation of the vibration mode shapes and frequencies of the dam-foundation-reservoir system and transformation of the equations of motion from the finite element coordinates to modal coordinates

6. Computation of the earthquake response in each of the uncoupled modal coordinates using a response spectrum or acceleration time history as the earthquake input, and then superposing the modal responses to obtain the total response.

The same finite element idealizations of the dam and foundation rock developed for the static analysis are also used for the calculation of earthquake response. However, for earthquake analysis the element properties should be evaluated using the *dynamic* elastic material properties of the concrete and the foundation rock. Formulations of the equations of motion for incompressible reservoir water, of the free vibration analysis, and of the earthquake response calculations are described in the following section.

7.2 System Equations of Motion

The equations of motion for a dam structure idealized by finite elements are:

$$\mathbf{m}\ddot{\mathbf{u}} + \mathbf{c}\dot{\mathbf{u}} + \mathbf{k}\mathbf{u} = \mathbf{p}(t) \qquad (7.1)$$

where **m**, **c**, and **k** = mass, damping, and stiffness matrices of the system evaluated by the procedures described in Chapter 3
u = vector of displacements of the finite element nodes
p(t) = vector of time varying external forces or of effective loads resulted from earthquake ground motion

In the case of earthquake ground motion, no dynamic external forces are applied directly to the structure. Instead, the structure is subjected to ground accelerations applied at the base of the structure. The base excitation produces inertia forces that depend on <u>total</u> accelerations $\ddot{\mathbf{u}}^t$ of the DOF's which are due to the relative motion within the structure plus the effect of support motions, i.e.:

$$\ddot{\mathbf{u}}^t = \ddot{\mathbf{u}} + \mathbf{r}\ddot{\mathbf{u}}_g \qquad (7.2)$$

where $\ddot{\mathbf{u}}_g$ = the vector of three components of the free-field ground accelerations at all support points
r = influence coefficient matrix which represents structural displacements resulting from a unit displacement in each component of the support motions

Thus, the equations of motion for a dam-foundation-reservoir system subjected to earthquake ground motion can be written as:

$$\mathbf{m}\ddot{\mathbf{u}} + \mathbf{c}\dot{\mathbf{u}} + \mathbf{k}\mathbf{u} = -\mathbf{m}\mathbf{r}\ddot{\mathbf{u}}_g + \mathbf{f}_h \qquad (7.3)$$

where $\mathbf{m}$ and $\mathbf{c}$ = mass and damping matrices of the dam
$\mathbf{k}$ = stiffness matrix of the dam and foundation rock
$-\mathbf{m}\ddot{\mathbf{u}}_g$ = effective earthquake loads
$\mathbf{f}_h$ = vector of hydrodynamic forces acting on the dam-water interface only

Note that the foundation rock contributes only to the stiffness matrix because its inertia and damping effects are ignored. Procedures for calculating hydrodynamic forces $\mathbf{f}_h$ for the incompressible reservoir water are presented in the following section.

7.3 Westergaard Analysis of Added-mass

The effect of reservoir water on the earthquake response of concrete dams was first considered by Westergaard (1933). He introduced the *added-mass* concept for an incompressible reservoir which has been used as the standard method in the earthquake response calculation of most gravity dams. In his analysis, the dam was idealized as a 2-D rigid monolith with vertical upstream face; the reservoir water was assumed to be incompressible and to extend to infinity; and the effects of surface waves were ignored. Based on these simplified assumptions, Westergaard indicated that the hydrodynamic pressures exerted on the face of the dam due to earthquake ground motion is equivalent to the inertia forces of a prismatic body of water attached firmly to the face of the dam and moving back and forth with the dam while the rest of reservoir water remains inactive. He also suggested a parabolic shape for this body of water with the base width equal to seven-eights of the height, as shown in Figure 7-1.

7.3.1 Arch Dam Extension of Westergaard Analysis

The Westergaard added-mass concept is also applicable to the earthquake analysis of arch dams, but it should be modified to account for the curvature and flexibility of the dam structure. In general, arch dams are curved in both the plan and elevation, and, thus, the orientation of the pressures normal to the dam face varies from point to point. When making this modification, it is also convenient to account for the dam flexibility by recognizing that the hydrodynamic pressure exerted at any point on the dam is proportional to the total normal acceleration at that point. The added mass calculated in this manner is known as the generalized added mass, because it is applicable to the general geometry of the upstream face of flexible arch

dams. This extension can be easily included in the finite element response analysis of arch dams and is available as an option in the GDAP (Ghanaat 1993) program.

The basic assumption in the *Generalized Westergaard Method* (Clough 1977) analysis is that the pressure at any point i on the face of the dam is expressed by the Westergaard parabolic shape shown in Figure 7-1, i.e.:

$$\mathbf{p}_i = \alpha_i \, \ddot{\mathbf{u}}'_{ni} \tag{7.4}$$

where $\alpha_i = \frac{7}{8}\rho_w \sqrt{H_i(H_i - Z_i)}$

$\ddot{\mathbf{u}}'_{ni}$ = total normal acceleration at point i
α_i = Westergaard pressure coefficient
ρ_w = mass density of water
H_i = depth of water at vertical section that includes point i
Z_i = height of point i above the base of the dam

It should be obvious that there is no rational basis for this assumption because limitations imposed in the original Westergaard analysis are not met. Furthermore, the same Westergaard pressure coefficient is used for all three components of the ground accelerations. The procedure, however, provides a somewhat reasonable generalization and is useful for the preliminary or feasibility studies of arch dams.

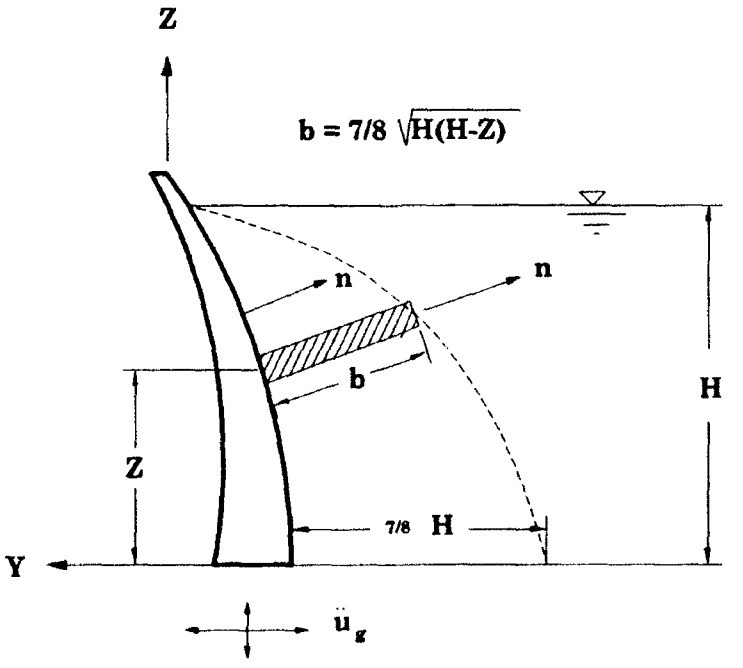

Figure 7-1 Westergaard Added-Mass Representation For Arch Dams

In the finite element analysis, $\ddot{\mathbf{u}}'_{ni}$ is expressed in terms of Cartesian coordinate components of the ground acceleration $\ddot{\mathbf{u}}_g$ and of the acceleration components of node i relative to the base of the dam $\ddot{\mathbf{u}}$. This relationship is given by the direction cosines between the Cartesian coordinates and the normal:

$$\ddot{\mathbf{u}}'_{ni} = \lambda_i\left(\ddot{\mathbf{u}} + \mathbf{r}\ddot{\mathbf{u}}_g\right) \tag{7.5}$$

where λ_i = a vector of normal direction cosines at node i
boldfaced terms = a vector or matrix quantity

7.3.2 Hydrodynamic Forces Acting on the Dam

The normal pressure p_i is now converted to an equivalent normal hydrodynamic force at node i by multiplying by the surface area A_i tributary to point i:

$$F_{ni} = -p_i A_i \tag{7.6}$$

The normal force F_{ni}, however, should be resolved into its Cartesian components given by:

$$\mathbf{F}_i = F_{ni}\lambda_i^T \tag{7.7}$$

Combining Equations 7.4, 7.5, and 7.6 with Equation 7.7 leads to:

$$\mathbf{F}_i = -\mathbf{m}_{ai}\left(\ddot{\mathbf{u}} + \mathbf{r}\ddot{\mathbf{u}}_g\right) \tag{7.8}$$

where

$$\mathbf{m}_{ai} = \alpha_i A_i \lambda_i^T \lambda_i \tag{7.9}$$

Here $\mathbf{m}_{ai}$ is a full 3 × 3 added-mass matrix associated with node i on the upstream face of the dam. Following the direct stiffness assembly procedure, the vector of hydrodynamic forces acting on the upstream nodes of the dam is given by:

$$\mathbf{f}_h = \sum_i \mathbf{F}_i = \mathbf{m}_a\left(\ddot{\mathbf{u}} + \mathbf{r}\ddot{\mathbf{u}}_g\right) \tag{7.10}$$

where $\mathbf{m}_a$ is the added-mass matrix resulting from the hydrodynamic pressures acting on the upstream face of the dam. The added-mass terms associated with each node form a 3×3 full submatrix along the diagonal of $\mathbf{m}_a$, but the submatrices are not coupled.

7.3.3 Coupled Dam-Water Equations of Motion

Substituting Equation 7.10 into Equation 7.3, the equations of motion including the hydrodynamic effects of the reservoir can be written as:

$$(\mathbf{m}+\mathbf{m}_a)\ddot{\mathbf{u}}+\mathbf{c}\dot{\mathbf{u}}+\mathbf{k}\mathbf{u}=-(\mathbf{m}+\mathbf{m}_a)\mathbf{r}\ddot{u}_g \qquad (7.11)$$

The right-hand side of this equation is the effective earthquake loads, which depend on the added mass of the reservoir as well as the mass of the dam structure. In the computer implementation of the Westergaard added mass, the global matrix $\mathbf{m}_a$, need not be assembled separately. Instead, the added mass of the impounded water is combined with the mass of the concrete for each individual element on the upstream face of the dam, and then the mass matrix for the entire structure is assembled according to the standard procedure.

7.4 Finite Element Analysis of Incompressible Water

The Westergaard added mass discussed previously is computationally efficient, but it does not properly represent the hydrodynamic forces acting on arch dams. A better approach is to idealize the impounded water by the finite element method, which permits a realistic treatment of the complicated geometry of an arch dam reservoir. Assuming that water is incompressible, finite element solution of the dam-water interaction is represented by an equivalent added-mass matrix. The finite element formulation of an incompressible reservoir model with nodal pressures as unknowns is summarized by Kuo (1982) and Zienkiewicz (1971).

7.4.1 Equations of Motion

The equation of motion for hydrodynamic pressures of an incompressible and inviscid fluid is given by the wave equation:

$$\nabla^2 p = 0 \qquad (7.12)$$

where ∇^2 = Laplacian operator in three dimensions
$p = p(x,y,z,t)$ = hydrodynamic pressure in excess of the static pressure in the fluid domain Ω, as shown in Figure 7-2

The hydrodynamic pressures acting on the face of a dam are obtained by solving this equation, with appropriate boundary conditions. The boundary condition at the free surface R_s in the absence of surface waves is:

$$p = 0 \tag{7.13}$$

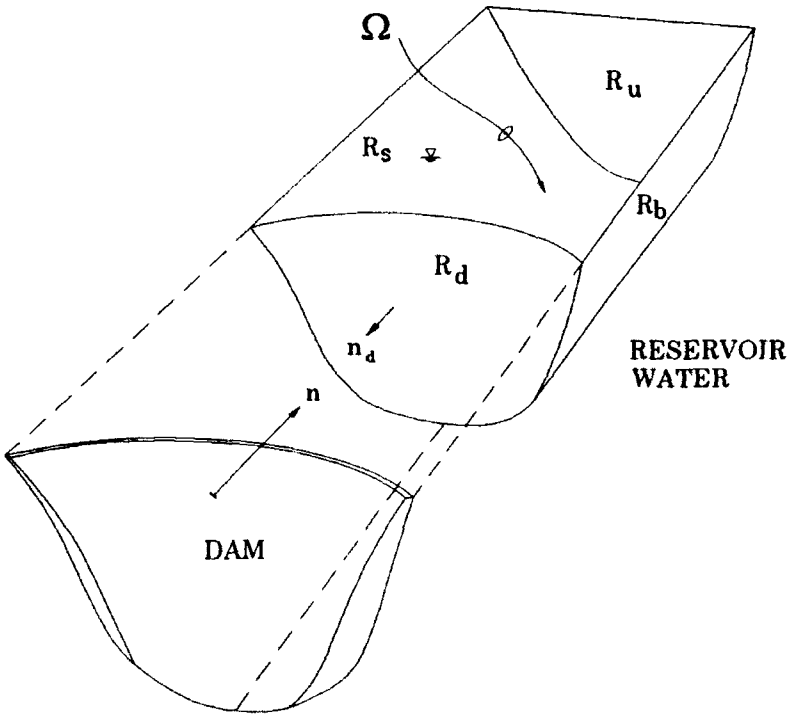

Figure 7-2 Dam and Reservoir Water

On the upstream face of the dam R_d, where the normal motion is prescribed, the boundary condition is:

$$\frac{\partial p}{\partial n} = -\rho \ddot{u}_{nd} \tag{7.14}$$

where ρ = mass density of water
$\ddot{u}_{nd}$ = total acceleration normal to upstream face of the dam
n = the direction normal to the boundary and is positive when pointing out of the fluid domain

A similar boundary condition may also be applied at the reservoir boundary R_b:

$$\frac{\partial p}{\partial n} = -\rho \ddot{u}_{nb} \tag{7.15}$$

where $\ddot{u}_{nb}$ is the normal component of the ground motion at the reservoir boundary. However, the computer program GDAP (Ghanaat 1993) assumes that the reservoir boundary R_b does not move, thus the pressure on the dam due to the motion of the reservoir boundary is ignored. The finite element discretization of the reservoir water cannot be applied to a reservoir of infinite extent. It is necessary to truncate the reservoir model at an appropriate distance from the upstream face of the dam, at which location the boundary condition is given by:

$$\frac{\partial p}{\partial n} = -\rho \ddot{u}_{nu} \tag{7.16}$$

where $\ddot{u}_{nu}$ is the acceleration normal to the upstream boundary R_u. The acceleration, $\ddot{u}_{nu}$ can be obtained from the continuum solution (Hall and Chopra 1980), or from the finite element solution (Saini, Bettes, and Zienkiewicz 1978) of a fluid domain extending to infinity from the truncated boundary. In the former solution, constant depth is assumed for the infinite fluid domain, whereas the latter uses specially developed infinite elements extending to infinity. However, if the upstream extent of the incompressible reservoir is greater than three times the dam height (Clough et al. 1984 (Apr)(Nov)), the acceleration at the truncated boundary has a small effect on the hydrodynamic pressures at the face of the dam and, thus, can be set to zero in practical applications.

7.4.2 Finite Element Discretization

The solution of the wave equation for hydrodynamic pressure is obtained numerically using the Galerkin FEM. The Galerkin form of the hydrodynamic pressure equation, Equation 7.12, is given by:

$$\int_{\Omega} \mathbf{N}^T \nabla^2 p \, d\Omega = 0 \tag{7.17}$$

where interpolation functions N for pressure are selected as weighting functions. This equation applies only to the pressures within the region Ω without reference to boundary conditions specified in Equations 7.13 to 7.16. To produce boundary conditions, Green's Theorem (or integration by parts) is applied to Equation 7.17, yielding integrals on both the region Ω and its boundary R_d:

$$\int_{\Omega} \nabla \mathbf{N}^T \nabla p \, d\Omega + \rho \int_{R_d} \mathbf{N}^T \rho \ddot{u}_{nd} \, dR = 0 \qquad (7.18)$$

Accordingly, as shown in Figure 7-3, the fluid region Ω and interface boundary R_d are discretized into 2-D and 3-D finite elements with nodal pressures as unknowns. The pressure distribution within each element is given by:

$$p = \mathbf{N}\mathbf{p} \qquad (7.19)$$

where $\mathbf{N}$ = interpolation functions for pressure
$\mathbf{p}$ = vector of nodal pressures

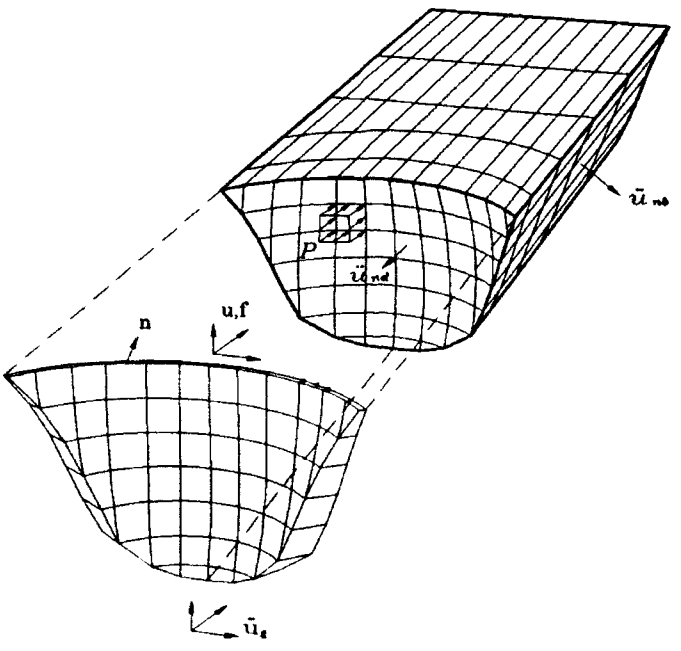

Figure 7-3 Dam and Water Finite Element Models

Substituting Equation 7.19 into Equation 7.18 gives the matrix form of the hydrodynamic pressure equation as follows:

$$\mathbf{gp} = \rho \mathbf{h}_d \ddot{\mathbf{u}}'_d \tag{7.20}$$

$$\mathbf{g} = \int_\Omega \nabla \mathbf{N}^T \nabla \mathbf{N} \, d\Omega \tag{7.21}$$

$$\mathbf{h}_d = \int_{R_d} \mathbf{N}^T \mathbf{n}^T \mathbf{N}_d \, dR \tag{7.22}$$

where matrix $\mathbf{g}$ = assembled for all 3-D elements in the fluid domain Ω
matrix $\mathbf{h}_d$ = assembled for the 2-D elements in contact with the dam face

These matrices are evaluated numerically using Gaussian quadrature as described previously. Here, $\mathbf{N}_d$ are the interpolation functions associated with the dam elements, and $\mathbf{n}$ is the outward normal from the dam for expressing the normal acceleration of the dam $\ddot{u}_{nd}$ in terms of three Cartesian components $\ddot{u}'_d$.

In the analysis of interaction between the dam and reservoir water, only the pressures at the upstream nodes of the dam are needed. Thus, Equation 7.20 is partitioned into quantities associated with the nodes on the dam upstream face (d) and all other nodes in the reservoir (r):

$$\begin{bmatrix} g_{rr} & g_{rd} \\ g_{dr} & g_{dd} \end{bmatrix} \begin{Bmatrix} p_r \\ p_d \end{Bmatrix} = \rho \begin{bmatrix} 0 & 0 \\ 0 & h_d \end{bmatrix} \begin{Bmatrix} 0 \\ \ddot{u}'_d \end{Bmatrix} \tag{7.23}$$

Eliminating noninterface quantities (r) from this equation gives:

$$\underline{g}\, p_d = \rho h_d \ddot{u}'_d \tag{7.24}$$

where $$\underline{g} = g_{dd} - g_{dr}\, g_{rr}^{-1}\, g_{rd} \tag{7.25}$$

is a full symmetric matrix coupling all nodal pressures at the upstream face of the dam, given by:

$$p_d = \rho \underline{g}^{-1} h_d \ddot{u}'_d \tag{7.26}$$

7.4.3 Hydrodynamic Forces Acting on the Dam

The pressure distribution acting on the upstream face of the dam is now available in terms of the computed nodal pressures p_d and the assumed pressure interpolation functions N. The nodal hydrodynamic forces that are equivalent to these pressure distributions are computed in a consistent manner using the principle of virtual displacements:

$$\mathbf{f}_h = -\boldsymbol{h}_d^T \boldsymbol{p}_d \tag{7.27}$$

Combining Equations 7.26 and 7.27 gives:

$$\mathbf{f}_h = -\rho \boldsymbol{h}_d^T \underline{\boldsymbol{g}}^{-1} \boldsymbol{h}_d \ddot{\boldsymbol{u}}_d^t \tag{7.28}$$

or

$$\mathbf{f}_h = -\boldsymbol{m}_a \ddot{\boldsymbol{u}}_d^t \tag{7.29}$$

where

$$\boldsymbol{m}_a = \rho \boldsymbol{h}_d^T \underline{\boldsymbol{g}}^{-1} \boldsymbol{h}_d$$

is an equivalent added-mass matrix, representing the inertial effects of the incompressible reservoir. This is a symmetric full matrix that couples all DOF on the upstream face of the dam.

7.4.4 Coupled Dam-Water Equations of Motion

The dam structure and the impounded water are coupled through the hydrodynamic forces $\mathbf{f}_h$ at the interface nodes as indicated in Figure 7-3. The equations of motion for the coupled dam-reservoir water system is obtained by the direct substitution of Equation 7.29 into Equation 7.3. However, prior to this substitution, $\mathbf{f}_h$ must be expanded to include all DOF's of the dam structure. Thus, Equation 7.29 is written as:

$$\mathbf{f}_h(t) = \begin{Bmatrix} 0 \\ \mathbf{f}_{dh} \end{Bmatrix} = \begin{bmatrix} 0 & 0 \\ 0 & \boldsymbol{m}_d \end{bmatrix} \begin{Bmatrix} \ddot{\boldsymbol{u}}_s^t \\ \ddot{\boldsymbol{u}}_d^t \end{Bmatrix} = \boldsymbol{m}_a \ddot{\boldsymbol{u}}^t \tag{7.30}$$

where $\ddot{\boldsymbol{u}}_s^t$ is a vector of total acceleration associated with all DOF's of the dam-foundation system, excluding the nodes on the upstream face. Introducing this equation into Equation 7.3 and expanding the total acceleration in terms of the acceleration relative to the fixed base and the ground acceleration give:

$$(\mathbf{m}+\mathbf{m}_a)\ddot{\mathbf{u}}+\mathbf{c}\dot{\mathbf{u}}+\mathbf{k}\mathbf{u}=-(\mathbf{m}+\mathbf{m}_a)\mathbf{r}\ddot{u}_g \qquad (7.31)$$

This equation is in the form of the standard earthquake response equation of motion, with the effects of reservoir water expressed as the added-mass matrix, $\mathbf{m}_a$. However, the program GDAP does not expand $\mathbf{m}_a$ to a matrix that includes all DOF's because it is not computationally efficient. Instead, the effective earthquake forces and the generalized-coordinate mass matrix, due to the added-mass, are computed separately.

7.5 Modal Analysis

The finite element model of an arch dam system represented by Equation 7.31 includes a large number of DOF's. The solution of this equation for the time history of response can be performed directly by a step-by-step method dealing simultaneously with all DOF's in the response vector by a procedure equivalent to that described for a single degree of freedom (SDOF) in Section 7.6.1 However, it is computationally advantageous to transform the equation of motion, Equation 7.31, to modal coordinates before carrying out the analysis. The reason for this is that, in most cases, the significant response of the dam structure can be adequately described by the few lowest vibration modes, and thus solution of the complete set of equations in the finite element coordinates is avoided.

Transformation to modal coordinates is accomplished by using the free vibration mode shapes of the system. For damping ratios less than 0.2, a range which includes the concrete arch dams, the effects of damping on vibration frequencies are neglected. Therefore, vibration mode shapes and frequencies of the dam structure are conveniently computed for the undamped structure.

The modal coordinates for the arch dam structure are obtained by solving the eigenproblem:

$$\mathbf{k}\boldsymbol{\phi}=\omega^2(\mathbf{m}+\mathbf{m}_a)\boldsymbol{\phi} \qquad (7.32)$$

for the undamped free vibration mode shapes ϕ and frequencies ω. Note that these modal properties are for the combined dam-water-foundation system because the stiffness of the foundation rock and the added-mass of the incompressible reservoir water are incorporated in Equation 7.32.

Applying the modal coordinate transformation:

$$\mathbf{u} = \Phi \ddot{\mathbf{y}} \tag{7.33}$$

where $\Phi = [\phi_1, \phi_2, \cdots, \phi_n]$

and $\mathbf{y} = [y_1, y_2, \cdots, y_n]^T$

to Equation 7.31 leads to a set of uncoupled modal coordinate response equations of the form:

$$\ddot{y}_n + 2\xi_n \omega_n \dot{y}_n + \omega_n^2 y_n = \frac{L_n}{M_n} \ddot{u}_g(t) \tag{7.34}$$

where $L_n = \phi_n^T (\mathbf{m} + \mathbf{m}_a)\mathbf{r}$

$M_n = \phi_n^T (\mathbf{m} + \mathbf{m}_a)\phi_n.$

This modal equation represents a SDOF equation of motion for mode n of the dam structure, which can be solved independently of the others.

7.5.1 Calculation of Frequencies and Mode Shapes

The first step in dynamic analysis based on mode superposition method is evaluation of the natural frequencies and mode shapes of undamped free vibration of the dam structure. These are obtained by solving the eigenproblem given in Equation 7.32 using the iterative procedures. Most iterative eigensolution procedures are based on some variation of the Stodola method (Clough and Penzien 1975, Wilson 1982), in which an initial mode shape is assumed, and it is adjusted iteratively until an adequate approximation of the true mode shape is achieved; the frequency of vibration is then obtained from the equation of motion. One such iterative procedure is the *subspace iteration* method (Bathe and Wilson 1976) which has been implemented in the GDAP (Ghanaat 1993) program as well as in several general-purpose structural analysis programs.

The subspace iteration method iterates simultaneously on a group of eigenvectors to solve for the lowest p mode shapes and frequencies satisfying:

$$\mathbf{k}\Phi = (\mathbf{m} + \mathbf{m}_a)\Phi\Omega^2 \tag{7.35}$$

where $\Omega^2 = \mathbf{diag}(\omega_i^2)$

and $\Phi = [\phi_1, \phi_2, \cdots, \phi_p]$

In addition to Equation 7.35, the mode shapes also satisfy the orthogonality conditions:

$$\Phi^T \mathbf{k} \Phi = \Omega^2 ; \quad \Phi^T (\mathbf{m} + \mathbf{m}_a) \Phi = \mathbf{I}$$

where **I** is a unit matrix of order p because Φ contains only p mode shapes. The solution starts with establishing q starting iteration vectors ($q>p$), which are adjusted in each iteration step and used as trial vectors for the next iteration until convergence to the required p frequencies and mode shapes is obtained. If $\mathbf{X}_1$ contains the p starting iteration vectors, then the k'th iteration is described as:

$$\mathbf{k}\overline{\mathbf{X}}_k = (\mathbf{m} + \mathbf{m}_a)\mathbf{X}_{k-1} \tag{7.36}$$

The unscaled improved eigenvectors in $\overline{\mathbf{X}}_k$ are obtained by solving Equation 7.36. But they must be normalized and orthogonalized before they can be used in the subsequent iteration cycle. This is achieved by computing the generalized stiffness and mass matrices for the p-dimensional subspace associated with the $\overline{\mathbf{X}}_k$ and then solving the corresponding eigenproblem. The generalized stiffness and mass matrices associated with $\overline{\mathbf{X}}_k$ are given by:

$$\mathbf{k}_k^* = \overline{\mathbf{X}}_k^T \mathbf{k} \overline{\mathbf{X}}_k \tag{7.37}$$

$$\mathbf{m}_k^* = \overline{\mathbf{X}}_k^T \mathbf{m} \overline{\mathbf{X}}_k + \overline{\mathbf{X}}_k^T \mathbf{m}_a \overline{\mathbf{X}}_k \tag{7.38}$$

The corresponding eigenproblem:

$$\mathbf{k}_k^* \hat{\mathbf{Y}}_k = \mathbf{m}_k^* \hat{\mathbf{Y}}_k \Omega_k^2 \tag{7.39}$$

is solved for the mode shapes $\hat{\mathbf{Y}}_k$ and frequencies Ω_k^2. Then the scaled improved approximation to the eigenvectors are given by:

$$\mathbf{X}_k = \overline{\mathbf{X}}_k \hat{\mathbf{Y}}_k \tag{7.40}$$

The entire iterative cycle is repeated many times until the process converges to the true mode shapes and frequencies as follows:

$$\Omega_k^2 \rightarrow \Omega^2 \quad \text{and} \quad \mathbf{X}_k \rightarrow \Phi \quad \text{as } k \rightarrow \infty$$

7.6 Response-Spectrum Mode Superposition

The natural frequencies and mode shapes of undamped free vibration of the dam structure are used to compute the dam response to earthquake ground motion. For design and preliminary evaluation purposes, it is usually sufficient to compute only the maximum values of the response due to earthquake. The maximum response values for the dam structure are obtained by response-spectrum mode superposition. First, the maximum response values for each mode of vibration modeled by an equivalent SDOF system are directly obtained from the earthquake response spectrum, and then the modal maxima are combined to obtain estimates of the maximum total response.

The response of each mode of vibration is obtained by solving the modal equation of the form presented in Equation 7.34. The response of mode n with natural frequency ω_n, damping ξ_n, generalized mass M_n, and the modal earthquake-excitation factor L_n to a specified ground acceleration $\ddot{u}_g(t)$ is given by:

$$Y_n = \frac{L_n}{M_n} V_n(t) \tag{7.41}$$

where $V_n(t)$ can be evaluated by numerical integration of the Duhamel integral (Clough and Penzien 1975 (pp 102 - 105)):

$$V_n(t) = -\frac{1}{\omega_{nD}} \int_0^t \ddot{u}_g(\tau) \exp\left[-\xi\omega_n (t-\tau)\right] \sin \omega_{nD} (t-\tau) d\tau \tag{7.42}$$

In this equation, $\omega_{nD} = \omega_n \sqrt{1-\xi_n^2}$ is the *damped vibration frequency* of the structure. But the difference between the damped and undamped frequencies is negligible for damping ratios less than 20 percent, and it is normally ignored in

practical analyses. The maximum value of Equation 7.42, which is called the spectral displacement for frequency ω_n, may be expressed as:

$$S_{dn} = \max|Y_n(t)| \tag{7.43}$$

These equations indicate S_{dn} depends not only on the ground-motion history but also on vibration frequency and damping of the particular mode represented by a SDOF oscillator. A plot of S_{dn} as a function of natural vibration frequency or period and for a specified damping value is denoted as the *displacement response spectrum* for the given earthquake accelerogram $\ddot{u}_s(t)$. Similar response-spectrum plots can be developed for other response quantities. The pseudo-velocity S_{vn} and pseudo-acceleration S_{an} are two such quantities that have units of velocity and acceleration, respectively, and are related to S_{dn} as follows:

$$S_{vn} = \omega_n S_{dn} = \frac{2\pi}{T_n} S_{dn} \tag{7.44}$$

$$S_{an} = \omega_n S_{vn} = \omega_n^2 S_{dn} \tag{7.45}$$

The displacement, pseudo-velocity, and pseudo-acceleration response spectra all provide the same information, and any one of them can be used. But all three response spectra can also be presented in a compact tripartite or four-way logarithmic plot as shown in Figure 7-4. As illustrated in this figure, for a given period and damping value (for example for T = 1 sec, ξ = 5%), $S_v = 190$ is read from the vertical logarithmic scale, while $S_d = 30$ and $S_a = 1.22$ are read from the logarithmic scales oriented at 45 degrees (0.7854 radians) to the period scale.

Finally, the maximum modal displacement expressed in terms of S_a^* or S_d is:

$$Y_{n,max} = \frac{L_n}{M_n} S_{dn} = \frac{L_n}{M_n} \frac{S_{an}}{\omega_n^2} \tag{7.46}$$

and the maximum relative displacement vector is

$$u_{n,max} = \phi_n Y_{n,max} = \phi_n \frac{L_n}{M_n} \frac{S_{an}}{\omega_n^2} \tag{7.47}$$

* Use of S_a is more common than S_d and S_v

The ratio L_n/M_n is a participation factor indicating the degree to which mode n is excited by the ground motion.

7.6.1 Combination of Modal Responses

The previous section demonstrated that the maximum response for each individual mode of the dam structure can be obtained directly from the earthquake response spectrum. In general, because the modal maxima do not occur at the same time, they must be combined by approximate procedures to estimate the maximum total response. Two common procedures for combining the modal maxima are the square root of the sum of the squares (SRSS) and the complete quadratic combination (CQC) methods. Assuming that only p lower modes contribute significantly to the total response, the SRSS combination of the modal maxima $u_{ni,max}$ to a single input spectrum in n direction is given by:

$$u_{max} = \sqrt{\sum_{i=1}^{p} (u_{ni,max})^2} \tag{7.48}$$

The SRSS method usually provides a conservative estimate of the maximum response when the vibration periods of the dam structure are well separated. But it underestimates the total response for the closely spaced vibration periods, because it ignores the correlation between the adjacent modes. A better alternative is to use the CQC method (Wilson, Der Kiureghian, and Bayo 1981) which includes all cross-modal terms as expressed by:

$$u_{max} = \sqrt{\sum_{i=1}^{p} \sum_{j=1}^{p} u_{ni,max} \rho_{ij} u_{nj,max}} \tag{7.49}$$

where $u_{i,max}$ = modal maximum response corresponding to mode i
ρ_{ij} = modal correlation coefficients

For a constant modal damping ξ, this coefficient is given by:

$$\rho_{ij} = \frac{8\xi^2(1+r)r^{\frac{3}{2}}}{(1-r^2)^2 + 4\xi^2 r(1+r)^2} \tag{7.50}$$

where $r = \omega_j/\omega_i$ is the frequency ratio

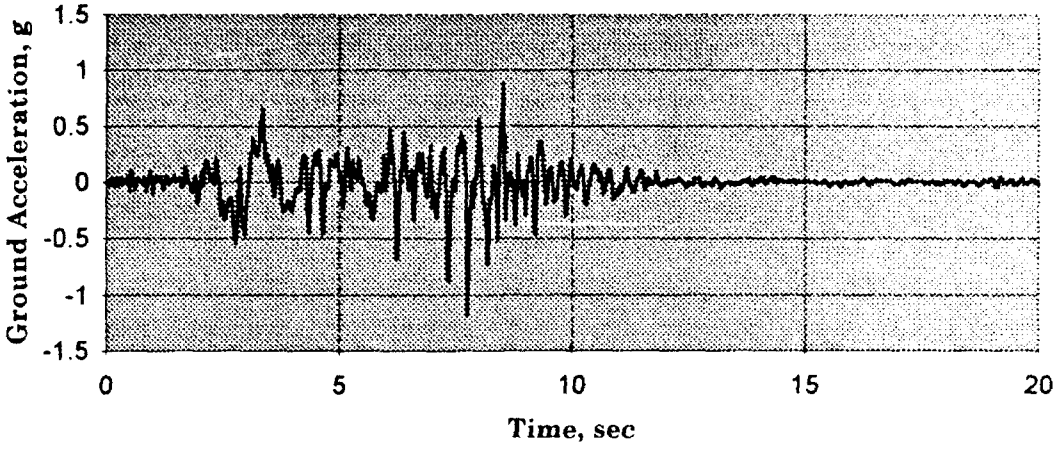

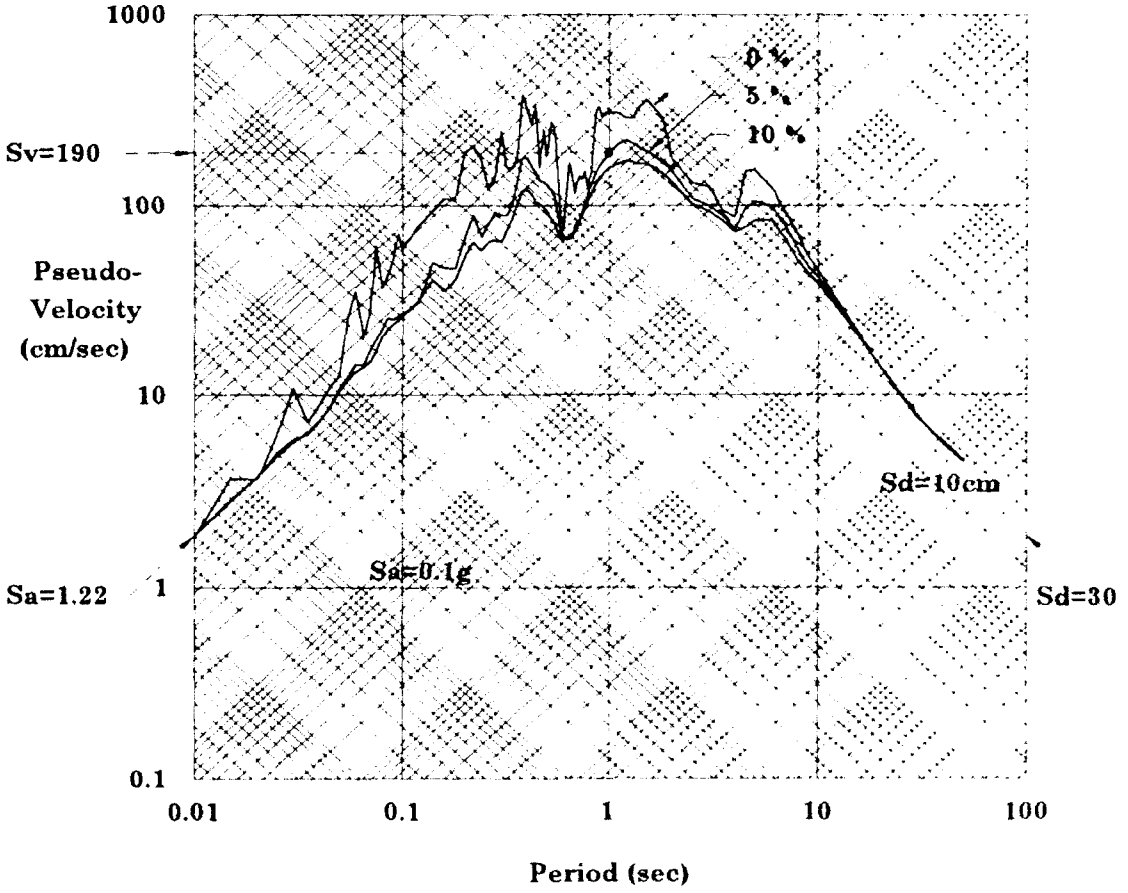

Figure 7-4 Four-way Logarithmic Plot of Response Spectrum For S14W Component of Pacoima Dam Accelerogram (shown for damping ratios of 0,5, and 10 percent)

7.6.2 Combining for Multicomponent Response Spectra

The maximum total response to a single response-spectrum input has just been described. For a three-component response-spectrum input, the following directional combination methods may be used:

SRSS: $$u = \sqrt{\sum_{n=1}^{3} u_{ni}^2} \tag{7.51}$$

Algebraic Summation: $$u = \sum_{n=1}^{3} u_{ni} \tag{7.52}$$

The maximum modal displacement u_{ni}, as evident from Equation 7.47, takes the sign of the modal participation factor and may be positive or negative. Thus, the algebraic summation for multicomponent input to response in each mode must be performed prior to combination of the modal responses, otherwise the signs are lost.

The SRSS combination of directional responses can be performed in any order with the SRSS modal combination but should be applied after the CQC combination of modal responses.

7.7 Time-History Mode-Superposition

The complete response history of the dam structure to earthquakes could be determined by computing the response history for each vibration mode separately and then combining the modal responses to obtain the total response. The time-history mode-superposition method involves the same analysis steps previously described for the response-spectrum method, except that the response computation is carried out for the entire duration of the ground shaking. The equation of motion for the *nth* vibration mode of the dam described earlier is given by:

$$\ddot{y}_n + 2\xi_n \omega_n \dot{y}_n + \omega_n^2 y_n = \frac{L_n}{M_n} \ddot{u}_g(t) \tag{7.34}$$

Although modal response history can be obtained by numerical integration of the Duhamel integral (Equation 7.42), it is more common to directly solve the equation of motion (Equation 7.34) by numerical procedures. Among many procedures available for this purpose, the linear acceleration method (Clough and Penzien 1975) implemented in the GDAP (Ghanaat 1993) program is the simplest and is described here.

7.7.1 Linear Acceleration Method

The basic assumption of this method is that the acceleration varies linearly during each time-step Δt as illustrated in Figure 7.5. Assuming that the motion at time t is given, the acceleration, velocity, and displacement responses at t + τ, where τ ≤ t, are obtained as follows:

$$\ddot{y}_{t+\tau} = \ddot{y}_t + \left(\ddot{y}_{t+\Delta t} - \ddot{y}_t\right)\frac{\tau}{\Delta t} \tag{7.53}$$

$$\dot{y}_{t+\tau} = \dot{y}_t + \ddot{y}_t\tau + \left(\ddot{y}_{t+\Delta t} - \ddot{y}_t\right)\frac{\tau^2}{2\Delta t} \tag{7.54}$$

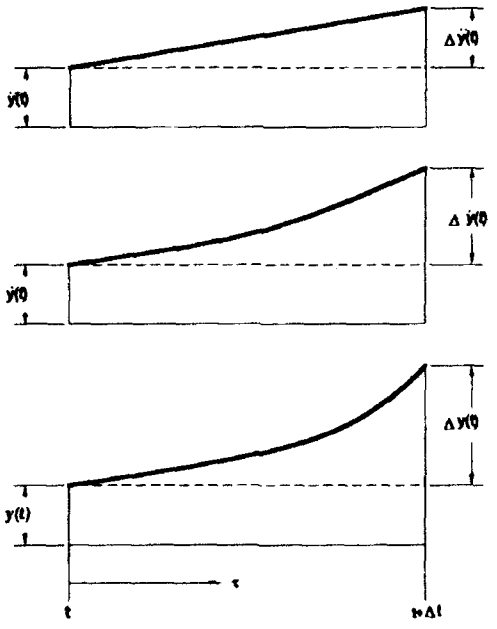

Figure 7-5 Motion of System During Time-Step Δt

$$\mathbf{y}_{t+\tau} = \mathbf{y}_t + \dot{\mathbf{y}}_t t + \tfrac{1}{2}\ddot{\mathbf{y}}_t t^2 + (\ddot{\mathbf{y}}_{t+\Delta t} - \ddot{\mathbf{y}}_t)\frac{t^3}{6\Delta t} \tag{7.55}$$

At the end of the time interval t+Δt, these expressions lead to:

$$\dot{\mathbf{y}}_{t+\Delta t} = \dot{\mathbf{y}}_t + (\ddot{\mathbf{y}}_{t+\Delta t} + \ddot{\mathbf{y}}_t)\frac{\Delta t}{2} \tag{7.56}$$

$$\mathbf{y}_{t+\Delta t} = \mathbf{y}_t + \dot{\mathbf{y}}_t \Delta t + (2\ddot{\mathbf{y}}_t + \ddot{\mathbf{y}}_{t+\Delta t})\frac{\Delta t^2}{6} \tag{7.57}$$

The equilibrium equation (Equation 7.34) at time t + Δt is written as:

$$\ddot{\mathbf{y}}_{t+\Delta t} + 2\xi\omega\dot{\mathbf{y}}_{t+\Delta t} + \omega^2\mathbf{y}_{t+\Delta t} = \mathbf{r}_{t+\Delta t} \tag{7.58}$$

Substituting Equations 7.56 and 7.57 into Equation 7.58, leads to an equation with $\ddot{y}_{t+\Delta t}$ as the only unknown. Solving for $\ddot{y}_{t+\Delta t}$ and substituting into Equations 7.56 and 7.57, the following relationship is established:

$$\begin{bmatrix} \ddot{y}_{t+\Delta t} \\ \dot{y}_{t+\Delta t} \\ y_{t+\Delta t} \end{bmatrix} = \mathbf{A}\begin{bmatrix} \ddot{y}_t \\ \dot{y}_t \\ y_t \end{bmatrix} + \mathbf{L}r_{t+\Delta t} \tag{7.59}$$

where

$$\mathbf{A} = \begin{bmatrix} -\beta/3 - \kappa & \dfrac{-\beta - 2\kappa}{\Delta t} & \dfrac{-\beta}{\Delta t^2} \\ \Delta t(1/2 - \beta/6 - \kappa/2) & 1 - \beta/2 - \kappa & \dfrac{-\beta}{2\Delta t} \\ \Delta t^2(1/3 - \beta/18 - \kappa/6) & \Delta t(1 - \beta/6 - \kappa/3) & 1 - \beta/6 \end{bmatrix} \quad ; \quad \mathbf{L} = \begin{bmatrix} \dfrac{\beta}{(\omega\Delta t)^2} \\ \dfrac{\beta}{2\omega^2\Delta t} \\ \dfrac{\beta}{6\omega^2} \end{bmatrix}$$

$$\beta = \left[\frac{1}{(\omega\Delta t)^2} + \frac{\xi}{(\omega\Delta t)} + \frac{1}{6}\right]^{-1} \quad ; \quad \kappa = \frac{\xi\beta}{(\omega\Delta t)}$$

The linear acceleration method provides an efficient step-by-step integration procedure so long as the time-step is sufficiently short. The choice of the time-step for linear analysis depends on the rate of variation of the applied load, and the dam vibration period T. The time-step must be short enough to provide satisfactory representation of these factors. The linear acceleration method is only conditionally stable and will give divergent solution if the time-step is greater than about one-

half the vibration period. The stability limit is determined by examining eigenvalues of the approximation operator **A**. An integration method is stable if and only if the spectral radius (absolute value of eigenvalues) $\rho(\mathbf{A}) \leq 1$. Figure 7-6 demonstrates stability characteristics of the linear acceleration method as a function of $\Delta t/T$.

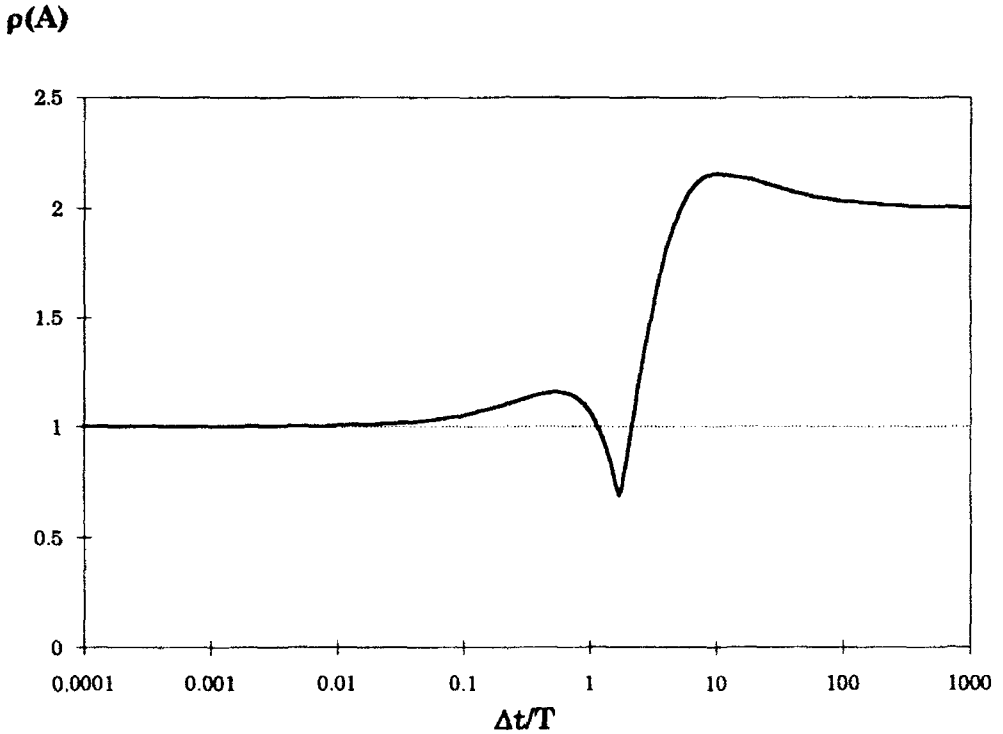

Figure 7-6 Spectral Radius $\rho(\mathbf{A})$ as a Function of $\Delta t/T$, ξ=0

It is noted that $\Delta t/T \leq 0.1$ provides a reasonable solution. For the earthquake analysis of arch dams, a 0.01-sec time-step provides an adequate description of the ground motion, and the shortest period of vibration that produces significant response generally is considerably longer than this time-step. Thus, the linear acceleration method with a 0.01-sec time-step should be effective in most arch dam analyses. For special cases, when the linear acceleration method requires very short time-steps to avoid instability, unconditionally stable methods such as the Newmark and Wilson θ methods (Bathe and Wilson 1976) may be used. Using these methods, integration parameters can be selected so that the stability will be maintained regardless of the $\Delta t/T$ ratio.

7.7.2 Total Response History

The modal displacement, velocity, and acceleration histories are obtained from Equation 7.59 by solving this recursive equation for entire duration of the ground motion. Knowing the modal response quantities, the contributions of the p lower modes to the dam response are given by:

$$\begin{aligned} u_n(t) &= Y_n(t)\phi_n \\ \dot{u}_n(t) &= \dot{Y}_n(t)\phi_n \qquad n = 1,2,...p \\ \ddot{u}_n(t) &= \ddot{Y}_n(t)\phi_n \end{aligned} \tag{7.60}$$

The element stresses associated with the dam deformations are determined using the stress-displacement relationship given in Chapter 3 (Equations 3.3 and 3.5). At each time-step the stresses associated with modal displacements $u_n(t)$ are:

$$\sigma_n(t) = [D][B]u_n(t) \tag{7.61}$$

Any internal forces can be determined from the nodal displacements and the element stiffness adjacent to the particular nodes. For example, the thrust forces at the dam-foundation interface for mode n are:

$$f_n(t) = \mathrm{k}u_n(t) \tag{7.62}$$

Finally, the total earthquake response of the dam due to all vibration modes is obtained by superposition as follows:

$$u(t) = \sum_{n=1}^{p} u_n(t) \tag{7.63a}$$

$$\dot{u}(t) = \sum_{n=1}^{p} \dot{u}_n(t) \tag{7.63b}$$

$$\ddot{u}(t) = \sum_{n=1}^{p} \ddot{u}_n(t) \tag{7.63c}$$

$$\sigma(t) = \sum_{n=1}^{p} \sigma_n(t) \tag{7.63d}$$

$$f(t) = \sum_{n=1}^{p} f_n(t) \tag{7.63e}$$

7.8 Results of Dynamic Analysis

The results of a typical dynamic analysis of arch dams include natural frequencies, vibration mode shapes, nodal displacements, and element stresses for a specified seismic input. The seismic inputs typically are the operating basis earthquake (OBE) and the maximum credible earthquake (MCE) ground motions specified in EM 1110-2-2201.

7.8.1 Response Spectrum

The natural frequencies and mode shapes of a dam structure are the basic vibration properties used for computing its maximum response using the response-spectrum method of analysis. They are obtained from the undamped free vibration analysis of the dam structure discussed previously. The natural frequencies and mode shapes provide insight into the basic dynamic response behavior of the dam structure, as well as some advance indications of the sensitivity of the dynamic response to earthquake ground motions having various frequency contents.

The maximum response quantities computed in a typical response-spectrum analysis include maximum nodal displacements and element stresses. The maximum modal displacements and stresses, if printed out, take the sign of the modal participation factor (Section 7.5), and may be positive or negative. But the maximum total nodal displacements and element stresses that are computed by SRSS or CQC combinations of the modal maxima are all positive. The maximum nodal displacements for 8-node solid and 3-D shell elements described in Chapter 5 consist of three translations corresponding to global DOF's of each element node. The maximum nodal displacements for thick-shell elements (Section 5.4) include three translations in the global directions and two rotations about two axes perpendicular to the midsurface normal.

For each element, the stresses are directly computed at the element integration points. But by using the interpolation functions, they may also be computed at the element nodal points, element center, or at the center of element surfaces. The element stresses are given in the global directions or in the direction of element local axes. The stresses defined in the element local axes are more practical for arch dams, because they can be interpreted as surface arch and cantilever stresses that better represent the arch dam behavior.

The maximum stresses for the GDAP eight-node solid element are given at the element center in the global directions and at the center of one element surface with respect to the local element axes which are useful when these elements are used to model the dam. The stresses for the eight-node solid elements consist of six components, three normal (σ_x, σ_y, σ_z) and three shear stresses (τ_{xy},τ_{yz},τ_{zx}) . The maximum stresses for the GDAP 3-D and thick-shell elements, primarily used to model the dam body, are provided with respect to local axes of the element surfaces. They are computed at 10 locations corresponding to eight midedge nodes and two center points on the element surfaces. At each point six stress components, three normal and three shear stresses similar to those described for the eight-node elements, are provided. The surface stresses for thick-shell elements are computed at eight integration points, four on each element surface. They include two normal stress components (σ_x, σ_y) in the direction of two surface axes (Figure 5.4) and three shear stresses (τ_{xy},τ_{yz},τ_{zx}); the stress component normal to the element surface is assumed to be zero (σ_z= 0).

In addition to the maximum nodal displacements and element stresses discussed previously, the GDAP program also computes the maximum nodal forces (thrusts) at the dam-foundation interface nodes as well as at any other selected points.

7.8.2 Time-history

The time-history mode-superposition method also requires undamped natural frequencies and mode shapes for computing response history of the dam structure to earthquakes. Thus, similar to the response-spectrum analysis, first an undamped free vibration analysis or eigensolution is carried out to compute vibration properties of the dam structure.

Similar to the response-spectrum method, the primary results of a time-history analysis include the nodal displacements and element stresses, except that they are computed for the entire duration of the earthquake ground shaking. Therefore, response quantities computed in this manner not only contain the maximum response values but also include variation of the response quantities with time. At each dam and foundation nodal point, three displacement histories corresponding to the translation DOF's are computed. These usually represent relative dynamic

displacements of a particular node with respect to ground displacements (fixed foundation boundary nodes). When thick-shell elements are used, two additional time-histories associated with two rotation DOF's at each element node can also be obtained. Some computer programs also have options for acquiring other response quantities such as the nodal velocity and nodal acceleration histories.

In the time-history analysis, stress histories for each finite element are computed at the same locations described previously for the response-spectrum analysis. For the shell elements, they include surface arch, cantilever and shear stresses which can be used to also compute the associated principal stress-histories on dam surfaces. For the eight-node solid elements also discussed previously, stress-histories at the element center are computed in the global direction, whereas at the center of the element surfaces they are given with respect to the particular surface local axes. These stress-histories, when examined, provide not only the extreme stress values but also the times at which they occur, the number of stress cycles exceeding allowable values, and the excursions beyond the allowable values, all of which will be discussed in Chapter 8.

8. EVALUATION AND PRESENTATION OF RESULTS

The presentation and evaluation of results of static and earthquake analyses are discussed in this chapter. It is assumed that the analysis has been performed using the GDAP (Ghanaat 1993) program, but the discussion can also be applied to results obtained by other programs.

8.1 RESULTS OF STATIC ANALYSIS

The basic results of static analysis for an arch dam include nodal displacements, element stresses, and arch thrusts exerted on the dam abutments. These response quantities should be evaluated for the usual, unusual, and extreme static loading combinations specified in EM 1110-2-2201. The results of static analysis should also be obtained and presented for each individual load to facilitate examination of the consistency of the results.

The static nodal displacements may be displayed in the form of deflected shapes across the arch sections or as 3-D plots for the entire dam structure. Figure 8-1 shows three such deflected shapes displayed across the arch sections for the hydrostatic pressures, temperature changes, and the combined hydrostatic plus temperature loads. As expected, this figure shows that an arch dam deflects downstream under water loads, whereas it moves upstream when subjected to loads due to the temperature increase. In the analysis, the deflected shapes for various loading combinations are obtained for the monolithic structure by applying the associated static loads (excluding gravity) simultaneously or separately. When applied separately, displacements for each individual load are computed alone and then are combined to obtain the total displacements for a particular loading combination. The magnitudes of the resulting deformations are not directly used in the design or safety evaluation of arch dams. But the deflection patterns should vary smoothly from point to point and are used to evaluate the adequacy of the design by visual means.

The current approach for the design and evaluation of arch dams is based explicitly on the values of induced stresses computed using the linear-elastic analysis. Whenever the overall stresses in the structure are below the allowable values as specified in EM 1110-2-2201, the design is considered to be adequate. A well-designed arch dam will develop compressive stresses only under the static loads, and these are mostly much smaller than the compressive strength of the concrete.

Tensile stresses usually develop when the dam is subjected to multiple loading combinations which include severe temperature changes or other unfavorable loading conditions. Although limited tensile stresses can be tolerated under static loading conditions, they should be minimized by reshaping the dam whenever possible. However, it should be noted that tensile stress limits are seldom satisfied near the dam-foundation contact zone by an elastic analysis which ignores cracking and nonlinearity in the foundation joints. At this location, the tensile stresses can be interpreted as openings of the dam-foundation interface joint or of joints within the foundation rock below.

Since maximum stresses in an arch dam usually occur at the faces of the structure, stresses resolved into arch, cantilever, and principal stresses at the upstream and downstream faces of the dam are the primary stresses used for the evaluation of the analysis results. However, shear stresses induced in the body of the dam by bending and twisting moments should also be examined to assure that they are within the allowable limits. The arch and cantilever stresses are ordinarily displayed as stress contours, whereas the principal stresses are shown in the form of vector plots on each face of the dam (Figure 8-2). The evaluation of the adequacy of a new design or safety assessment of an existing dam involves comparing the maximum computed stresses with the allowable compressive and tensile strengths of the concrete. The largest compressive stresses should be less than the compressive strength of the concrete by the factors of safety established in EM 1110-2-2201 for each particular loading combination.

8.2 RESULTS OF EARTHQUAKE ANALYSIS

The design and evaluation of arch dams for earthquake loading are generally based on the results of linear-dynamic analysis as described in this manual. In most cases, the linear analysis provides satisfactory results for evaluation of the dam response to low- or moderate-intensity earthquake ground motions. This level of ground motion corresponds to the OBE for which the resulting deformations are usually expected to be within the linear-elastic range of the concrete. The OBE is defined as a level of ground motion with a 50 percent probability of being exceeded during the service life of the dam, which is normally assumed to be 100 years as specified in EM 1110-2-2201. In this case, the evaluation of earthquake performance is based on simple stress checks in which the calculated elastic stresses are compared with the specified allowable tensile stresses. However, under more severe MCE, it is

possible that the calculated stresses would exceed the tensile strength of the concrete, indicating that damage would occur. If the damage is significant, the actual earthquake performance of the dam can be evaluated only by a nonlinear analysis that includes the basic nonlinear behavior mechanisms such as joint opening, tensile cracking, and foundation failure. A complete nonlinear earthquake analysis to account for all of these nonlinear mechanisms is not currently possible, although the effects of contraction joint opening during major earthquakes can be studied using a recently developed modeling technique and numerical procedure implemented in the ADAP-88 program (Fenves, Mojtahedi, and Reimer 1989). Consequently, the linear method of analysis continues to be the primary tool in practice for the evaluation of earthquake performance of arch dams. The evaluation process for damaging earthquakes, however, is quite complicated and requires both judgment and careful interpretation of the numerical results. Presentation and interpretation of the results of response-spectrum and time-history analyses are discussed in the following sections.

8.2.1 Results of Response-Spectrum Analysis

The basic dynamic characteristics of an arch dam are obtained from the study of its undamped natural frequencies and mode shapes that are computed prior to performing the response-spectrum analysis. The examination of these results provides some advance indications of the sensitivity of the dam response to earthquakes having various frequency contents, as well as the deflection patterns that would dominate the earthquake response. For example, the four lowest mode shapes and frequencies shown in Figure 8-3 indicate that the example dam model has several closely spaced vibration frequencies below 10 Hz and that the contribution of each of these modes to the earthquake response of the dam appears to be significant, because their frequencies occur in the dominant frequency range of most earthquakes.

The basic results of a response-spectrum analysis consist of the maximum nodal displacements and element stresses. As discussed in the preceding chapter, these are first computed separately for each mode of vibration, and then the resulting modal maxima which do not occur at the same time during the earthquake are combined by the SRSS or CQC method to obtain an estimate of the maximum dynamic response to a specified component of the earthquake ground motion. In addition, because the responses to the three earthquake components (two horizontal

plus vertical) are developed independently, the maximum dynamic responses due to the earthquake components are further combined by the SRSS method to include the effects of all three components. It is obvious that the resulting dynamic responses obtained in this manner have no sign and may be interpreted as being positive or negative. In particular, the maximum element stresses σ_d are assumed to be tension (positive) or compression (negative).

8.2.1.1 Total Response

In the response-spectrum method of analysis, total stresses due to static plus earthquake loads are the single response quantity used to evaluate the earthquake performance of an arch dam. The evaluation involves comparison of the total stresses with the specified allowable tensile and compressive stresses of the concrete. As discussed in EM 1110-2-2201, the allowable compressive stresses are obtained from the dynamic compressive strength of the concrete by applying appropriate factors of safety. The allowable tensile stress is equal to the dynamic tensile strength of the concrete which is obtained from splitting tensile tests modified by applying adjustment factors to account for the seismic strain rate and the nonlinear characteristics of the stress-strain curve as discussed by Raphael (1984).

Total stresses are obtained by combining dynamic stresses σ_d obtained from the response-spectrum analysis with static stresses σ_{st}. The static stresses are computed for the gravity, hydrostatic, and temperature changes expected to occur during the normal operation of the dam, as specified in EM 1110-2-2201. Since response-spectrum stresses have no sign, this combination should consider dynamic stresses to be positive or negative, leading to the maximum values of total tensile or compressive stresses:

$$\sigma_{max} = \sigma_{st} \pm \sigma_d$$

It should be noted that this combination of static and dynamic stresses is appropriate only if the σ_{st} and σ_d are oriented similarly. Thus, it is true for the arch or cantilever stresses, but generally it is not true for the principal stresses. The resulting total arch and cantilever stresses for the upstream and downstream faces of the dam are then displayed in the form of stress contours similar to those shown in Figure 8-4. In general, the maximum tensile and compressive stresses computed

in this manner for different points do not occur at the same time, and thus the contour plot does not represent concurrent data.

8.2.2 Evaluation of Results of Time-History Analysis

In the time-history analysis using GDAP, envelope values as well as the entire response histories of element stresses and nodal displacements of the dam to the design earthquake are computed. Thus, the results of such analyses include not only the maximum response values but also provide information on the variation of response with time which is essential for evaluation of the dam response to major earthquakes. The interpretation and presentation of response histories require a systematic postprocessing capability such as the one available in GDAP (Ghanaat 1993). The basic results of time-history analysis and procedures for their presentation and evaluation are described in the following paragraphs (Clough 1989).

8.2.2.1 Mode Shapes and Nodal Displacements

Vibration mode shapes and frequencies are only required for the response-spectrum and the time-history mode-superposition methods. But they may be computed even when the direct method of time-history analysis mentioned in Section 7.5 is used, because they are useful for developing a basic understanding of the dynamic response. The computed vibration modes may be presented as shown in Figure 8-3.

The resulting displacement histories for a time-history analysis may be presented as shown in Figure 8-5, for the upstream, cross-stream, and vertical directions. As a minimum, displacement histories for several points along the dam axis at the crest and at midheight elevations should be displayed and evaluated. These displacement histories can be used to identify the time and duration at which the critical stresses occur. This is because the critical stresses correspond to the time-steps at which the displacements reach their maximum. Displacement results are also used in the design of open joints for separating two adjacent independent structural components.

8.2.2.2 Envelopes of Maximum and Minimum Stresses

The envelopes of maximum and minimum stresses are among the first results to be examined. They are displayed as contour plots of the arch stresses and cantilever

stresses on each face of the dam. Contours of the maximum arch and cantilever stresses represent the largest static plus dynamic tensile (positive) stresses that have occurred at any location in the dam during the earthquake ground shaking (Figure 8-4). Similarly, the contours of minimum stresses correspond to the largest compressive (negative) arch and cantilever stresses that are developed in the dam. It is clear that the envelope stresses for different locations occur at different times and, thus, are not concurrent.

These contours are used to identify regions where the tensile stresses exceed the tensile strength of the concrete. It is only these regions that must be examined for possible damage. The extent and severity of damage is determined by further evaluation accounting for the time-dependent nature of the dynamic response which is described in the following sections.

Contours of the minimum stresses show the extreme compressive stresses that could develop in the dam during the earthquake excitation. They are compared with the allowable compressive stresses to ensure that they meet the required factors of safety for the earthquake loading, but generally they are not a critical factor with regard to dam safety.

8.2.2.3 Envelopes of Maximum and Minimum Principal Stresses

Time-histories of principal stresses for any point on the faces of the dam are easily computed from the arch, cantilever, and shear stresses at that point. When the effects of static loads are considered, the static and dynamic arch, cantilever, and shear stresses must be combined prior to the calculation of the principal stresses. The resulting time-histories of principal stresses are then used to determine the envelopes of the maximum and minimum principal stresses similar to those obtained for the arch and cantilever stresses. When displayed in the form of vector plots (Figures 8-6 and 8-7), they can be used to determine the direction of tensile cracking.

8.2.2.4 Simultaneous or Concurrent Critical Stresses

The envelopes of maximum stresses discussed in Section 8.2.2.2 indicate the over-stressed areas where the tensile strength of the concrete is exceeded. For each stress point showing an arch stress value exceeding the tensile strength of the concrete (called the *critical arch stress points*), the time-step when the peak arch

stress is reached is determined. This is repeated for each point having a cantilever stress value exceeding the tensile strength of the concrete (called the *critical cantilever stress points*). This information is then used to determine the concurrent (or simultaneous) states of stress corresponding to the time-steps at which the critical arch and cantilever stresses reach their maxima. The concurrent arch and cantilever stresses are displayed as contour plots (Figure 8-8) and can be interpreted as snap shots of the worst stress conditions. They are evaluated similar to the envelope stresses, except that concurrent stresses which occur at the same time indicate the true stress distribution corresponding to critical time-steps during the earthquake excitation. Compared to the envelope stresses, the concurrent stresses are not necessarily all tension, and the overstressed regions will be smaller.

8.2.2.5 Time-history of Critical Stresses

When the envelope of maximum stresses and concurrent stresses show tensile stresses that exceed the allowable value, the stress histories for the critical points are examined for a more detailed evaluation (Figure 8-9). For each critical arch and cantilever stress point, the stress history for the point on the opposite face of the dam should be also examined. For example, a pair of arch stress histories as shown in Figure 8-9 can be used to evaluate the linear variation of arch stress through the dam thickness at critical time-steps. Noting that the vertical contraction joints in arch dams cannot resist tension, the arch tensile stress distribution through the thickness may be interpreted in terms of joint opening. Similar stress distribution should be also determined for the critical cantilever stress points. At the dam-rock interface, the critical tensile cantilever stresses can be interpreted as openings of the rock-concrete joints or of the joints within the rock below. For locations within the body of dam away from the foundation boundary, it can be expected that cracking will occur at the critical cantilever stress points. The time-history of cantilever stresses at each critical location should be examined to determine the number of cycles and the total duration of stress exceeding the tensile strength of the concrete. This would indicate whether the excursion beyond the allowable value (or cracking stress) is an isolated case or is repeated many times during the earthquake excitation. The estimated total duration of excursions beyond the allowable value is used to demonstrate whether the maximum stress cycles are merely spikes or have longer duration and thus could be more damaging. Acceptable limits for the number of times that the allowable stress can be safely exceeded have not yet been established. In practice, up to five stress cycles have been permitted based on

judgment but such performance has not been substantiated by experimental data. In addition, the number of adjacent finite elements that crack, the extent of cantilever cracks through the dam thickness, as well as arch stress distribution through the thickness should be established for the evaluation.

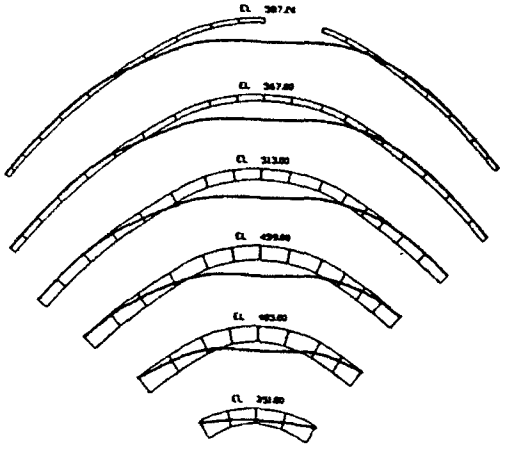

(a) Hydrostatic Pressure

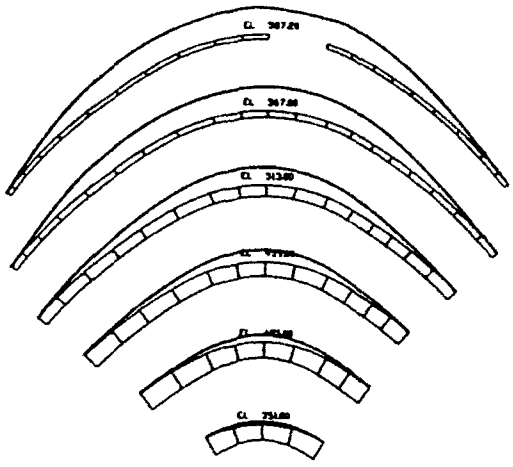

(b) Temperature Increase

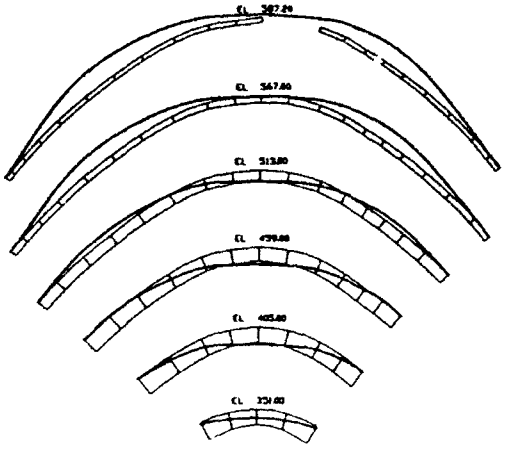

(c) Combined Water

Figure 8-1 Dam Deflections Due to Static Loads

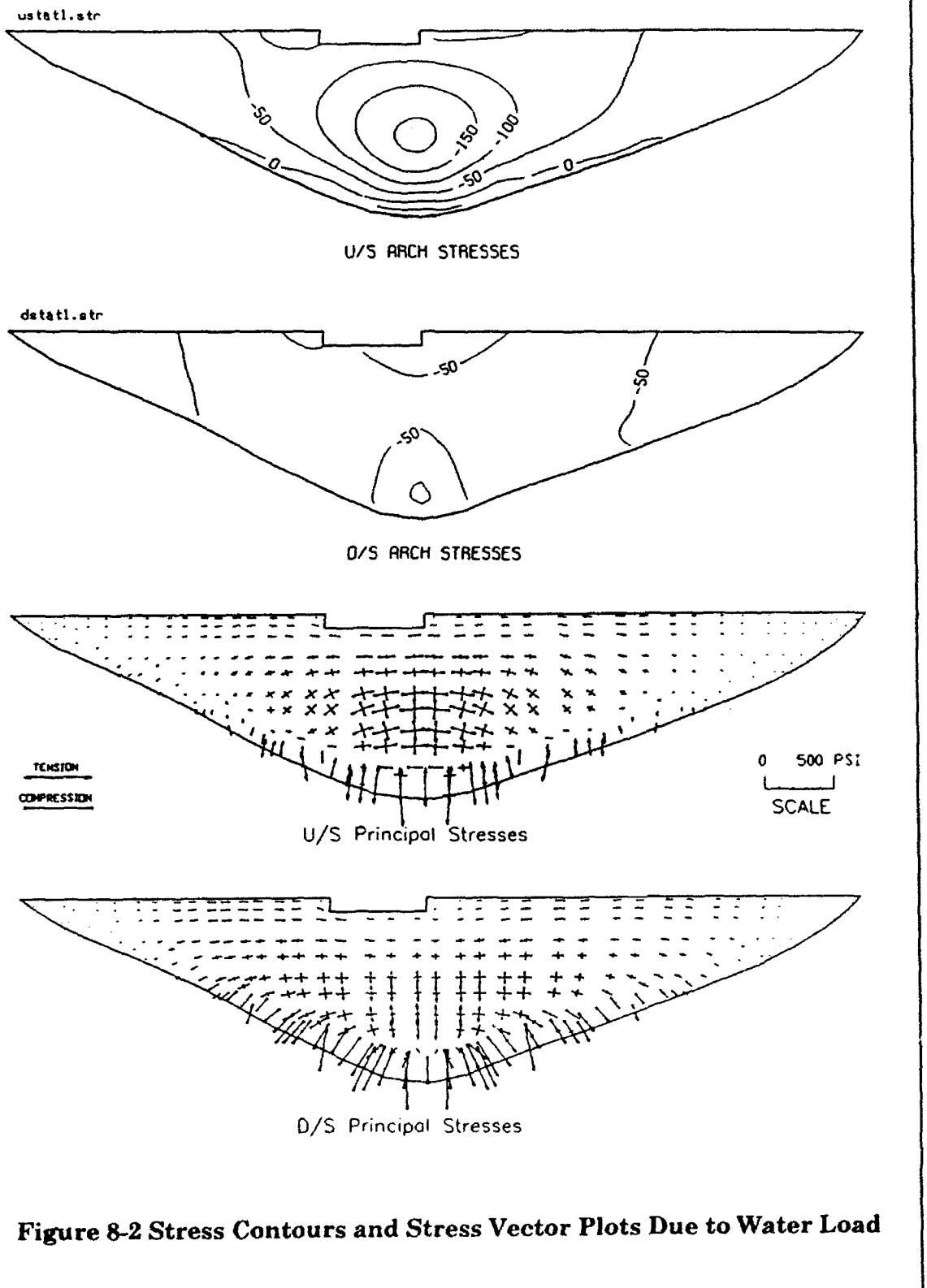

Figure 8-2 Stress Contours and Stress Vector Plots Due to Water Load

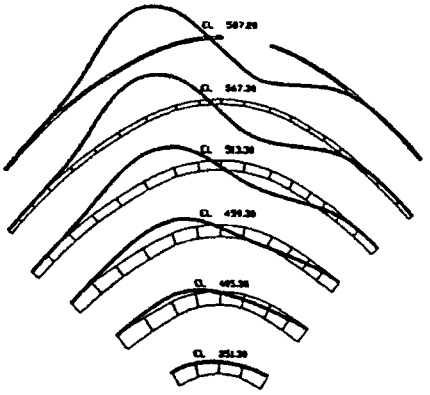

MODE-1
2.44 HZ

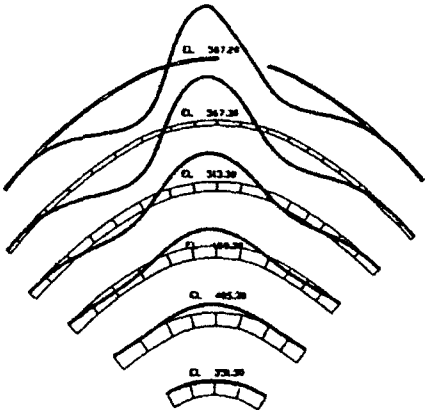

MODE-2
2.89 HZ

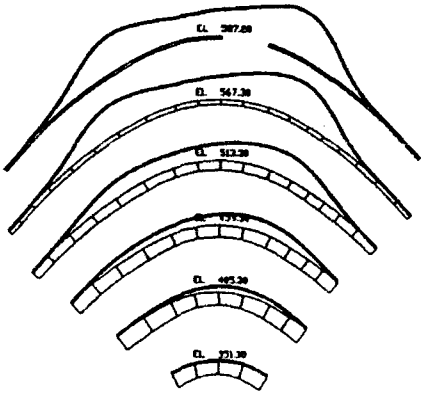

MODE-3
3.18 HZ

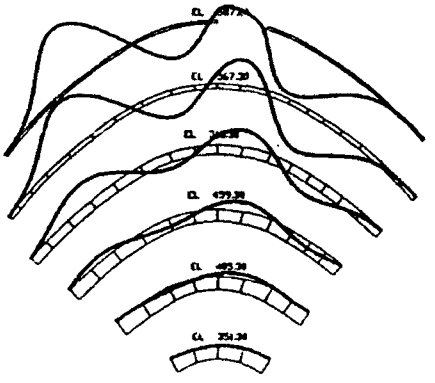

MODE-4
3.68 HZ

Figure 8-3 Four Lowest Vibration Mode Shapes

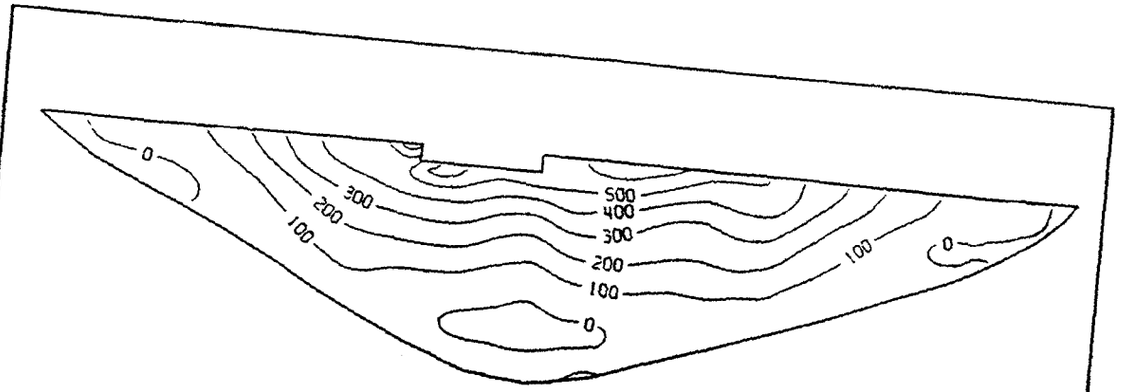

U/S ARCH STRESSES

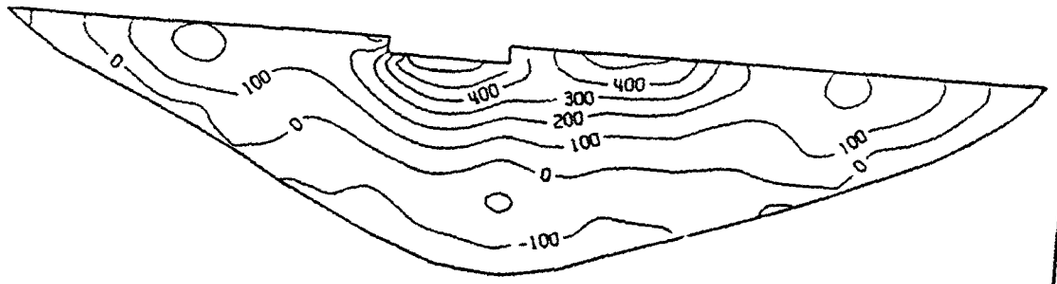

D/S ARCH STRESSES

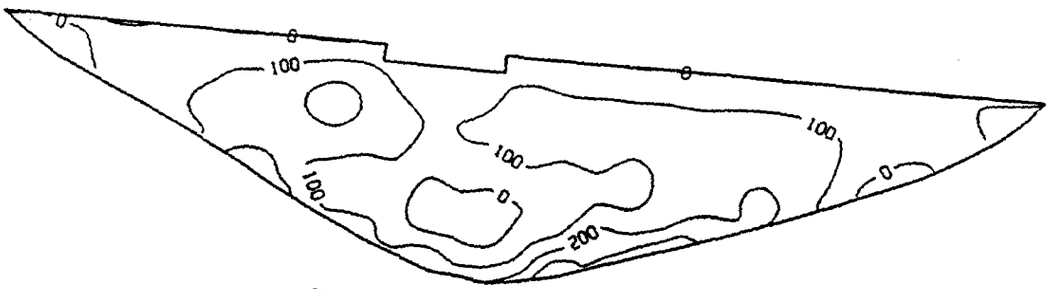

U/S CANTILEVER STRESSES

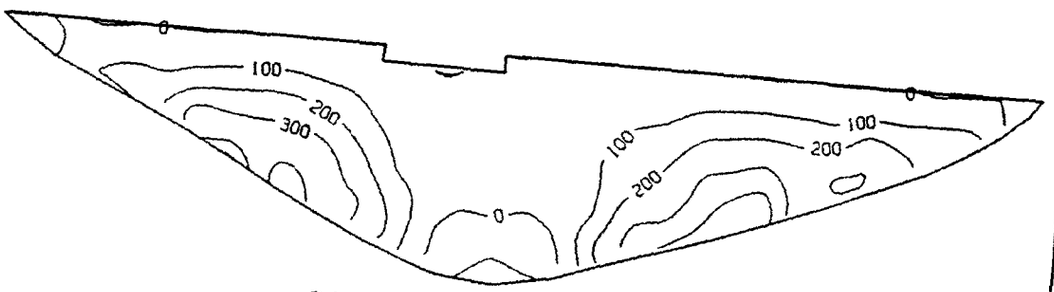

D/S CANTILEVER STRESSES

Figure 8-4 Envelopes of Maximum Arch and Cantilever Stresses

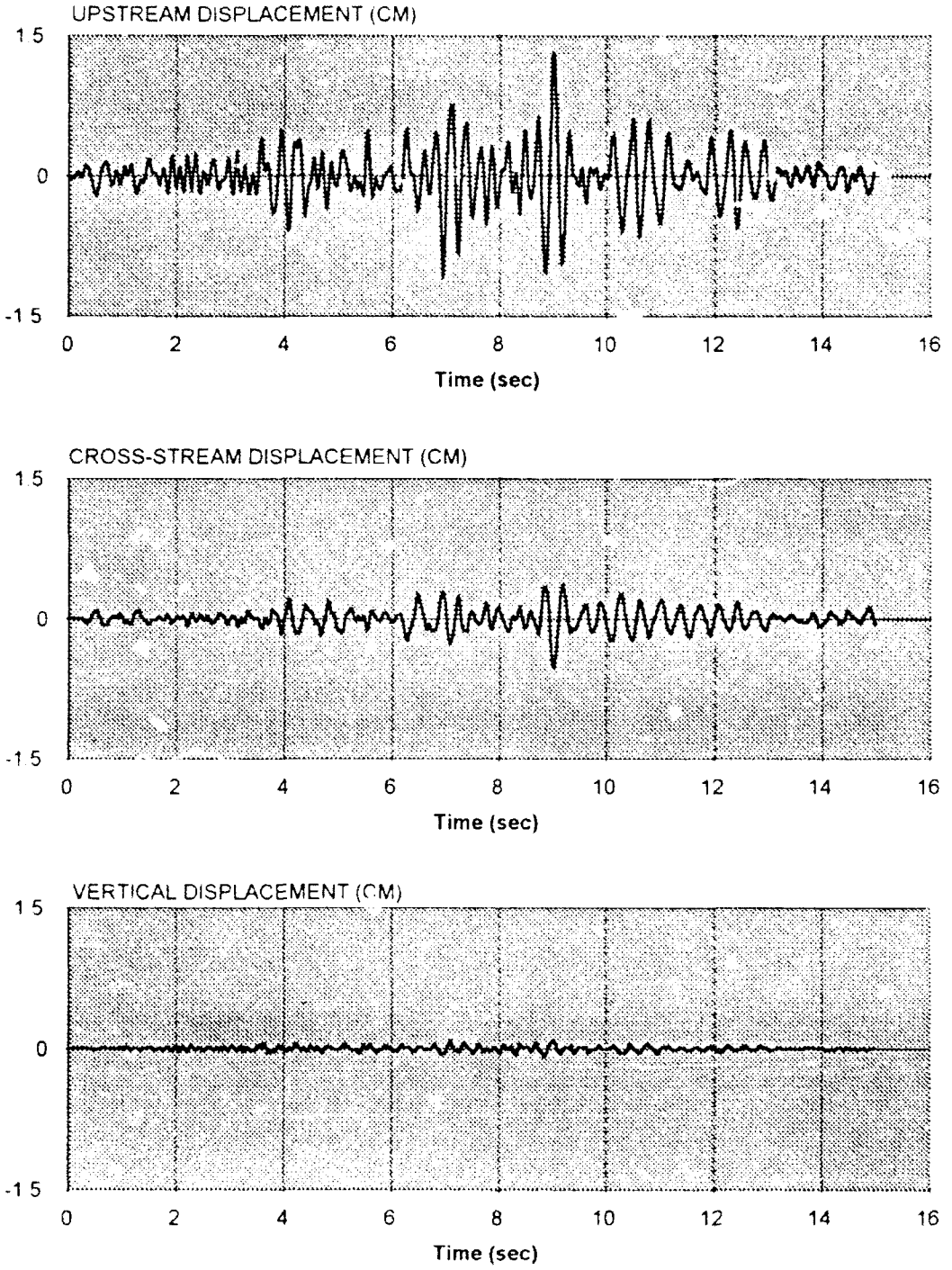

Figure 8-5 Displacement Response Histories of a Crest Node in Upstream, Cross Stream, and Vertical Directions

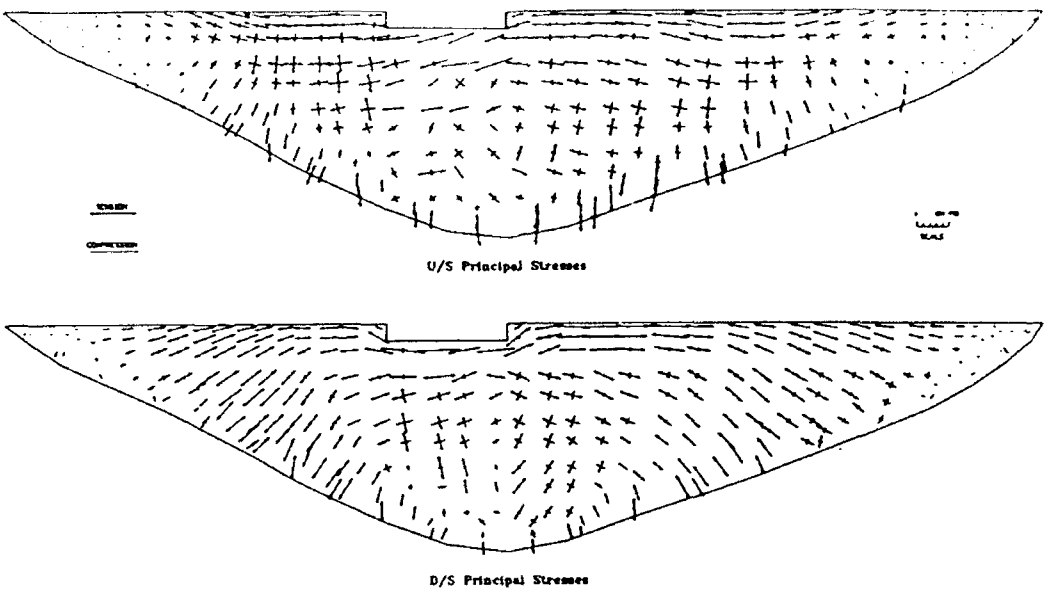

Figure 8-6 Envelope of Maximum Principal Stresses with Their Corresponding Perpendicular Pairs

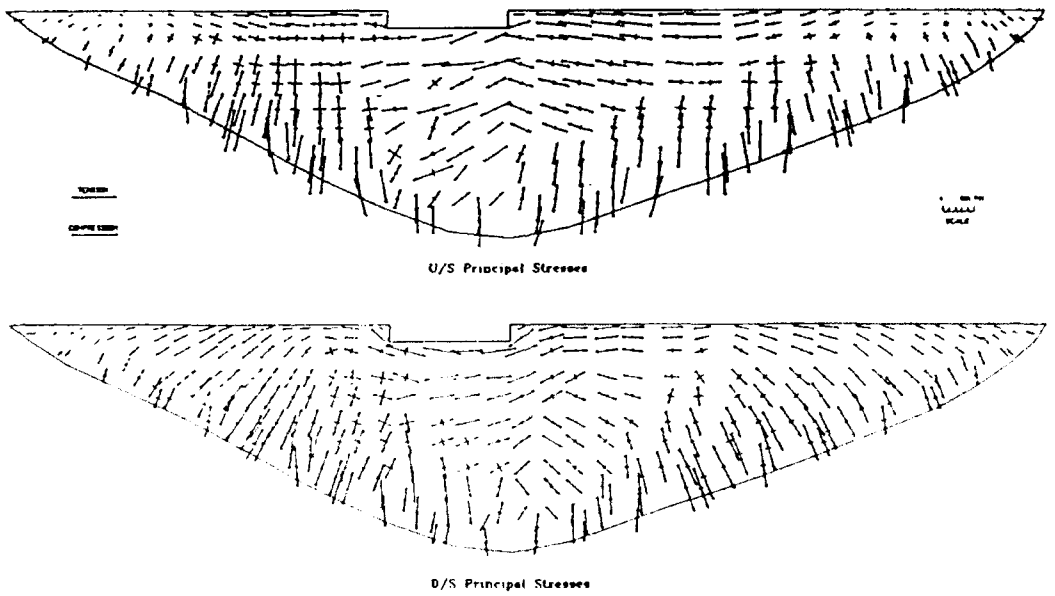

Figure 8-7 Envelope of Minimum Principal Stresses with Their Corresponding Perpendicular Pairs

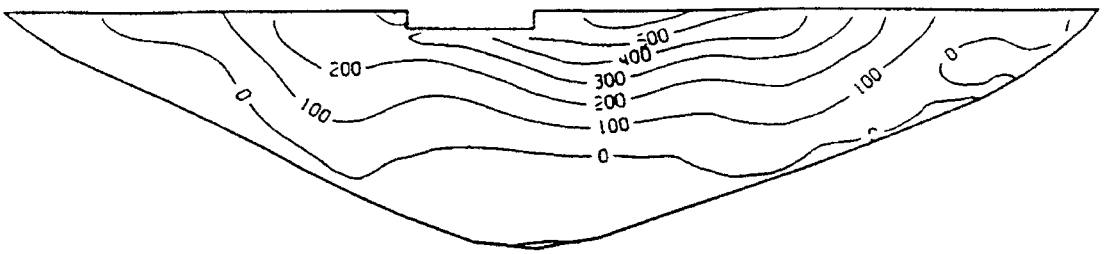

U/S ARCH STRESSES

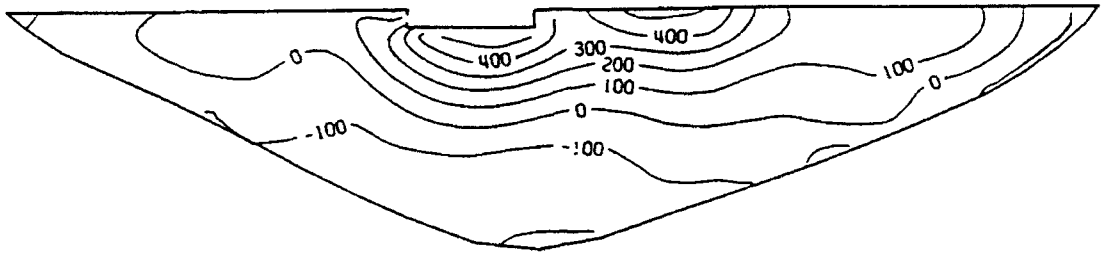

D/S ARCH STRESSES

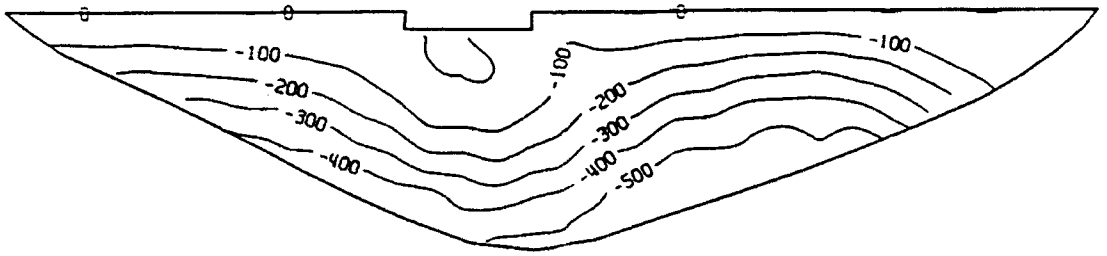

U/S CANTILEVER STRESSES

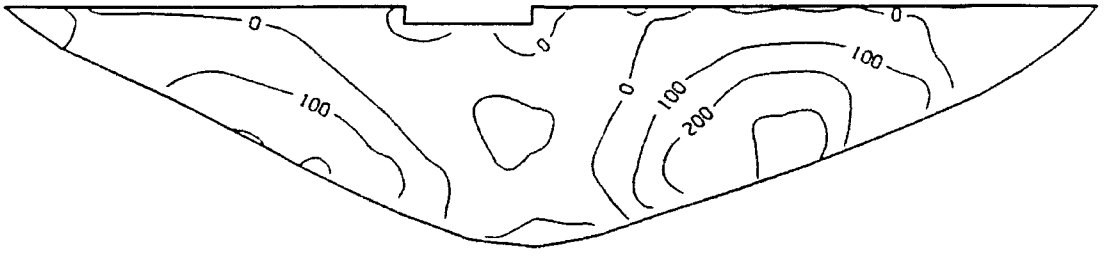

D/S CANTILEVER STRESSES

Figure 8-8 Concurrent Arch and Cantilever Stresses at Time = 9 sec

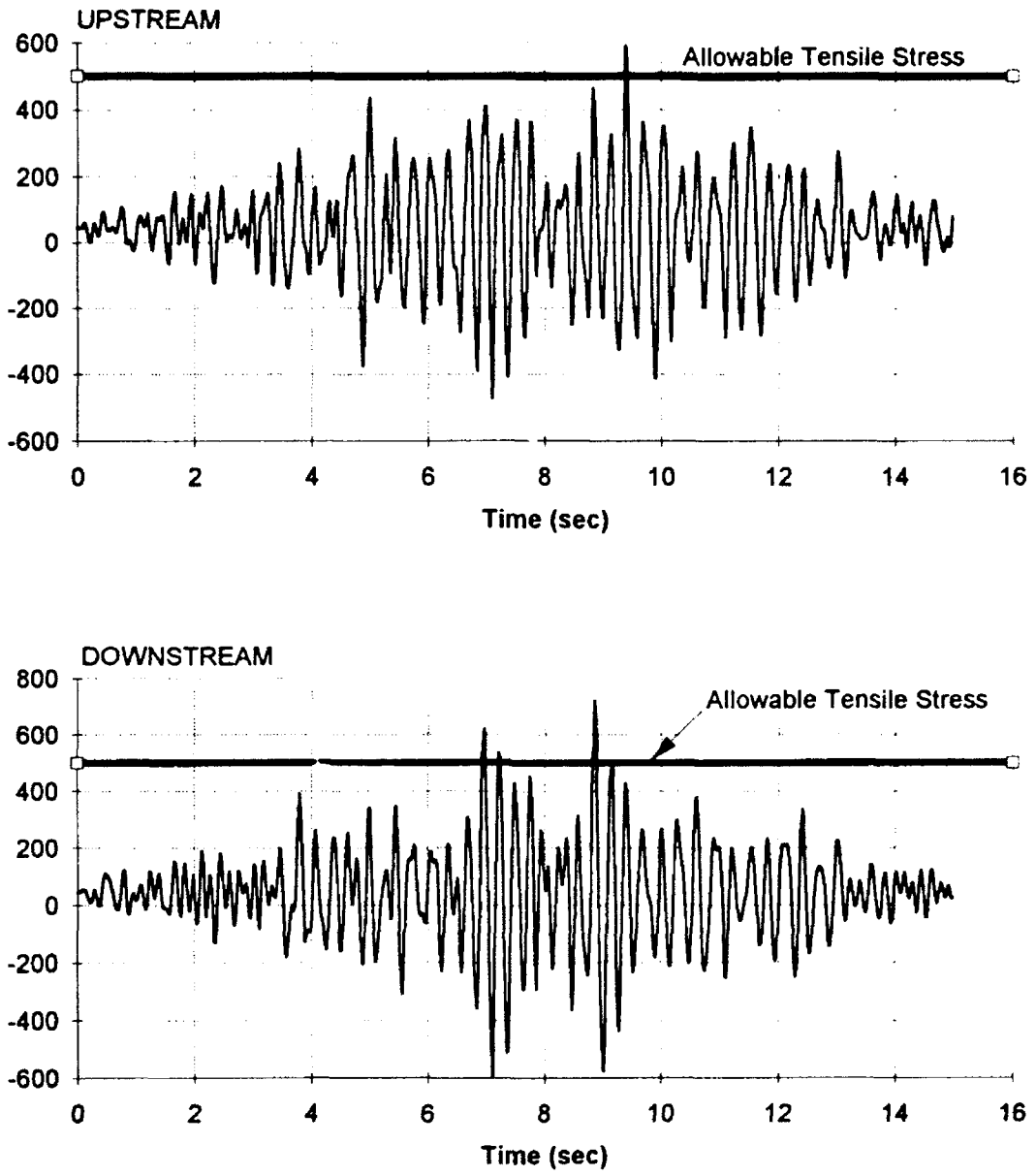

Figure 8-9 Time-histories of Arch Stresses (in psi) at Two Opposite Points on Upstream and Downstream Faces of Dam

REFERENCES

Bathe, K.- J., Wilson, E. L., and Peterson, F.E. 1974. "SAP, A general Structural Analysis Program," Report No. UCB/EERC 73-11, University of California Earthquake Engineering Research Center, Berkeley.

Bathe, K.-J., and Wilson, E.L. 1976. *Numerical Methods in Finite Element Analysis,* Prentice-Hall, Englewood Cliffs, NJ.

Chopra, A. K. 1988 (Oct). *"Earthquake Response Analysis of Concrete Dams,"* Chapter 15, Advanced Dam Engineering For Design, Construction, and Rehabilitation, Jansen, Robert B., ed., Van Nostrand Reinhold, New York, pp 416 - 465.

Clough, R. W. 1977 (Feb). *Lecture Notes.* unpublished document.

Clough, R. W. 1980. *Nonlinear Mechanisms in the Seismic Response of Arch Dams,* Proceedings, International Research Conference on Earthquake Engineering, June-July 1980, Skopje, Yugoslavia.

Clough, R. W. 1989. Meeting Notes prepared for the U.S. Army Corps of Engineers, U. S.Army Engineer District, Jacksonville, FL.

Clough, R. W. , and Penzien, J. 1975. Dynamics of Structures, McGraw-Hill, New York.

Clough, R. W., Chang, K. T., Chin, H.-Q., Stephen, R. M., Wang, G.-L., and Ghanaat, Y. 1984 (Apr). "Dynamic Response Behavior of Xiang Hong Dian Dam," Report No. UCB/EERC 84/02, University of California Earthquake Engineering Research Center, Berkeley.

Clough, R. W.,Chang, K. -T., Chin, H.-Q., Stephen, R. M., Ghanaat, Y., and Qi, J.-H. 1984 (Nov). "Dynamic Response Behavior of Quan Shui Dam," Report No. UCB/EERC 84/20, University of California Earthquake Engineering Research Center, Berkeley.

Clough, R. W., and Chang, K.T. 1987 (Jun). *"Proceedings of China-U.S. Workshop on Earthquake Behavior of Arch Dams,"* Beijing, China.

Dahlquist, G., and Bjorck, A. 1974. Numerical Methods, Prentice Hall, Englewood Cliffs, NJ.

Duron, Z. H., and Hall, J. F. 1988 (Oct). "Experimental and Finite Element Studies of the Forced Vibration of Morrow Point Dam," *Journal of Earthquake Engineering and Structural Dynamics,* Vol 16, No. 7, pp 1021-1039.

Fenves, G. L., Mojtahedi, S., and Reimer, R. B. 1989 (Nov). "ADAP-88: A Program For Nonlinear Earthquake Analysis of Concrete Arch Dams," *Report No. UCB/EERC-89/12,* University of California Earthquake Engineering Research Center, Berkeley.

Fok, H. -L., and Chopra, A., K. 1985. "Earthquake Analysis and Response of Concrete Arch Dams," *Report No. UCB/EERC-85/07.* University of California Earthquake Engineering Research Center, Berkeley.

Ghaboussi, J., Wilson,E. L., and Taylor, R. L. 1971. "Isoparametric Finite Elements with Imcompatible Deformation Modes," Proceedings of O. N. R. Symposium, University of Illinois, Urbana, IL.

Ghanaat, Y. 1993. "User's Manual - GDAP - Graphics-Based Dam Analysis Program," Instruction Report ITL-93-3, U. S. Army Engineer Waterways Experiment Station, Vicksburg, MS.

Hall, J. F. and Chopra, A. K. 1980. "Dynamic Response of Embankment. Concrete-Gravity and Arch Dams Including Hydrodynamic Interaction," *Report No. UBC/EERC -80/39,* University of California Earthquake Engineering Research Center, Berkeley.

Headquarters, Department of the Army. 1993. "Engineering and Design: Arch Dam Design," EM 1110-2-2201, Washington, DC.

Herzog, M. A. M. 1989(Jul). "The Influence of Reservoir Loading on Dam Stresses and Deflections," *Journal of Water Power & Dam Construction.*

Hurty, W. C., and Rubinstein, M. F. 1964. *Dynamics of Structures,* Prentice-Hall, Englewood Cliffs, NJ.

Kuo, J. 1982. "Fluid-Structure Interactions: Added Mass Computations for Imcompressible Fluid," *Report No. UCB/EERC-82/09,* University of California Earthquake Engineering Research Center, Berkeley.

Malvern, L. E. 1969. *Introduction to the Mechanics of a Continuous Medium,* Prentice-Hall, Englewood Cliffs, NJ.

Pawsey, S. F. 1970. "The Analysis of Moderately Thick to Thin SHELLS by the Finite Element Method," *Report No. UC/SESM-70/12,* Structural Engineering Laboratory, University of California, Berkeley.

Pilkey, W., Saczalski, K., and Schaffer, H. 1974. *Structural Mechanics Computer Programs,* University Press of Virginia, Charlotteville, VA.

Raphael, J. M. 1984 (Mar - Apr). "The Tensile Strength of Concrete," *ACI Journal,* Proceedings Vol 81, pp 158-165.

Saini, S.S., Bettes, P., and Zienkiewicz, O.C. 1978. "Couples Hydrodynamic Response of Concrete Gravity Dams Using Finite and Infintie Elements, " Journal of Earthquake Engineering and Structural Dynamics, Vol 6, pp 363-74.

Timoshenko, S. P., and Goodier, J. N. 1970. *Theory of Elasticity,* 3rd ed., McGraw-Hill, New York.

U. S. Bureau of Reclamation. 1965 (Oct). "Control of Cracking in Mass Concrete Structures," *Engineering Monograph No. 34,* U.S. Department of the Interior, Denver, CO.

U. S. Bureau of Reclamation. 1977. "Design of Arch Dams," *Design Manual For Concrete Arch Dams,* U.S. Department of the Interior, Denver, CO.

Westergaard, H.M. 1933. "Water Pressures on Dams During Earthquakes," Transactions, American Society of Civil Engineers, Vol 98.

Wilson, E.L. 1982. "New Approaches For The Dynamic Analysis of Large Structural Systems," Report No. UCB/EERC-82/04, University of California Earthquake Engineering Center, Berkeley.

Wilson, E.L., Der Kiureghian, A., and Bayo, E.P. 1981. "Short Communication: A Replacement for the SRSS Method in Seismic Analysis," Journal of Earthquake Engineering and Structural Dynamics, Vol 9, pp 187-194.

Zienkiewicz, O.C. 1971. *The Finite Element Method in Engineering Science,* 2nd ed., McGraw-Hill, New York.

REPORT DOCUMENTATION PAGE

Form Approved
OMB No 0704-0188

1. AGENCY USE ONLY (Leave blank)	2. REPORT DATE	3. REPORT TYPE AND DATES COVERED
	July 1993	Final report

4. TITLE AND SUBTITLE

Theoretical Manual for Analysis of Arch Dams

5. FUNDING NUMBERS

6. AUTHOR(S)

Yusof Ghanaat

7. PERFORMING ORGANIZATION NAME(S) AND ADDRESS(ES)

QUEST Structures
1900 Powell St., Suite 210
Emeryville, CA 94608

8. PERFORMING ORGANIZATION REPORT NUMBER

9. SPONSORING / MONITORING AGENCY NAME(S) AND ADDRESS(ES)

U.S. Army Engineer Waterways Experiment Station
Information Technology Laboratory
3909 Halls Ferry Road, Vicksburg, MS 39180-6199

10. SPONSORING / MONITORING AGENCY REPORT NUMBER

Technical Report ITL-93-1

11. SUPPLEMENTARY NOTES

Available from National Technical Information Service, 5285 Port Royal Road, Springfield, VA 22161.

12a. DISTRIBUTION / AVAILABILITY STATEMENT

Approved for public release; distribution is unlimited.

12b. DISTRIBUTION CODE

13. ABSTRACT (Maximum 200 words)

This manual is a companion to Engineer Manual (EM) 1110-2-2201, "Engineering and Design: Arch Dam Design" (Headquarters, Department of the Army 1993), and is intended to provide a theoetical background for the linear structural analysis of concrete arch dams. It is also designed to describe analytical procedures employed in the computer program, Graphics-Based Dam Analysis Program (GDAP) (Ghanaat 1993), and to provide an overview of the trial load method of arch dam design and analysis.

The manual contains an overview and discussion of the general aspects of the finite element procedures, including system idealization, isoparametric element formulation, and solution techniques for the static and dynamic analyses of arch dams used in the computer program GDAP. It also presents general discussions on the concepts, assumptions, and limitations of the trial load method.

14. SUBJECT TERMS

Arch dam
Dynamic analysis
Earthquake analysis
Finite element
Trial load method

15. NUMBER OF PAGES
108

16. PRICE CODE

17. SECURITY CLASSIFICATION OF REPORT	18. SECURITY CLASSIFICATION OF THIS PAGE	19. SECURITY CLASSIFICATION OF ABSTRACT	20. LIMITATION OF ABSTRACT
UNCLASSIFIED	UNCLASSIFIED		

WATERWAYS EXPERIMENT STATION REPORTS PUBLISHED UNDER THE COMPUTER-AIDED STRUCTURAL ENGINEERING (CASE) PROJECT

	Title	Date
Technical Report K-78-1	List of Computer Programs for Computer-Aided Structural Engineering	Feb 1978
Instruction Report O-79-2	User's Guide: Computer Program with Interactive Graphics for Analysis of Plane Frame Structures (CFRAME)	Mar 1979
Technical Report K-80-1	Survey of Bridge-Oriented Design Software	Jan 1980
Technical Report K-80-2	Evaluation of Computer Programs for the Design/Analysis of Highway and Railway Bridges	Jan 1980
Instruction Report K-80-1	User's Guide: Computer Program for Design/Review of Curvilinear Conduits/Culverts (CURCON)	Feb 1980
Instruction Report K-80-3	A Three-Dimensional Finite Element Data Edit Program	Mar 1980
Instruction Report K-80-4	A Three-Dimensional Stability Analysis/Design Program (3DSAD)	
	Report 1: General Geometry Module	Jun 1980
	Report 3: General Analysis Module (CGAM)	Jun 1982
	Report 4: Special-Purpose Modules for Dams (CDAMS)	Aug 1983
Instruction Report K-80-6	Basic User's Guide: Computer Program for Design and Analysis of Inverted-T Retaining Walls and Floodwalls (TWDA)	Dec 1980
Instruction Report K-80-7	User's Reference Manual: Computer Program for Design and Analysis of Inverted-T Retaining Walls and Floodwalls (TWDA)	Dec 1980
Technical Report K-80-4	Documentation of Finite Element Analyses	
	Report 1: Longview Outlet Works Conduit	Dec 1980
	Report 2: Anchored Wall Monolith, Bay Springs Lock	Dec 1980
Technical Report K-80-5	Basic Pile Group Behavior	Dec 1980
Instruction Report K-81-2	User's Guide: Computer Program for Design and Analysis of Sheet Pile Walls by Classical Methods (CSHTWAL)	
	Report 1: Computational Processes	Feb 1981
	Report 2: Interactive Graphics Options	Mar 1981
Instruction Report K-81-3	Validation Report: Computer Program for Design and Analysis of Inverted-T Retaining Walls and Floodwalls (TWDA)	Feb 1981
Instruction Report K-81-4	User's Guide: Computer Program for Design and Analysis of Cast-in-Place Tunnel Linings (NEWTUN)	Mar 1981
Instruction Report K-81-6	User's Guide: Computer Program for Optimum Nonlinear Dynamic Design of Reinforced Concrete Slabs Under Blast Loading (CBARCS)	Mar 1981
Instruction Report K-81-7	User's Guide: Computer Program for Design or Investigation of Orthogonal Culverts (CORTCUL)	Mar 1981
Instruction Report K-81-9	User's Guide: Computer Program for Three-Dimensional Analysis of Building Systems (CTABS80)	Aug 1981
Technical Report K-81-2	Theoretical Basis for CTABS80: A Computer Program for Three-Dimensional Analysis of Building Systems	Sep 1981
Instruction Report K-82-6	User's Guide: Computer Program for Analysis of Beam-Column Structures with Nonlinear Supports (CBEAMC)	Jun 1982

(Continued)

WATERWAYS EXPERIMENT STATION REPORTS PUBLISHED UNDER THE COMPUTER-AIDED STRUCTURAL ENGINEERING (CASE) PROJECT

(Continued)

	Title	Date
Instruction Report K-82-7	User's Guide: Computer Program for Bearing Capacity Analysis of Shallow Foundations (CBEAR)	Jun 1982
Instruction Report K-83-1	User's Guide: Computer Program with Interactive Graphics for Analysis of Plane Frame Structures (CFRAME)	Jan 1983
Instruction Report K-83-2	User's Guide: Computer Program for Generation of Engineering Geometry (SKETCH)	Jun 1983
Instruction Report K-83-5	User's Guide: Computer Program to Calculate Shear, Moment, and Thrust (CSMT) from Stress Results of a Two-Dimensional Finite Element Analysis	Jul 1983
Technical Report K-83-1	Basic Pile Group Behavior	Sep 1983
Technical Report K-83-3	Reference Manual: Computer Graphics Program for Generation of Engineering Geometry (SKETCH)	Sep 1983
Technical Report K-83-4	Case Study of Six Major General-Purpose Finite Element Programs	Oct 1983
Instruction Report K-84-2	User's Guide: Computer Program for Optimum Dynamic Design of Nonlinear Metal Plates Under Blast Loading (CSDOOR)	Jan 1984
Instruction Report K-84-7	User's Guide: Computer Program for Determining Induced *Stresses and* Consolidation Settlements (CSETT)	Aug 1984
Instruction Report K-84-8	Seepage Analysis of Confined Flow Problems by the Method of Fragments (CFRAG)	Sep 1984
Instruction Report K-84-11	User's Guide for Computer Program CGFAG, Concrete General Flexure Analysis with Graphics	Sep 1984
Technical Report K-84-3	Computer-Aided Drafting and Design for Corps Structural Engineers	Oct 1984
Technical Report ATC-86-5	Decision Logic Table Formulation of ACI 318-77, Building Code Requirements for Reinforced Concrete for Automated Constraint Processing, Volumes I and II	Jun 1986
Technical Report ITL-87-2	A Case Committee Study of Finite Element Analysis of Concrete Flat Slabs	Jan 1987
Instruction Report ITL-87-1	User's Guide: Computer Program for Two-Dimensional Analysis of U-Frame Structures (CUFRAM)	Apr 1987
Instruction Report ITL-87-2	User's Guide: For Concrete Strength Investigation and Design (CASTR) in Accordance with ACI 318-83	May 1987
Technical Report ITL-87-6	Finite-Element Method Package for Solving Steady-State Seepage Problems	May 1987
Instruction Report ITL-87-3	User's Guide: A Three Dimensional Stability Analysis/Design Program (3DSAD) Module	Jun 1987
	Report 1: Revision 1: General Geometry	Jun 1987
	Report 2: General Loads Module	Sep 1989
	Report 6: Free-Body Module	Sep 1989

(Continued)

WATERWAYS EXPERIMENT STATION REPORTS PUBLISHED UNDER THE COMPUTER-AIDED STRUCTURAL ENGINEERING (CASE) PROJECT

(Continued)

	Title	Date
Instruction Report ITL-87-4	User's Guide: 2-D Frame Analysis Link Program (LINK2D)	Jun 1987
Technical Report ITL-87-4	Finite Element Studies of a Horizontally Framed Miter Gate Report 1: Initial and Refined Finite Element Models (Phases A, B, and C), Volumes I and II Report 2: Simplified Frame Model (Phase D) Report 3: Alternate Configuration Miter Gate Finite Element Studies–Open Section Report 4: Alternate Configuration Miter Gate Finite Element Studies–Closed Sections Report 5: Alternate Configuration Miter Gate Finite Element Studies–Additional Closed Sections Report 6: Elastic Buckling of Girders in Horizontally Framed Miter Gates Report 7: Application and Summary	Aug 1987
Instruction Report GL-87-1	User's Guide: UTEXAS2 Slope-Stability Package; Volume I, User's Manual	Aug 1987
Instruction Report ITL-87-5	Sliding Stability of Concrete Structures (CSLIDE)	Oct 1987
Instruction Report ITL-87-6	Criteria Specifications for and Validation of a Computer Program for the Design or Investigation of Horizontally Framed Miter Gates (CMITER)	Dec 1987
Technical Report ITL-87-8	Procedure for Static Analysis of Gravity Dams Using the Finite Element Method – Phase 1a	Jan 1988
Instruction Report ITL-88-1	User's Guide: Computer Program for Analysis of Planar Grid Structures (CGRID)	Feb 1988
Technical Report ITL-88-1	Development of Design Formulas for Ribbed Mat Foundations on Expansive Soils	Apr 1988
Technical Report ITL-88-2	User's Guide: Pile Group Graphics Display (CPGG) Post-processor to CPGA Program	Apr 1988
Instruction Report ITL-88-2	User's Guide for Design and Investigation of Horizontally Framed Miter Gates (CMITER)	Jun 1988
Instruction Report ITL-88-4	User's Guide for Revised Computer Program to Calculate Shear, Moment, and Thrust (CSMT)	Sep 1988
Instruction Report GL-87-1	User's Guide: UTEXAS2 Slope-Stability Package; Volume II, Theory	Feb 1989
Technical Report ITL-39-3	User's Guide: Pile Group Analysis (CPGA) Computer Group	Jul 1989
Technical Report ITL-89-4	CBASIN–Structural Design of Saint Anthony Falls Stilling Basins According to Corps of Engineers Criteria for Hydraulic Structures; Computer Program X0098	Aug 1989

(Continued)

WATERWAYS EXPERIMENT STATION REPORTS PUBLISHED UNDER THE COMPUTER-AIDED STRUCTURAL ENGINEERING (CASE) PROJECT

(Continued)

	Title	Date
Technical Report ITL-89-5	CCHAN–Structural Design of Rectangular Channels According to Corps of Engineers Criteria for Hydraulic Structures; Computer Program X0097	Aug 1989
Technical Report ITL-89-6	The Response-Spectrum Dynamic Analysis of Gravity Dams Using the Finite Element Method; Phase II	Aug 1989
Contract Report ITL-89-1	State of the Art on Expert Systems Applications in Design, Construction, and Maintenance of Structures	Sep 1989
Instruction Report ITL-90-1	User's Guide: Computer Program for Design and Analysis of Sheet Pile Walls by Classical Methods (CWALSHT)	Feb 1990
Technical Report ITL-90-3	Investigation and Design of U-Frame Structures Using Program CUFRBC Volume A: Program Criteria and Documentation Volume B: User's Guide for Basins Volume C: User's Guide for Channels	May 1990
Instruction Report ITL-90-6	User's Guide: Computer Program for Two-Dimensional Analysis of U-Frame or W-Frame Structures (CWFRAM)	Sep 1990
Instruction Report ITL-90-2	User's Guide: Pile Group–Concrete Pile Analysis Program (CPGC) Preprocessor to CPGA Program	Jun 1990
Technical Report ITL-91-3	Application of Finite Element, Grid Generation, and Scientific Visualization Techniques to 2-D and 3-D Seepage and Groundwater Modeling	Sep 1990
Instruction Report ITL-91-1	User's Guide: Computer Program for Design and Analysis of Sheet-Pile Walls by Classical Methods (CWALSHT) Including Rowe's Moment Reduction	Oct 1991
Instruction Report ITL-87-2 (Revised)	User's Guide for Concrete Strength Investigation and Design (CASTR) in Accordance with ACI 318-89	Mar 1992
Technical Report ITL-92-2	Finite Element Modeling of Welded Thick Plates for Bonneville Navigation Lock	May 1992
Technical Report ITL-92-4	Introduction to the Computation of Response Spectrum for Earthquake Loading	Jun 1992
Instruction Report ITL-92-3	Concept Design Example, Computer Aided Structural Modeling (CASM) Report 1: Scheme A Report 2: Scheme B Report 3: Scheme C	 Jun 1992 Jun 1992 Jun 1992
Instruction Report ITL-92-4	User's Guide: Computer-Aided Structural Modeling (CASM) - Version 3.00	Apr 1992
Instruction Report ITL-92-5	Tutorial Guide: Computer-Aided Structural Modeling (CASM) - Version 3.00	Apr 1992

(Continued)

Technical Report ITL-93-1
July 1993

US Army Corps of Engineers
Waterways Experiment Station

Computer-Aided Structural Engineering (CASE) Project

Theoretical Manual for Analysis of Arch Dams

by Yusof Ghanaat
QUEST Structures

Prepared for Headquarters, U.S. Army Corps of Engineers